# Timing of Brittle Deformation in the Cañon City Embayment, CO: Laser Ablation U-Pb Dating of Carbonate Fractures

By



Marc Center
B.S. University of Kansas 2022

Submitted to the graduate degree program in Geology and the Graduate Faculty of the University of Kansas in partial fulfillment of the requirements for the degree of Bachelor of Science.

Chair: Rick Devlin

Co-supervisor: Andreas Moeller

Co-supervisor: Douglas Walker

Date Approved: 11 May 2022

## Abstract

Currently, little is known about the exact timings of brittle deformation present in the Rocky Mountain Front Range. U-Pb carbonate dating via laser ablation is an emerging field that greatly broadens the potential to date deformation features, especially fault-hosted carbonate deposits. We have tested the feasibility of dating carbonate veins on samples from three different locations in the Cañon City embayment of the Rocky Mountain Front Range.

The results indicate that it is possible to date the carbonate veins crosscutting the Jurassic Morrison Fm. with low uncertainty, 110.4 ± 1.4 Ma, using this approach, which puts this in the timeframe of continuing sedimentation in the basin, prior to uplift of the Rocky Mountains. Fault-hosted carbonate veins in the Ordovician Harding Fm. yield scattered data interpreted as reflecting repeated precipitation of carbonate with the oldest event at ~100 Ma and the youngest between ~12 Ma and ~6 Ma. Ages range from early Cretaceous to Neogene and likely reflect the results of multiple fluid flow events associated with uplift in the area. Fluid events probably coincide with the different stages of uplift, which created the total current elevation (~2-3km) of the Colorado Plateau and Rocky Mountains. Major regional events include the flat slab subduction during the Laramide Orogeny and lithospheric delamination. However, the evidence of deformation occurring prior to the Laramide Orogeny poses new questions about the region. U-Pb carbonate dating using laser ablation - inductively coupled mass spectrometry (LA-ICP-MS) is highly applicable to the Front Range and future work will use this method to create a detailed deformation history of the area.


Keywords: Cañon City embayment, Rocky Mountain Front Range, laser ablation inductively coupled plasma mass spectrometry, geochronology, uranium lead dating of carbonate veins

# Acknowledgments

My sincere gratitude is given to my mentor and advisor Dr. Andreas Möller. This project would not have been possible without your guidance and expertise on the subject. Thank you for taking the time to provide constructive feedback on this paper and for your support with every step of this project. Your keen interest and dedication have helped push me to challenge myself and become a better student and person. I would also like to thank Dr. Douglas Walker and Dr. Rick Devlin for being committee members and taking the time to read this thesis and provide constructive feedback to improve it. Your unique insights and support have greatly enhanced my experience and benefitting knowledge as a result of working on this project. It is a pleasure to thank my partner Makenna Harris for her support and encouragement as I worked on this project. Thank you for engaging in many practice presentations and drafts. I also owe gratitude to my friends and family who supported me endlessly throughout this process.

Table of Contents

List of Figures

List of Tables

## Chapter 1: Introduction

Tectonic processes on Earth play a major role in the dynamics that dictate the shape and terrain of continents as they are seen today. As lithospheric plates collide and subduct, they create new topography on land by uplifting the continental crust, in this case, the Rocky Mountains were formed through a series of uplift events driven by these processes starting with the Laramide orogeny from 80 Ma to 40 Ma (e.g., Karlstrom et al., 2012). The occurrence of some brittle deformation features in the area likely coincides with the timings of this orogenic event. To determine if this is true, LA-ICP-MS U-Pb geochronology techniques were applied to a variety of fault-hosted carbonates and veins to establish the exact timings of these features.

Geochronology is a critical part of gaining a full understanding of geologic history, providing the absolute timing of events, including deformation. Creating a more detailed account of the deformation history in the Colorado Front Range was initially limited to the relation of tilted and untitled strata summarized in a review of the state-of-knowledge by Cather (2004). This study will explore the hypothesis that U-Pb carbonate dating of brittle deformation features (fractures, faults) via laser ablation can directly date discrete deformation events. This should contribute to a more detailed understanding of the formation of the Rocky Mountain front Range in general, and the complex geometry of the Canon City embayment in particular.

Carbonate-forming fluid flowing along fault surfaces has the potential to precipitate calcite while incorporating uranium. Therefore, fault-hosted calcite deposits and calcite growth associated with slip events, seen as slickenfibers, have the potential to be used to date brittle deformation events by the U-Pb method (e.g., Roberts and Walker, 2016). This study aims to test the feasibility of this method for dating brittle deformation in the Cañon city embayment region.

To do this, carbonate samples from joints/faults were collected from Cañon City, CO and processed into ca. 100µm thick polished sections to be analyzed by LA-ICP-MS.

The Front Range, for the purpose of this work, is defined as the southern part of the Rocky Mountains in the state of Colorado. The Cañon City embayment is in part bounded by the Dakota Sandstone Fm. which forms steeply dipping ridges around the city. Samples were selected from a variety of host rocks with the aim of testing each one's viability for dating. These include fault-hosted carbonates in the Ordovician Harding Fm and veins cross cutting the Jurassic Morrison Fm. Sample locations and overall research area can be seen in Figure 1.

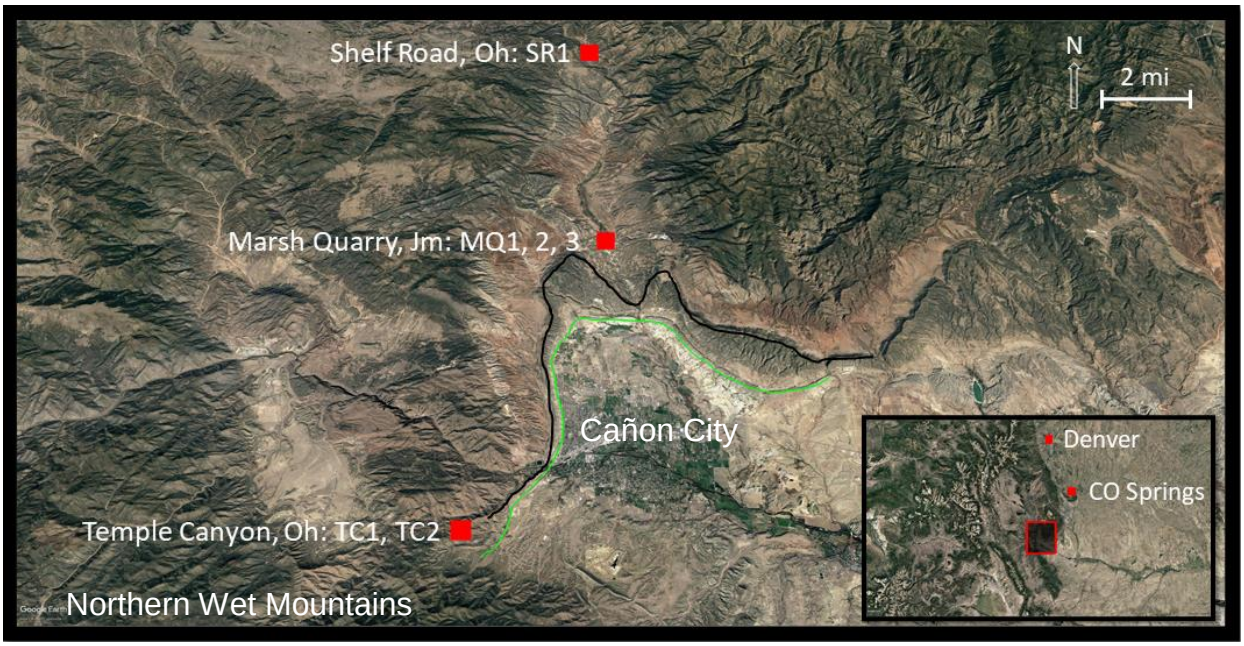


**Figure 1**. Google Earth satellite image map of the Cañon City Embayment, CO, and research area. Red squares indicate sample locations with accompanying labels including the location name and sample names. The embayment is outlined with the steeply dipping Dakota Fm. sandstone strata outlined in black. The upper extension of the city is outlined in green. To the southwest of the city is the Wet Mountains, shown here is the northern boundary of this feature labeled in white in the bottom left-hand corner. The smaller map in the inset provides an overview image of part of Colorado to place the research area in context with Denver and Colorado Springs. The research area is highlighted in red with a shaded area.

# Chapter 2: Geologic Setting

## Previous Work 2.1

Dating calcite ($CaCO_3$) and other carbonate minerals by U-Pb or U-series geochronology initially focused on speleothems (Woodhead et al. 2006, 2010, 2012, 2019) and pedogenic carbonates (e.g., Richards et al., 1998), which show the most promise in terms of capturing uranium during crystallization. Reviews of the approach by Rasbury & Cole (2009) and Roberts et al. (2020) shows speleothems to have the highest U and lowest Pb and thus the best characteristics for highly precise dates. Diagenetic carbonates and terrestrial veins on the other hand show a wide range of U and Pb concentrations and therefore potentially require a larger number of samples to be tested. Aside from the use on speleothems, the technique has been applied to many other geological systems to determine the age of deposition, diagenesis, ore deposits and fossils (Jahn and Cuvellier, 1994; Rasbury et al., 1997; Richards et al., 1998; Rasbury and Cole, 2009; Li et al., 2014; Roberts and Walker, 2016; Roberts et al., 2017; Roberts et al., 2020; Rasbury et al., 2021; Smeraglia et al., 2021). Initially, carbonate dating was conducted using chemical dissolution and isotope dissolution to be analyzed through thermal ionization mass spectrometry (TIMS) (e.g., Richards et al., 1998). More recent efforts utilize laser ablation ICP-MS techniques; Roberts et al. (2020) and Rasbury et al. (2021) summarize the state-of-the-art of LA-ICP-MS U-Pb carbonate dating and contribute novel ideas on the U-Pb systematics of carbonates.

Currently, there is no published information on the exact timing of brittle deformation features in the Cañon city embayment region. Work by Beaudoin et al. (2018) on the Bighorn Basin in Wyoming used U-Pb dating of calcite veins to examine the stress evolution of the area. Previous work by Erslev et al. (2004) has examined the minor faulting in the Colorado Front

Range and indicate that the majority of faulting in Cañon City Embayment is in the form of left and right-lateral strike slip faults with a minority of faults being thrust faults. There is also record of the orientation of faults that bound the Wet Mountains (surrounding the embayment on the south-west side) being dominantly northwest-striking thrust faults (Erslev et al., 2004). The Ilse fault system within the Wet Mountain arch exhibits similar attitudes as an interconnected series of faults. These systems propagate northward from the Wet Mountain arch to central CO. Overlying structure formations in the Cañon City Embayment are summarized in a review of faulting on the east side of the embayment by Marshall (1959). The synclinal formation of the embayment developed as a monocline during the upwarping of Cooper Mountain on the eastern side and down warping on the western side. The resulting tensional forces of the area then likely surpassed the limits of the tensile strength of the rocks, thus, creating the Fourmile Creek Thrust Fault and a system of tear faults. The new U-Pb carbonate geochronology work undertaken in this study plans to expand what is currently known about deformation and related fluid flow in the Rocky Mountain Front Range.

## Regional Stratigraphy 2.2

The regional stratigraphy of the Cañon City embayment is made up of Phanerozoic sedimentary strata overlying a basement of mainly Paleoproterozoic granitic gneisses, exposed to the west and north of the city (Fig. 1). Descriptions of the regional strata here stem from field observations made at different sites including Twin Mountain, Temple Canyon, Marsh Quarry, and a log created while measuring bed thickness at Shelf Road. This study focuses on three main sites; Shelf Road, Marsh Quarry and Temple Canyon, (Figure 1) therefore, descriptions will be focused on exposures at these locations.

Outcrops along Shelf Road expose highly weathered basement directly below the contact that represents the Great Unconformity. Above the basement lies the Ordovician Manitou Fm. (Om) made up deep red carbonate limestone interbedded with greyish-whitish chert layers, it typically weathers as blocky and rounded outcrops and is a cliff-former. Resistant interbeds of chert protrude out of the outcrop face on the cm-scale. Overlying this is the Ordovician Harding Fm. (Oh) pertinent to this study as 2 of the samples were in the Harding Fm. The Harding Fm consists of three main packages with of interbedded sandstone with varying color and thickness ranging from red to white to yellow. The Ordovician Fremont Fm. (Of) overall is a greyish dolomitic limestone. While the lower Fremont Fm. is tan and contains fossil hash, the middle Fremont Fm. is tan to white and interbedded with chert nodules, typically smoother in texture than the lower Fremont Fm. Exposures at Shelf Rd outcrops of the upper Fremont Fm. show autobrecciation with carbonate subangular clasts on the centimeter to decimeter scale in a fine-grained red stained carbonate matrix. Williams Canyon Fm tops this but no observations of it were made during this study. This is overlain by the Pennsylvanian/Permian Fountain Fm (Pf), a deep red sandstone conglomerate sequence with rounded quartzite clasts on the centimeter scale. Above this is the Jurassic Morrison Fm (Jm) with thick layers of silt and shale exhibiting colors ranging from grey to green to red. The Dakota Sandstone Fm that outlines the Canon City Embayment overlies the Morrison Fm and is made up of tan sandstone (Figure 1). A stratigraphic column representing the relative thickness and weather profiles for the local stratigraphy is shown in Figure 2 below.

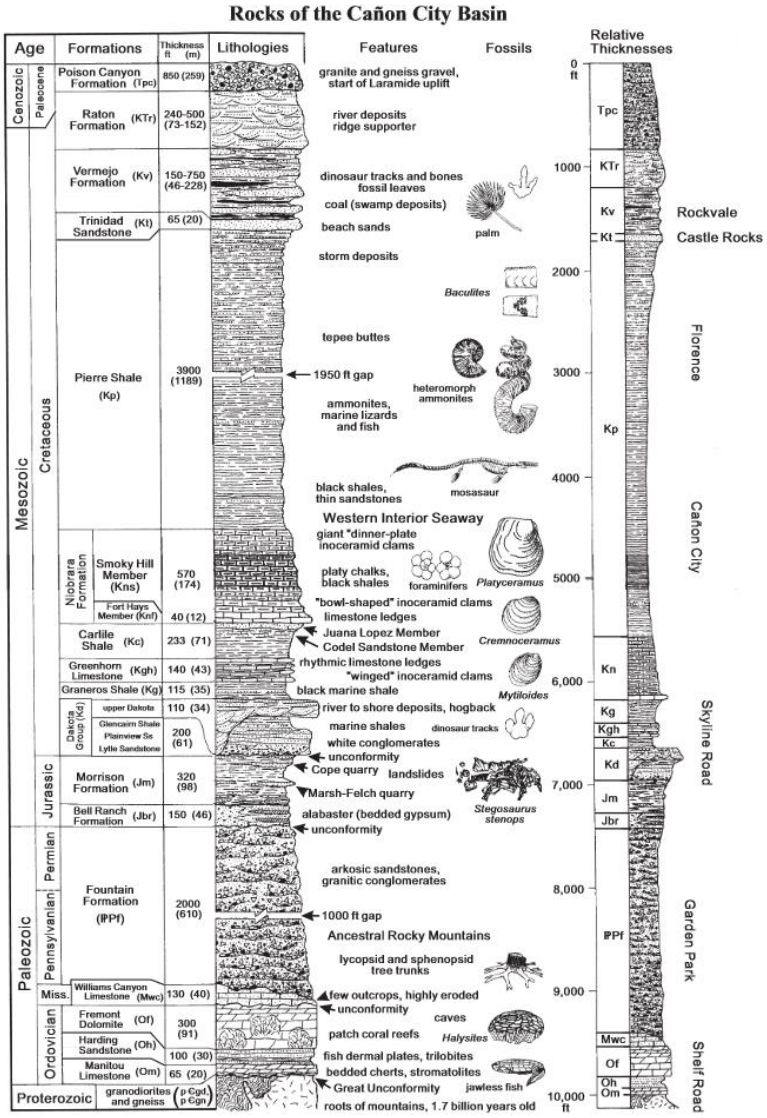


**Figure 2.** Stratigraphic column showing the stratigraphy of Cañon City including the weathering pattern of the outcrops, texture, fossil composition, relative thickness, age, and unconformities from the area. Note that in this study units above the Morrison Fm were not examined. Figure originally created by Evanoff, (1996) and modified in 2006 by the Royal Gorge Region organization.

Certain stratigraphic layers are not visible in the research areas (Temple canyon, Marsh Quarry, and Shelf Rd) or were not identifiable in the field, this includes the Bell Ranch Fm which should be between the Fountain Fm. and the Morrison Fm. It is also noteworthy that, while outside the scope of this work, the Cretaceous Pierre Shale Fm is an important unit in the

stratigraphy of the area as it provides fundamental timings of uplift and basin formation (Cather, 2004).

## Geologic History 2.3

The Colorado Plateau and Rocky Mountains, which are at an average elevation of ca. 2 km and ca. 3.2 km respectively, reflect multiple periods of uplift (e.g., Aslan et al. 2010; Karlstrom et al., 2012). The underlying causes of uplift are a subject of debate, different hypotheses are summarized by Heitmann et al. (2021). To reiterate the review by Heitmann et al. (2021), suggested causes of uplift include lower-crustal flow, removal of the Farallon slab during the Laramide orogeny, lithospheric foundering, hydration during the mid-Cenozoic and mantle upwelling, or as an isostatic response from denudation during the late Cenozoic. The Laramide orogeny occurred during the time frame of approximately 70 Ma to 40 Ma (e.g., Karlstrom et al., 2012), some studies propose that impacts of the Laramide orogeny were exhibited earlier, closer to 100 Ma, west of the Rocky Mountain belt (e.g., Carrapa et al., 2019). Synorogenic deposition and tilting is documented by Jacob and Albertus, (1985) who examined several angular unconformities in the region that supported the conclusion Laramide thrusting and deformation initiated in the late Cretaceous to early Paleocene. Constraints on Laramide timing were based on the synchronous deposition of sediments on the flanks of the Front Range during the Cretaceous (e.g., Erslev et al., 2004, 2006).

During the time frame 70-40 Ma, the low angle of subduction was the main cause for uplift while also hydrating and removing parts of the lithospheric base underlying the area (Karlstrom et al., 2012). Hernández-Uribe and Palin, (2019) state that the shear-removal of the subcontinental lithospheric mantle was as much as ca. 80 km which caused asthenospheric upwelling and isostatic rebound during this period.

Examinations of paleo-elevation proxies conclude that the region reached half its current elevation at the end of the Laramide and achieved its current elevation by 16 million years before the present (Heitman et al., 2021). Post Laramide uplift occurred during the period of 35 Ma to 25 Ma as an ignimbrite flare-up[1] occurred resulting from the fragmentation of the Farallon slab (Karlstrom et al., 2022). From 20 Ma to the present, the ignimbrite flare-up stopped, and the region experienced basaltic volcanism occurring along with extensional strain (Karlstrom et al., 2022). See Figure 3 below for a visual summary of this process from Karlstrom et al. (2022).

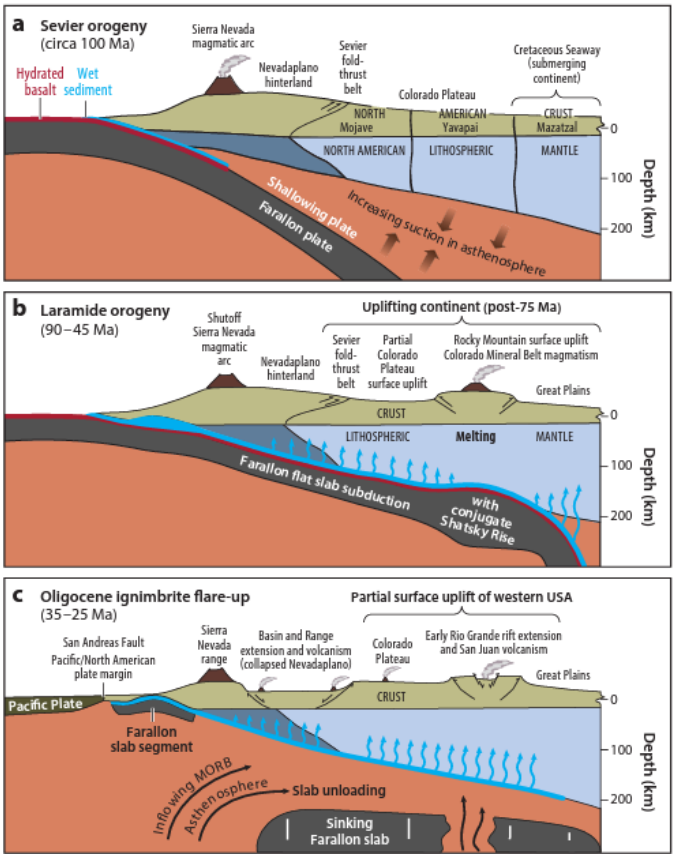


**Figure 3**. Visual interpretation of the different series of uplift processes that contributed to the modern elevation of the Rocky Mountains and Colorado Plateau, figure from Karlstrom et al. 2022.

[1] A type of arc volcanism that occurs following slab removal of the subducting slab underneath a thick crust, that is separate from arc volcanism in proximity of the trench (Karlstrom et al., 2022).

Several studies suggest significant portions of uplift are much younger, occurring at ca. 10 Ma. This is evident by the incision rates of the Colorado River that became much more rapid around this time (e.g., Aslan et al. 2010). Karlstrom et al. (2012) suggest that uplift <10 Ma makes up 25 to 50 % of uplift after the late Cretaceous exhibited in the Colorado Plateau and Rocky Mountains. Evidence from a technique using the vesicles in vesicular basalts indicate that there was slower uplift between the period of 25 Ma and 5 Ma (ca. 40 m/m.y. i.e., meters per million years) after which there was an onset of rapid uplift ca. 220 m/m.y. (Sahagian et al., 2002). This study aims to correlate the results of U-Pb dating of carbonates with hypothetical forces and timings of deformation/uplift in the region.

# Chapter 3: Methods

## Field Methods 3.1

Samples for this study were collected during field camp, a 6-week capstone course at the University of Kansas with the aim of introducing and teaching students how to conduct field work and map geologic structures. While visiting different areas including Marsh Quarry, Temple Canyon and Shelf Road, carbonate samples were collected along fault surfaces, which were identified in the field. Carbonates are abundant in the Earth's crust across all regions and can form from fluid flows with signature element ratios (Rasbury et al., 2021). Calcite ($CaCO_3$) and other carbonate minerals such as dolomite, aragonite, and magnesite etc. can form in many geologic settings. These environments include diagenetic, biogenetic, igneous, metamorphic, and hydrothermal environments (Roberts et al., 2020). Because calcite has the potential to incorporate uranium when it crystalizes, it also has the potential to be a useful chronometer for U-Pb and U-Th (Roberts et al., 2020).

Samples were collected from the Shelf Road area, Marsh Quarry, and the Temple Canyon area. Samples SR1 and SR2 from Shelf Road which is north of Cañon City were taken from fault surfaces in the Harding Fm (Oh) along the roadside. From Marsh Quarry carbonate samples MQ3, MQ2, and MQ1 were taken along fault planes in the Jurassic Morrison Fm (Jm). In the Temple Canyon area samples TC1 and TC2 were taken from the Harding Fm (Oh). The sample location and research area are shown in Figure 1. Faults in the Harding Fm were clearly visible by the slickensides and striations along the fault surfaces, due to the offsets being more visible because of the unit's high level of competency. Fault surface orientations could not be tracked in situ within the Morrison Fm, due to the weathered exposures of the host rock. Samples were collected from ground material and loose specimens in outcrops near the Marsh Quarry.

***Shelf Road (SR1, SR2)***

While measuring the stratigraphic section along the outcrop exposed at Shelf Road, a fault surface was identified along the roadside. Here, slickenlines marked by striations along the fault surface were present in the form of carbonate precipitate. This precipitate was collected from the fault surface and put into a sample bag, the orientation of the fault and sample were recorded via field images and a measured attitude (Figure 4Figure 5,Figure **6**).

**Figure 4**. Outcrop image from Shelf Road of the fault surface with accompanying carbonate precipitates, example outlined in red. Fault surface is within the Harding Fm., an 11 cm long pocketknife is shown for scale.

**Figure 5**. Overview image of the fault surface in the Harding Fm. along Shelf Road, note the pocketknife for scale. There is no apparent vertical offset on the fault, it is likely a sinistral strike-slip fault.


**Figure 6**. Image of the measured attitude of the fault striking NW and dipping relatively steeply at 75 degrees. Measurement was collected using a digital Brunton on a smartphone.

***Marsh Quarry (MQ1, MQ2, MQ3)***

During a hike along the Marsh Quarry area public trail, just north of Cañon City, pink and white carbonate pieces were found on the ground and in the outcrop. These samples exhibited striations; slickenfibers that were indicative of a fault surface. A scratch test and hydrochloric acid, that produced strong fizzing, was used to identify the material as carbonate. Layers of carbonate veins are present in the silty layers of the Morrison Fm. with thicknesses from a few mm to ca. 3 cm. Samples were collected from the outcrop and bagged up to be processed in the lab. Outcrop and sample images can be seen below (Figure 7Figure 8Figure 9).

**Figure 7**. Outcrop image along the Marsh Quarry trail showing weathered surface of the Morrison Fm, carbonate vein is present as broken up pink layer. Note the rhombohedral shape of the fracturing. Quarter for scale.

**Figure 8.** Second outcrop image from along the Marsh Quarry trail showing exposures of the Morrison Fm shales and siltstones. The carbonate vein is a darker shade of pink and slightly thinner (ca. 2 mm) than the one in Fig. 7. Quarter for scale.

**Figure 9**. Sample image of a broken off fault surface with evident striations on the surface of the carbonate vein. Note that the color of the carbonate is different across the surface ranging from dark pink to light pink to white, with evidence for the pink, younger, carbonate overgrowing the white, older, carbonate material. Quarter for scale.

***Temple Canyon (TC1, TC2)***

At the Temple Canyon site, southwest of Cañon City, there is a fault surface in the upper to middle Harding Fm. that shows slickensides. The slickensides consist of a white carbonate precipitate along the fault surface. The strike of the fault is roughly northwest with a high angle of dip to the southeast. A sledgehammer was used to break off a chunk of the sample, labeled TC1. A second sample (TC2) was collected using the same methods, from a highly brecciated, conglomeratic outcrop of the lowermost Harding Fm (Figure 10,Figure **11**).

**Figure 10**. Field image of the fault surface at Temple Canyon where sample TC1 was collected where the blue pen is resting. Carbonate precipitate is visible as the smooth white surface in the image above.

**Figure 11.** Field image of a second fault surface in the Temple Canyon area found in the lowermost Harding Fm. where sample TC2 was collected. Blue pen for scale. Note the grey color of the sandstone and angular clasts of quartz visible in the image.

Lab Methods 3.2

***Sample Preparation***

After the samples were collected in the field, they were brought back to the isotope geochemistry laboratories at the University of Kansas where they were broken into smaller pieces to be made into polished thick sections. Samples were labeled and a line was drawn on their surfaces to orientate broken parts to the original body of the sample. Once the samples were broken down, they were cleaned in deionized water in an ultrasonic bath to remove any surface dust and debris that might contaminate the isotopic results in the mass spectrometer (see Figure 12). Samples from Marsh Quarry were sorted based on color, with 3 distinct variations. Two of each were collected, this included two white samples with relatively thicker fiber growths, two pink samples with medium thickness, and two dark pink samples that were thinner (ca. 2-3 mm). These samples were named MQ3, MQ2 and MQ1 respectively (the two specimens for each type were labeled, e.g., MQ3-1 and MQ3-2). Afterwards, Marsh Quarry and Shelf Road samples were processed into thick sections by KU Geology technician Pike Holman after first embedding them in 1-inch blue epoxy discs. Samples TC1 and TC2 were processed by Holman into thick sections after having the pore space filled in with epoxy.

**Figure 12.** Processed and cleaned samples from Marsh Quarry trail are visible in the center petri dish (??cm diameter), note the variations in color ranging from white, pink, and dark pink. In the upper dish contains the processed samples from Shelf Road.

Polished thick sections (ca. 100µm) of each processed sample underwent petrographic and fluorescence analysis to determine the structural patterns and composition. Each sample was orientated such that the epoxy puck was cut perpendicular to the vein i.e., into the veins structure rather than along its surface. This meant all crystal fibers are visible to allow ablation across the width of the fault, and thereby detect potential age differences between episodes of mineral growth. Mechanisms for this growth likely evolve from the opening of fractures and space accommodation as the fracture widens. Samples were analyzed for microstructures such as fracturing and orientation of mineral growths, which could give clues to the overall orientation of the brittle deformation. Petrographic analysis was conducted using a microscope and imaged via microscope camera system (Figure 13,Figure **14**,Figure **15**,Figure **16**,Figure **17**,Figure **18**).

The composition of samples from the Marsh Quarry are dominantly calcite ($CaCO_3$) with no discernable mineral variations (Figure 14,Figure **15**,Figure **16**,Figure **17**). Note the high order birefringence indicative of carbonate in the figures. The orientation of fibers and structures varied between samples which had a direct influence on the choice of traversal. To obtain a date that is most representative of the age of the entire specimen, traversals were set to cross individual fibers. MQ1 exhibits a fibrous growth pattern that extends in the direction of the center vein and has perfect cleavage at 95/85º (Fig. Figure **14**). MQ2 samples were similar but there is a distinct change in fiber orientation in MQ2-2 while MQ2-1 remains the same although fibers appear to bend towards the center vein (Fig.**Figure 15**). 2 different traversals were created for MQ2-2, 1 traversal per 2 sessions of sample ablation, to see if there was a spatial correlation in terms of uranium concentration. Note the shearing fractures across the specimen MQ2-1 in figure Figure **15**. MQ3-2 exhibited the same shearing fractures across the fibrous growth pattern

(Fig.Figure **17**). MQ3-1 shows much larger fibrous growths (ca. ≥130µm) with very little fracturing.

Specimens from Shelf Road contain visible white carbonate layers with varying thicknesses (ca. <140µm) that were the targets of traversals (Fig.**Figure 18**). The main body of SR1 and SR2 is a complex of an ultra-fine-grained quartz and presumed carbonate cement. Some round growths of carbonate are visible in the main body of each specimen, these growths were large enough in some cases to fit a single 130µm circular spot into them. Samples from Temple Canyon (TC1 & TC2) are chiefly made up of large, and highly fractured rounded quartz clasts on the millimeter scale cemented with carbonate seen as black material in figure 13. Ablation was not possible in this case due to the fineness of the carbonate cement.

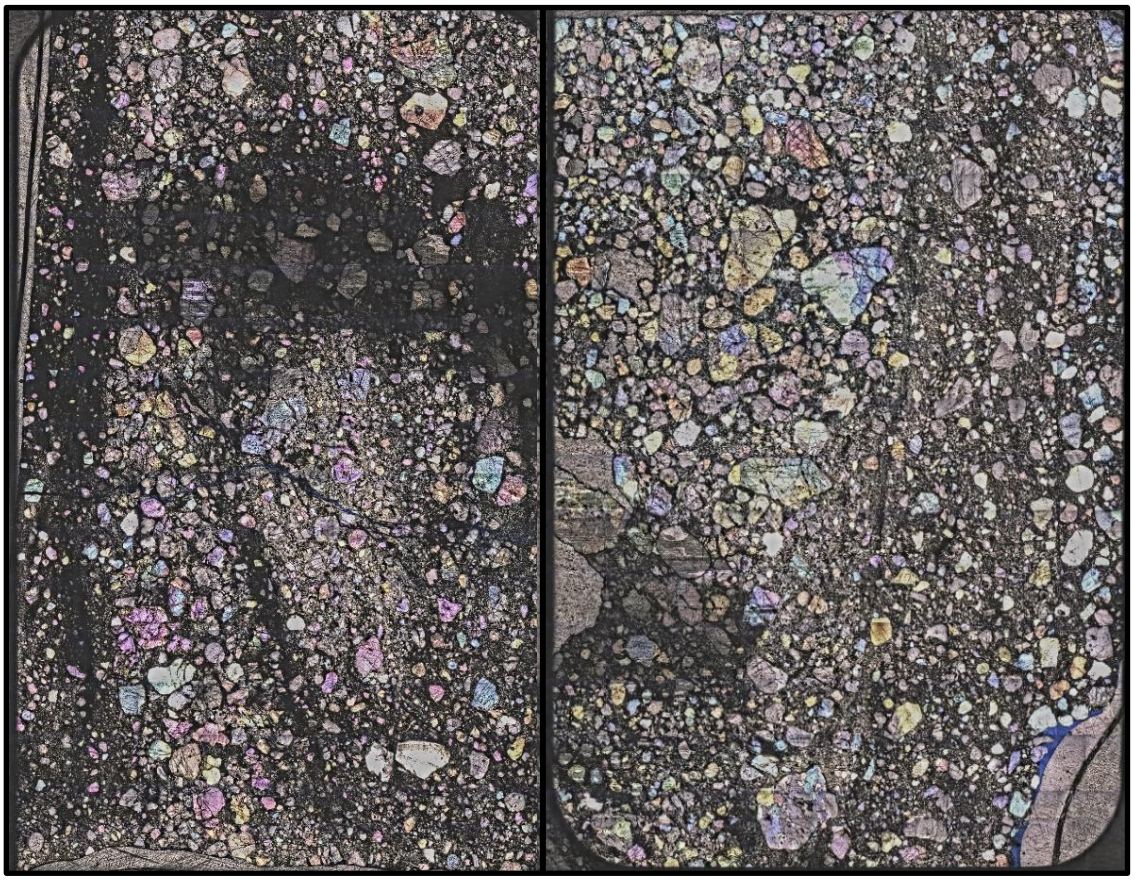

**Figure 13**. Two microscope images of TC1. left is the upper portion of TC1 and on the right is the lower portion of the same sample. Image created from mosaic function in Chromium 2.1 after inserting the samples into the laser for

analysis. Large, rounded grains are quartz, they are heavily fractured and vary in size from 200um to <30um. The black in the thick section is where the highest concentration of carbonate cement is present. On the left of both thick sections represents the fault surface where the carbonate was precipitated.

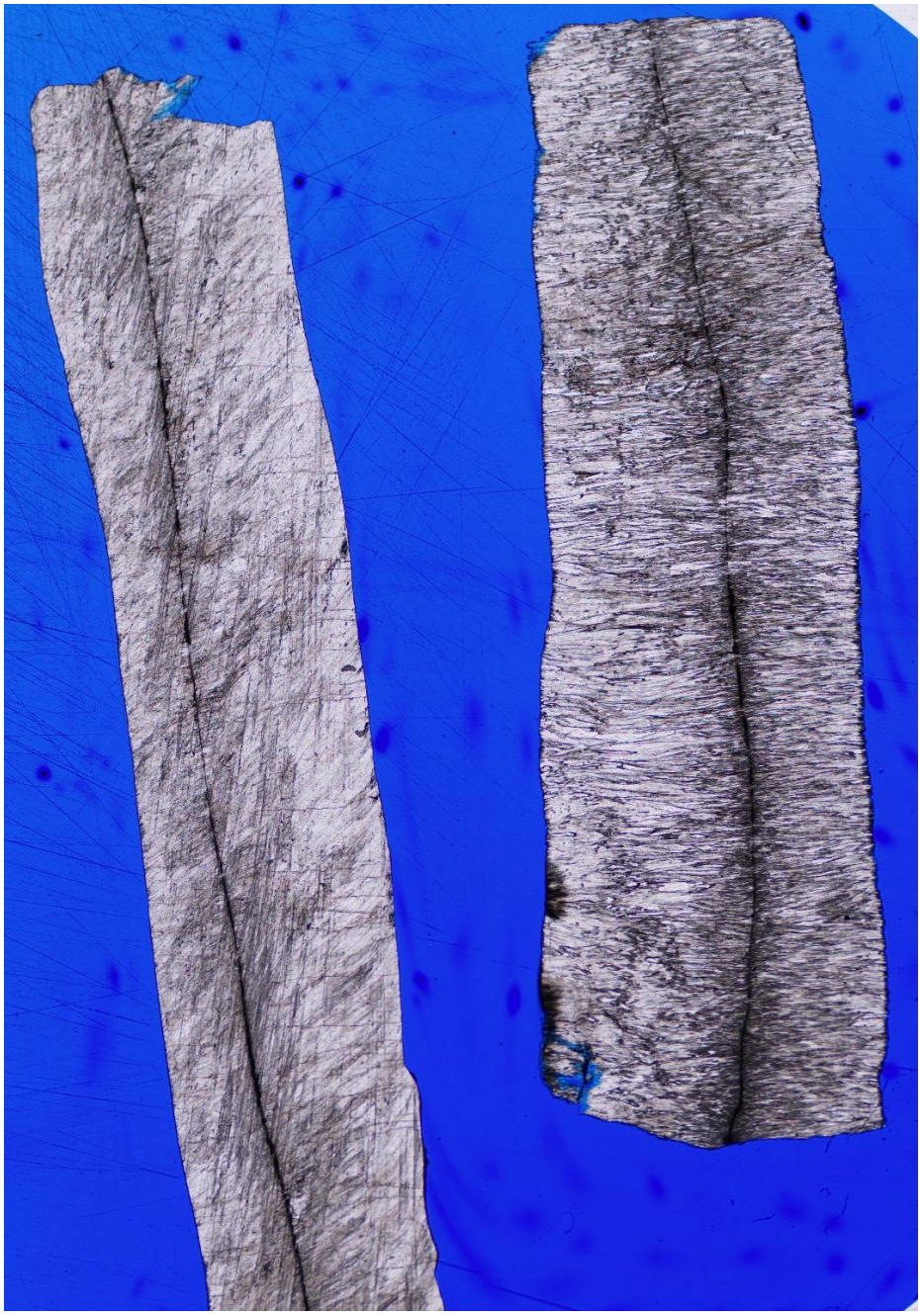

**Figure 14**. Plain polarized light image of sample MQ1, the sample distinguished by its dark pink color. Note the fibrous growth pattern which extends towards a center vein. Cleavage is perfect at 95/85º. Sample exhibits high order birefringence indicative of carbonates. On left is sample MQ1-1 and on the right is sample MQ1-2. Center vein is parallel to the orientation of the fault plane.

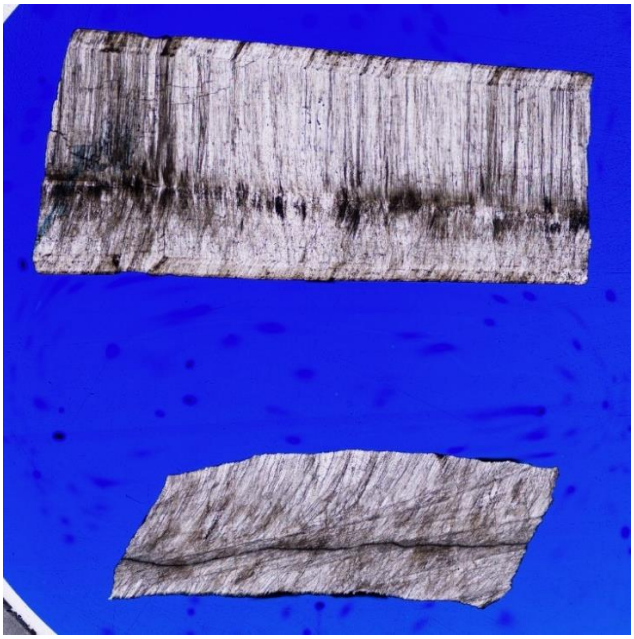

**Figure 15.** Sample images (PPL) for MQ2 with the medium pink color. Upper piece of the sample (MQ2-2) exhibits fiber growths perpendicular to center vein until reaching the outer edges where there is a clear difference in orientation. The outer layers of fibers represent presumably the earliest growths of carbonate. Lower sample (MQ2-1) has shearing fractures across prior fiber orientation. Center vein grows parallel to the orientation of the fault plane.

**Figure 16.** Plain polarized light image of sample MQ3-2, it possesses the same shearing fractures across its structure and fiber growths in the direction of the center of the vein. This was the whitest hand sample. Center vein grows parallel to the orientation of the fault plane.

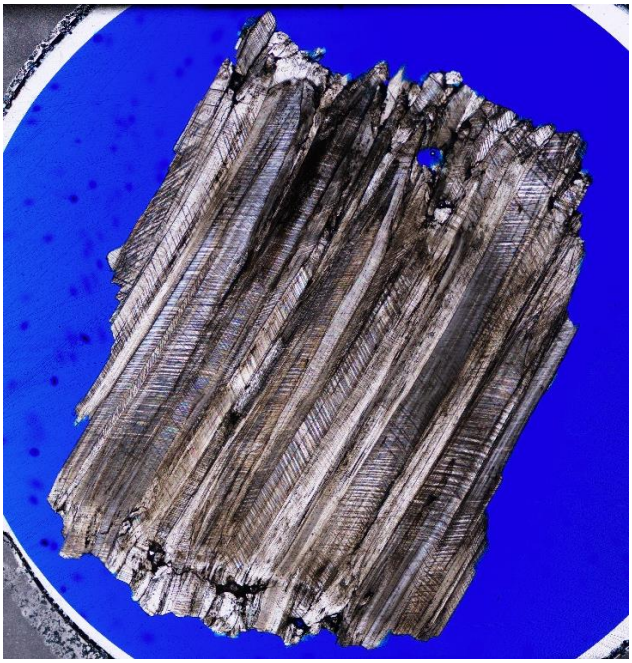

**Figure 17.** Plain polarized light image of MQ3-1 which is one of the white samples but with the largest grain size. Fibers are wider than 130µm and orientated without a center vein unlike the other samples. Towards the edges of the sample are different growth orientations for the fibers similar to observations in sample MQ2-2 (Figure 15). Fibers grow perpendicular to fault plane.

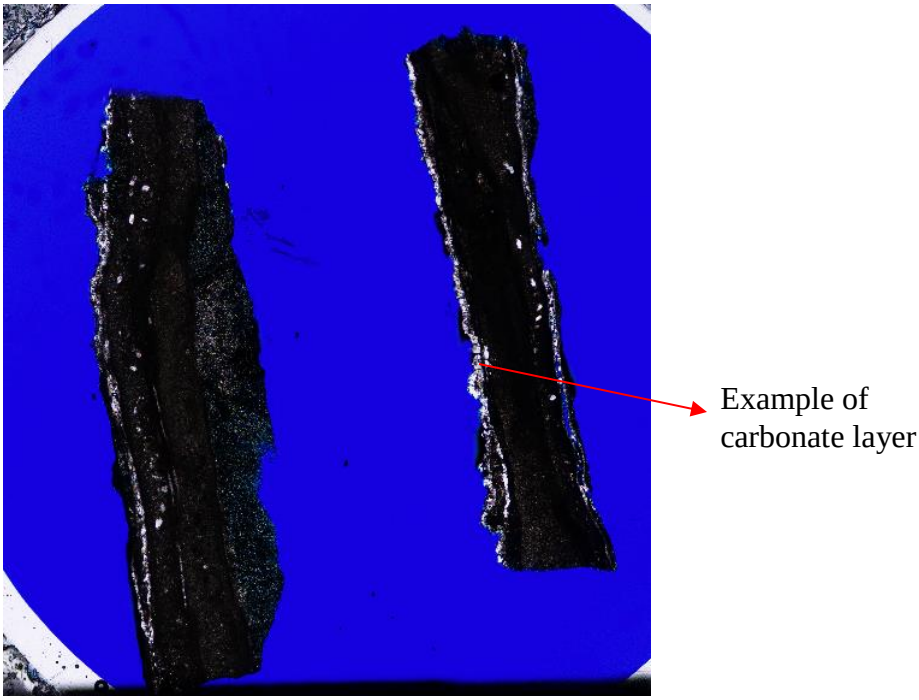


**Figure 18.** Plain polarized light image of SR1, the center of the sample is mainly very fine grained quartz while the carbonate comprises the white layers seen on the edges of the sample and smaller spots throughout the body of it. Carbonate layers are parallel to fault plane.

***LA-ICP-MS U-Pb Methodology***

U-Pb geochronology was used in attempts to determine the age of each sample. U-Pb isotopes were determined in polished, approximately 100 µm thick sections and the unpolished surfaces on samples from Temple Canyon and Shelf Road. Isotope ratios were obtained from the carbonate veins using laser-ablation induced coupled plasma mass spectrometry *(*LA-ICP-MS*)* in the isotope geochemistry labs at the University of Kansas. The instrument used for this experiment was a Photon Machines Analyte.G2 193nm excimer laser and Thermo Scientific Element2 mass spectrometer. The correction of Pb-Pb ratios was done using a standard NIST614 glass by creating a sequence of standard-sample bracketing in the task file. Reference material DBTL (Hill et al. 2016) was used to correct the U-Pb fractionation, and this calibration was checked for accuracy supported using the WC1 reference material (Roberts et al., 2017). Standard laser ablation parameters were used for the carbonate samples with a fluence of 2.7 J/cm^-2, and a 130 µm circular spot ablated for 30 seconds at 10 Hz. Carrier gases included the use of He (1.01 l/min) and Ar (1.1 l/min). The program Chromium 2.4 was used to place spots on each sample and create a standard task file to gather the data. Data were processed using IOLITE 2.5 (Paton et al. 2010, 2011) including editing of outliers. Concordia plots and age calculations were produced in IsoplotR (Vermeesch, 2018).

The unpolished surface samples underwent the same procedures, however, it required additional work to put in a sample mount and adjust the focus on the z-axis to properly ablate its more irregular surface. The SR_Surf sample was broken off from the same carbonate sample that produced SR1-2 and the TC_Surf sample was taken from TC2 along the edge where the thickest carbonate cement was visible. These samples were placed in a sample mount and held in place using museum wax, see Figure 19 below.

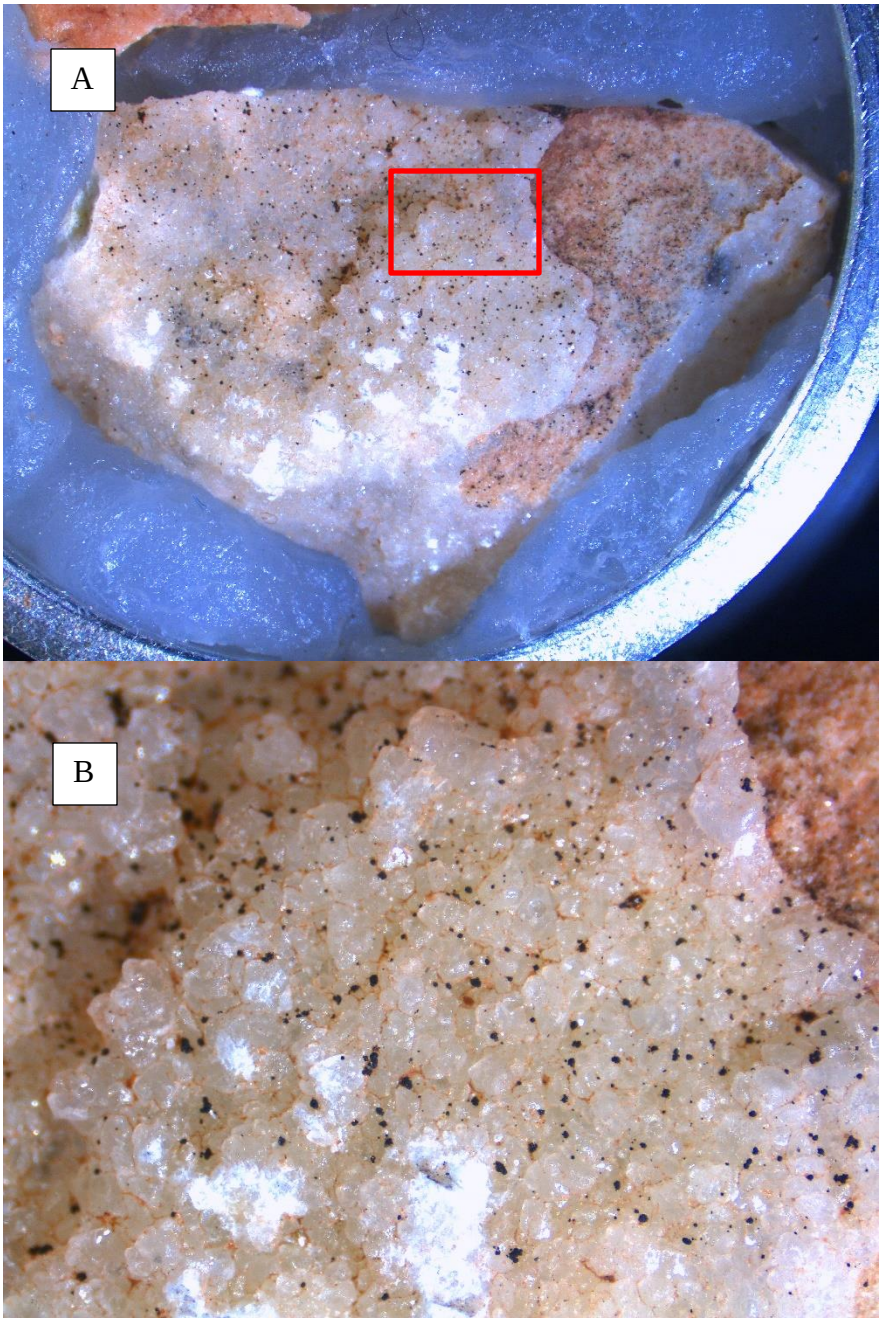


**Figure 19**. These images serve as an example for what the unpolished surface samples looked like after being prepared for ablation. A.) Image of SR_Surf in the sample mount held in place with museum wax, note the euhedral calcite crystals on its surface. B.) Close up of the space outlined in red on image A, the surface of the euhedral calcite is more evident, this is where ablation was targeted for this sample.

# Chapter 4: Results

## LA-ICP-MS U-Pb

LA-ICP-MS data produced from 2 sessions across 12 samples gave varying results, with some samples successfully producing dates with low uncertainties (ca. 1.5%) while others lacked sufficient radiogenic Pb to calculate a date. Sample ablation occurred successfully with all samples except for some portions of the surface samples where the relief of the unpolished surfaces made it too difficult to focus.

### *Marsh Quarry Samples (MQ1, MQ2, MQ3)*

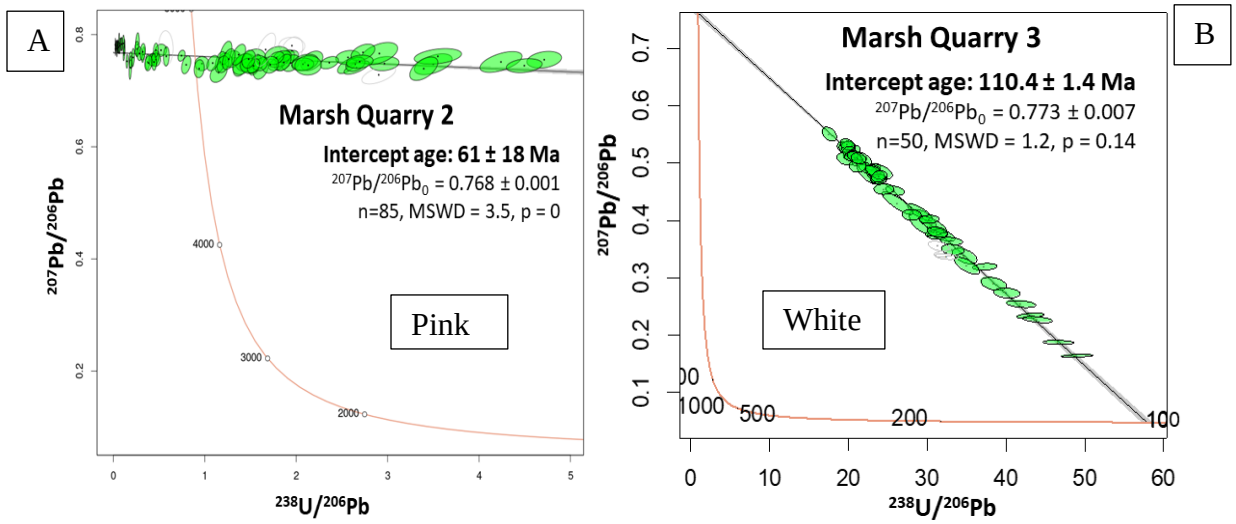


**Figure 20.** TW-concordia diagrams for U-Pb carbonate dating of brittle deformation features in the Cañon City embayment. **A:** limited spread in U-Pb gives an imprecise Laramide age for vein MQ2-2, consistent with field evidence (Figure 9). **B:** precise age for MQ3 coinciding with basin formation and sedimentation. Diagrams created using IsoplotR (Vermeesch, P., 2018).

Sample MQ3-1, white vein carbonate from the Jurassic Morrison Fm. produced an intercept date of **110.4 ± 1.4 Ma** for over 50 data points (Figure 20). The traverse across the sample using 130 µm ablation spots is shown in Figure 21. Overall, the sample showed no spatial correlation with regards to U and Pb distribution (Table 8).

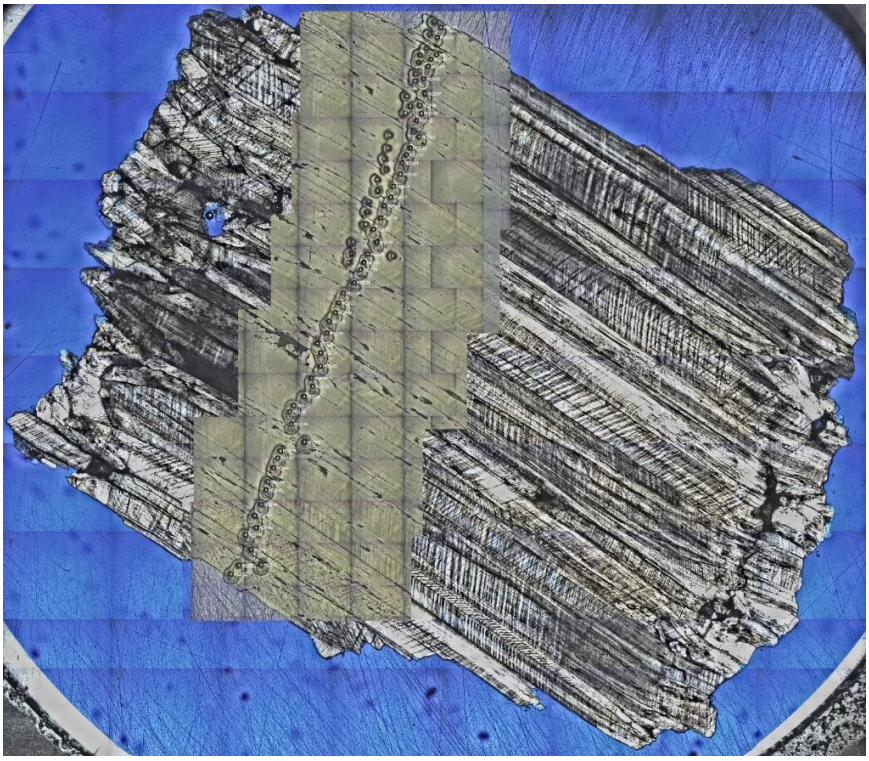

**Figure 21.** Laser ablation traverse along sample MQ3 from the Morrison Fm., across the carbonate fibers. The reflected light photo mosaic is overlain onto of a polarized transmitted light image of the sample. Note the larger fibers >150 µm in most cases, diameter of individual laser spots is 130 µm.

The sample MQ2-2 produced an age of 61 ± 18 Ma from 85 data points. In this case the first analytical session (not shown) found that U concentrations were too low along the center where fibers grew perpendicular to the central part of the vein. A new traverse in a second analytical session was done along the edges of the vein where there is a notable variation in fiber orientation and U concentrations were slightly higher, high enough to obtain a date, although with high uncertainty (ca. 30%), see Figure 20. A reflected light photo mosaic of this traverse can be seen below in Figure 22. Samples MQ3-2, MQ2-1, MQ1-1, and MQ1-2 did not contain enough traces of U to produce a meaningful date (Table 4, Table **5**, Table **6**, Table **9**).

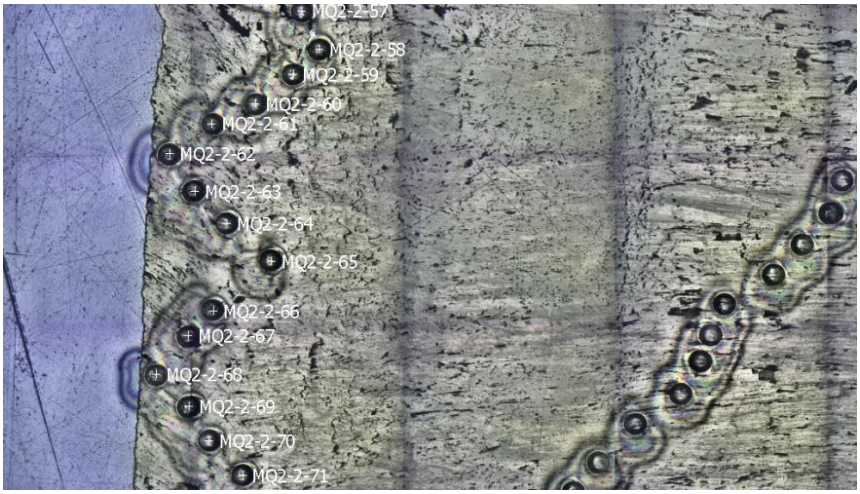


**Figure 22.** Portion of sample MQ2-2 shown in reflected light. Note that only some of the traverse is shown here. Higher concentrations of U were found along the vein edges where fibers were orientated at an angle to the center of the sample. A zig-zag traverse path was analyzed on both sides of the vein to obtain as much data of this area as possible. An example of this pattern can be seen on the left (spots 57 through 71 are visible).

### *Shelf Road Samples (SR1, SR2)*

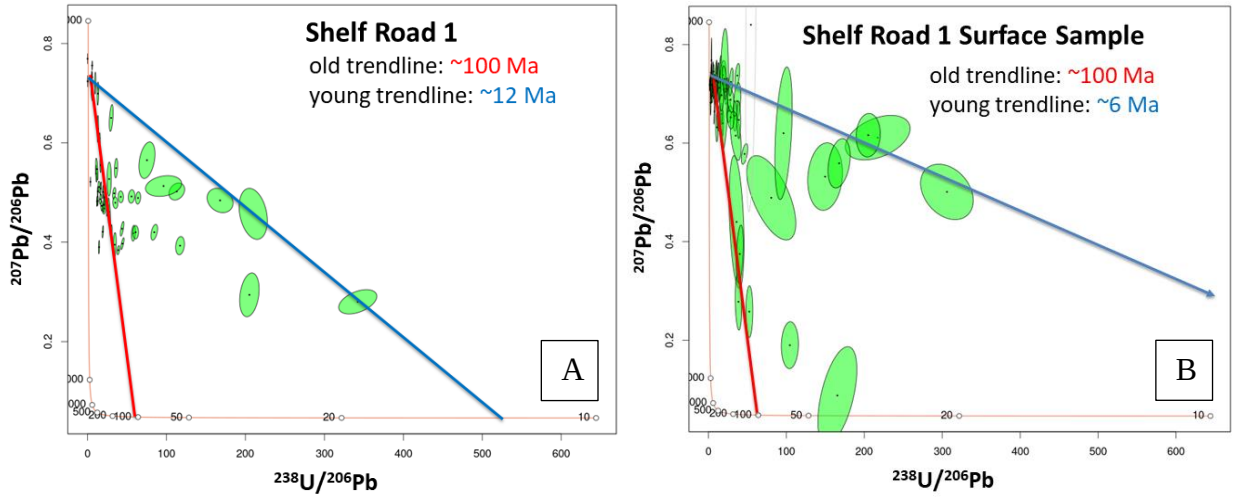


**Figure 23.** TW-concordia diagrams for U-Pb carbonate dating of brittle deformation features in the Cañon City embayment. **A:** Scattered U-Pb data of SR1 indicates different events between >100 Ma and 12 Ma. **B:** surface analyses of SR sample yield a similar range to SR1, but youngest array indicates a ca. 6 Ma event. Diagrams created using IsoplotR (Vermeesch, P., 2018).

The samples from the Ordovician Harding Fm. along Shelf Road exhibited scattered data within each sample. As shown in the TW-concordia diagrams (Figure 23 A, B) two data trends can be interpreted from the scattered data. A trend delineating a maximum date, and a trend that defines a minimum date. Due to the scattered nature of the data for these samples there is no

single trend that fits all data. Instead, trends were estimated, and these are shown in the TW-Concordia plots for SR1-2 and the SR_Surf samples (Fig. 23A, B). For both samples it is estimated that there are 2 projectable dates, the maximum at approximately 100 Ma, similar to the date obtained from MQ3-1, and the minimum either 6 Ma or 12 Ma, see Figure 23 A, B. No spatial correlation was found with regards to spot location and the estimated age group that the spots fell under. An example of the ablated spots from SR_Surf can be seen below in Figure 24 where the difference in relief is obvious and ablation pit depths vary.

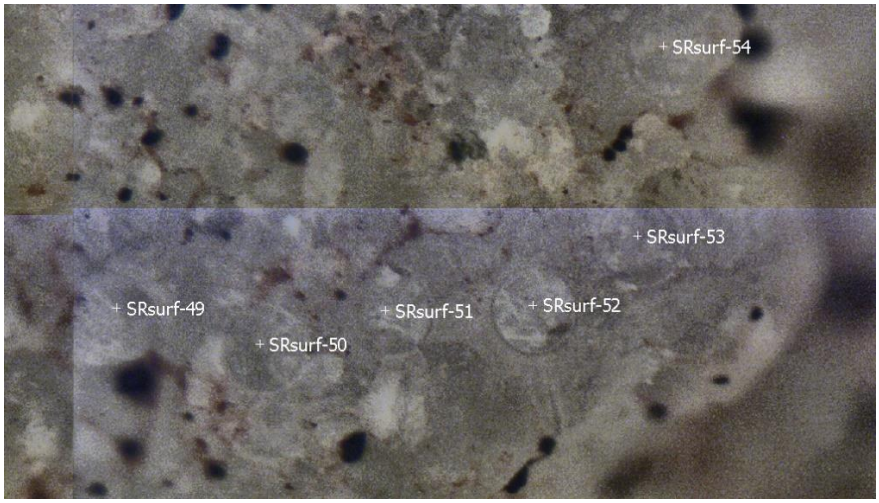


**Figure 24.** Image of the ablated surface from sample SR_Surf in a transmitted light microscopic view. Spots 49 through 54 are visible in this case to indicate the difference in relief seen by the varying levels of focus. The degree of ablation seems most complete in spot 52 but others appear too not have been fully ablated.

### *Temple Canyon Samples (TC1, TC2)*

Results from the carbonate vein samples from the Ordovician Harding Fm. at Temple Canyon were least successful of the three locations. The carbonate cement from each sample proved to be too fine grained to ablate, and the 130 µm ablation spots overlapped onto quartz grains from the sandstone. In most cases when a spot was ablated the sample would shatter at a microscopic scale and grains would break away. A new sample preparation method must be explored to ablate material where the carbonate cement is not very coarse. An example of the kind of data produced from the Temple Canyon samples can be seen below (**Figure 25**).

Additionally, an example of the surface of this fine-grained carbonate cement is visible in **Figure 26**.

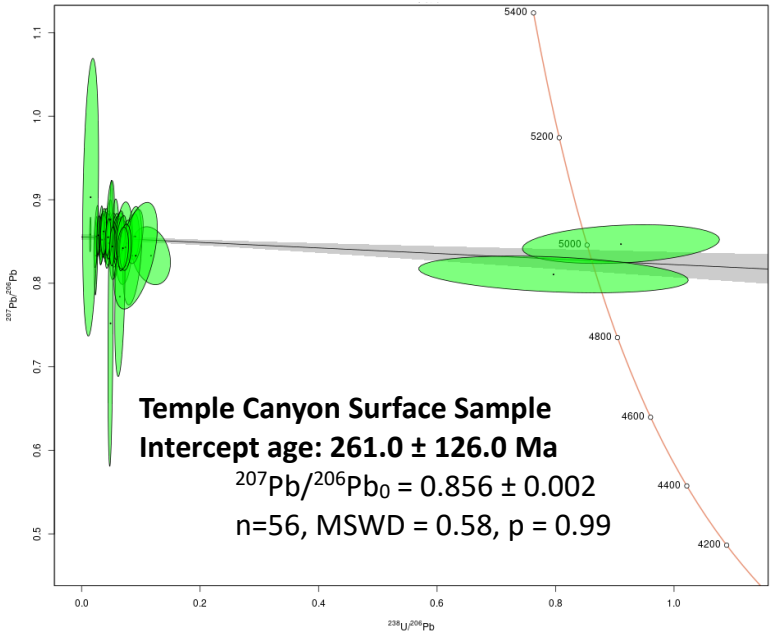


**Figure 25.** TW-Concordia plot from the TC_surf sample from the Ordovician Harding Fm at the Temple Canyon site. Uranium concentrations were too low to produce a meaningful date with a low uncertainty. Diagram created with IsoplotR (Vermeesch, P., 2018).

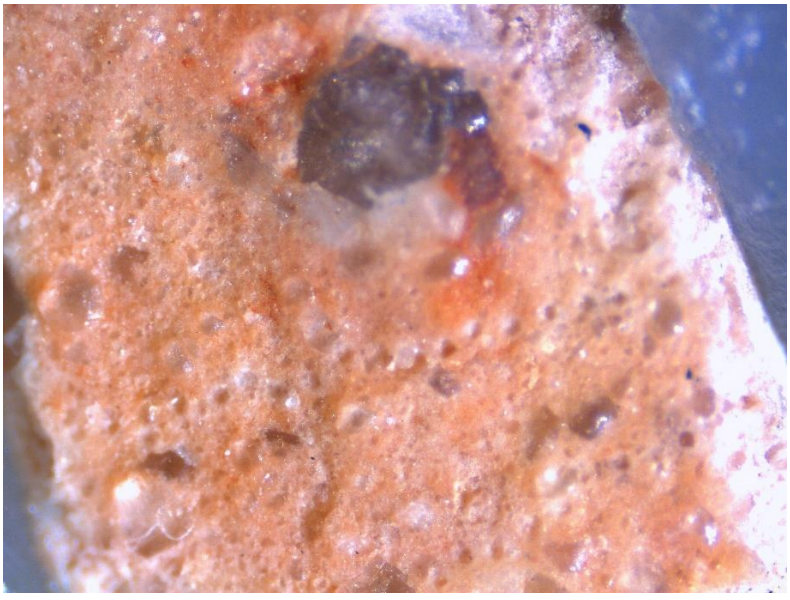

**Figure 26.** Example image from a binocular microscope of the surface ablation on TC_surf, the reddish pink matterial represents the extremely fine grained carbonate precipitate along a fault surface. The ablated pits have 130 µm diameter for scale and are visible as small craters on the sample surface.

***Parameters and Reference Material Data***

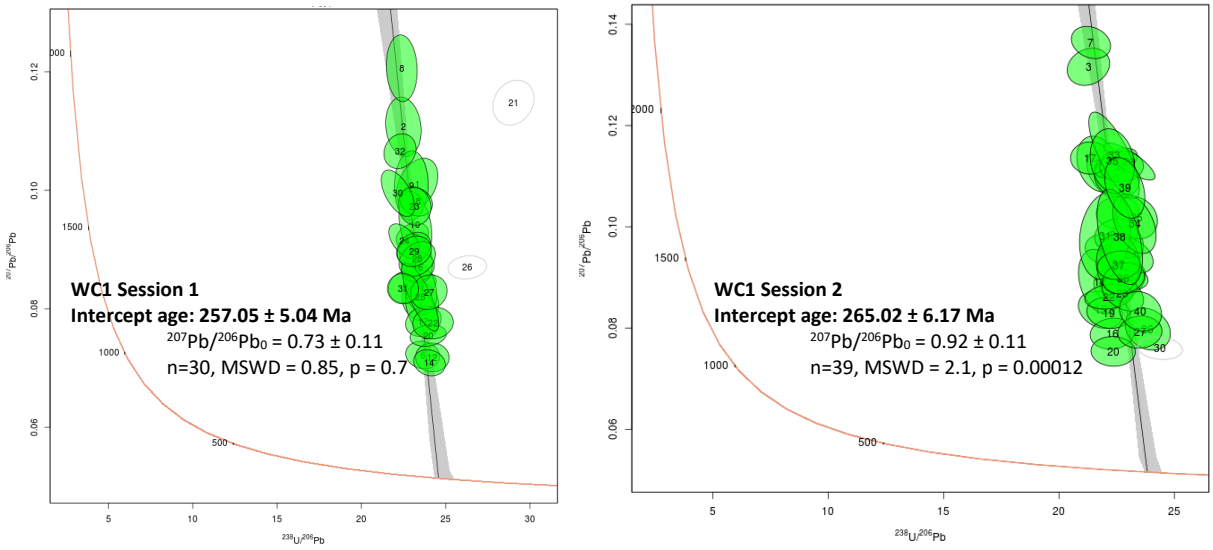


**Figure 27.** TW-Concordia plots for age validation reference material WC1 data from analytical sessions 1 and 2. WC1 is 254.4 ± 6.4 Ma old (Roberts et al., 2017).

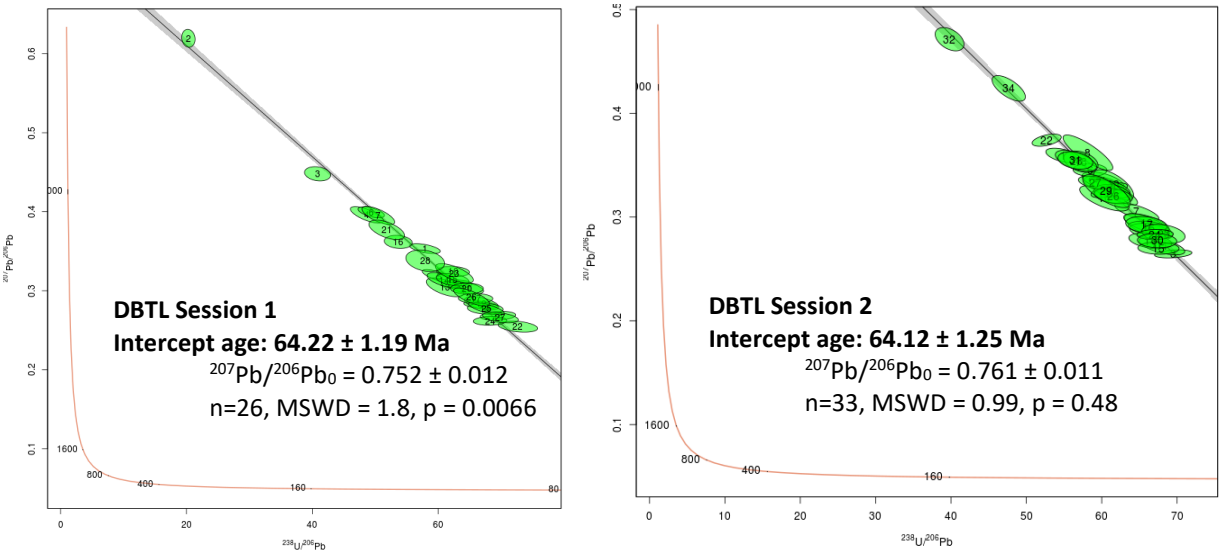


**Figure 28**. TW-Concordia plots for calibration reference material DBTL data from session 1 and 2. The reference literature age of DBTL is 64.04 ± 0.67 Ma old (Hill et al., 2016)

The results from the reference materials DBTL Hill et al. (2016) and WC1 (Roberts et al., 2017) were pooled from session 1 and 2 and plotted on a TW-concordia plot (Fig.Figure **27**Figure 28). Session 1 results for WC1 produced an age of 257.05 ± 5.04 Ma that is within the expected age range of 254.4 ± 6.4 Ma (Roberts et al., 2017). Session 2 results for WC1 produced

similar results (265.02 ± 6.17) within the expected maximum age range of 260.8 Ma. The ages from DBTL were 64.22 ± 1.19 Ma and 64.12 ± 1.25 Ma over sessions 1 and 2 respectively. The reference material is 64.04 ± 0.67 Ma old (Hill et al., 2016). A list of parameters used during data acquisition can be seen in table 1 below and for reference material data see Table 2Table 3Table 10Table 11.

**Table 1.** Data Reporting Table

| **Laboratory & Sample Preparation** | |
|---|---|
| Laboratory name | KU Isotope geochemistry laboratory |
| Sample type/mineral | carbonate |
| Sample preparation | Polished Thick Sections (ca. 100um) |
| Imaging | fluorescence |
| **Laser ablation system** | |
| Make, Model & type | Arf excimer 193 nm, Photon Machines Analyte G2, ATL |
| Ablation cell & volume | Helex 2, two-volume cell |
| Laser wavelength (nm) | 193 |
| Pulse width (ns) | 5 |
| **Fluence ($J.cm^{-2}$)** | 2.7 |
| **Repetition rate (Hz)** | 10 |
| **Spot size (um)** | 130 |
| Sampling mode / pattern | spot |
| Carrier gas | He, 1.01 l/min, Ar, 1.1 l/min |
| Ablation duration (secs) | 30 |
| Cell carrier gas flow (l/min) | Ar, 1.1 l/min |
| **ICP-MS Instrument** | |
| Make, Model & type | Thermo Element2 magnetic sector field ICP-MS |
| Sample introduction | Meinhard mixing bulb |
| RF power (W) | 1100 |
| Make-up gas flow (l/min) | Ar, 1.1 l/min |
| sampling depth | 4 |
| Detection system | single detector, counting & analog |
| Masses measured (integration time in ms) | 206Pb (40), 207Pb (88), 208Pb (8), 232Th (8), 238U (40) |
| Total integration time per reading (ms) | 184 |
| Total method time (secs) | 47 |
| IC Dead time (ns) | 4 |
| ThO+/Th+ (%) | U/UO <0.2 |
| 238+/232Th+ | 1.0 |
| **Data Processing** | |
| Gas blank (secs) | 17 |
| Calibration strategy | NIST 614 for Pb calibration, drift etc., DBTL for U-Pb |
| Reference Material info | NIST 614 (Jochum et al. 2009) |
| | DBTL (Hill et al. 2016) |
| Data processing package used / Correction for LIEF | IGOR PRO, Iolite 2.5 |
| Common-Pb correction, composition and uncertainty | none |
| Quality control / Validation | WC1 (Roberts et al. 2017) |

## Chapter 5: Discussion

The results of this study are consistent with the findings of several other studies that analyze fault-hosted carbonates as material for laser ablation dating e.g. (Roberts and Walker, 2016; Smeraglia et al., 2021). It is feasible to date carbonate veins; however, few samples yield precise results (~25% for this study). LA-ICP-MS U-Pb dating of carbonate veins in the Cañon City embayment is a feasible way of constraining the age of brittle deformation provided more strenuous sample screening is applied in the future. This process might involve ablating samples with a few spots after sample imaging to test for areas with relatively high uranium concentration. This worked well for sample MQ2-2 where there was a spatial correlation in uranium concentration along fiber growths with a different orientation and is also outlined in reviews of the technique by Roberts et al. (2020). The examination of uranium concentrations from each spot across the traversal for MQ2-2 show that U was absent except for the edges where the fibers were orientated at an angle to the center vein.

Results highlight a previously undocumented early onset of deformation in the Cañon City Embayment region, as early as 110 Ma. From the 12 samples analyzed, only 1 (MQ3) had a significant enough concentration of uranium to produce a date with low uncertainty (110.4 ± 1.4 Ma). U-Pb carbonate dates vary from Cretaceous (ca. 110 Ma) to Neogene (ca. 12-6 Ma) and are likely correlated to different uplift episodes, which created the current topography of the Front Range. Contrary to the initial hypothesis that the brittle deformation was mainly attributable to the Laramide orogeny, results from MQ3 (110.4 ± 1.4 Ma) predate the event and are more in line with earlier Cretaceous basin formation. Dates from MQ2 (61 ± 18 Ma) fall within the timing of the Laramide orogeny but need to be refined to be geologically useful.

The difference in ages across the same sample location are likely due to different fluid flow events. Triggered by Laramide deformation, it is probable that later uplift events and associated fluid flow recrystallized carbonate along fault surfaces. This is also a likely explanation for the variation in color across the sample location ranging from white to pink to dark pink, see Figure 9. Each color represents different generations of crystallization caused by these carbonate-forming fluid events. This idea is supported by the data from Shelf Road in the Ordovician Harding Fm. where samples were interpreted to have experienced multiple different fluid events between early Cretaceous (~ 100 Ma) to Neogene (~ 6-12 Ma), see Figure 24. Younger ages may have been triggered by the rapid onset of uplift from 10 Ma to recent. These would then be attributed to the uplift caused by mantle upwelling following the removal of the Farallon slab and lithospheric delamination. See Figure 29 below for an illustration of this process with respect to lithospheric hydration during the Cenozoic.

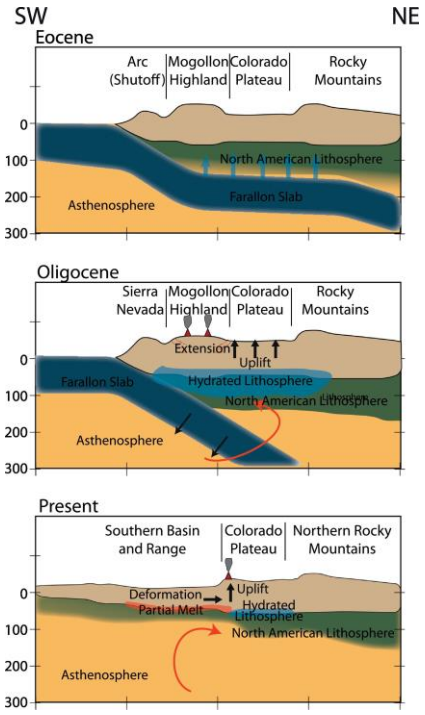


**Figure 29.** Illustrative cross section of the Colorado Plateau and Rocky Mountains to highlight potential uplifting forces with respect to water from Eocene to present. Note that the subducting slab shown in dark blue represents the Farallon Slab. Figure taken from Porter et al., (2017).

Carbonate is easily susceptible to diagenetic alteration, which must be recognized in order to produce geologically meaningful interpretations from the data. Relating petrographic analysis to characteristics expressed in the field should be employed to prevent misinterpretation (Rasbury et al., 2021). Samples from Marsh Quarry provide examples for deformation and diagenesis. This likely has an impact on the spatial correlation of uranium concentrations as seen in MQ2-2 (Figure 15). For comparison, sample MQ3 does not exhibit major deformation textures or different orientations of fiber growths. It is homogenous in color and fibers are wider than in other samples. It is assumed that the sample is relatively well preserved and unaffected by later diagenesis, so that the date obtained from it is reflects the original fracture fill event. In contrast, most of the other samples from the Marsh Quarry trail have evident deformation (MQ2-1 and both MQ1 samples, see Figure 15 and Figure 14). MQ2-2 did not have as much visible fracturing, but there is evidence of recrystallization by the reorientation of the fibers. The outer portion of the sample is likely the first crystal growth, assuming the fault surface continues to slip and open slowly (evident by the fibrous growths as stated by Smeraglia et al. 2021) and the carbonate continues to crystallize towards the center.

The purpose of this study was to test the feasibility of U-Pb dating of carbonate via LA-ICP-MS in the Cañon City Embayment. While it proved partly successful, there are several limitations that must be addressed. The number of samples studied here is limited and the vein orientations were not fully documented, as the scope of this study was merely to determine whether the methodology would work on the area. It will be prudent to completely document all brittle deformation orientations, including the attitude of both the fault surface and slickenfibers to determine the stress regime. Most samples did not contain enough uranium to be dated and much time was spent on sample prep rather than sample screening.

## Chapter 6: Conclusion

The U-Pb dating of carbonate veins in the Cañon City embayment region yielded ages ranging from early Cretaceous to Neogene. A date with low uncertainty, 110.4 ± 1.4 Ma, has been obtained from ca. 2cm thick fibrous, white carbonate veins cross cutting the Jurassic Morrison Fm. This date coincides with basin formation and sedimentation, and with the timing of the Sevier Orogeny. This is contrary to the initial hypothesis that brittle deformation features would mainly coincide with the Laramide Orogeny and younger uplift events. A younger age of 61 ± 18 Ma, with a higher uncertainty, has been determined on pink carbonate vein material from the Morrison Fm. consistent with macroscopic observations. Fault-hosted carbonate material from the Ordovician Harding Fm. at Shelf Road produced scattered results, interpreted to range from Early Cretaceous and Neogene (~100 Ma, ~12-6 Ma respectively). This is interpreted as representing multiple fluid flow events. Most carbonate vein samples collected from the Morrison Fm. have too little uranium concentrations to be dated. In samples from Temple Canyon carbonate cement between quartz grains was too thin to ablate with the 130µm spot size necessary. These results are promising enough to warrant further, more detailed investigations.

Future work will involve working with a much larger range of stratigraphic units and locations in the Front Range. Detailed field observations and petrographic observations must be done to correlate internal structures with ages to create meaningful geologic interpretations. Sr isotope measurement may help to identify possible fluid sources (e.g., basement vs. Phanerozoic sediments). Fluid inclusion work may be done to constrain the temperature and composition of the fluid. Cathodoluminescence will be used to map internal textures in samples before laser ablation ICP-MS analysis.

## References

Aslan, A., Karlstrom, K.E., Crossey, L.J., Kelley, S., Cole, R., Lazear, G., and Darling, A., 2010, Late Cenozoic evolution of the Colorado Rockies: Evidence for Neogene uplift and drainage integration, *in* Morgan, L.A., and Quane, S.L., eds., Through the Generations: geologic and anthropogenic field excursions in the Rocky Mountains from modern to ancient: Geological Society of America Field Guide v. 18, p. 21–54, doi: 10.1130/2010.0018(02).

Beaudoin, N., Lacombe, O., Roberts, N.M.W., and Koehn, D., 2018, U-Pb dating of calcite veins reveals complex stress evolution and thrust sequence in the Bighorn Basin, Wyoming, USA: Geology, v. 46, p. 1015–1018, https://doi.org/10.1130/G45379.1.

Carrapa, B., DeCelles, P.G., and Romero, M., 2019, Early inception of the Laramide Orogeny in southwestern Montana and northern Wyoming: implications for models of flat-slab subduction: Journal of Geophysical Research: Solid Earth, v. 124, p. 2102–2123, doi:10.1029/2018JB016888.

Cather, S., 2004, Laramide orogeny in central and northern New Mexico and southern Colorado: The geology of New Mexico: A geologic history, v. 11, p. 203-248.

Erslev, E.A., and Larson, S.M., 2006, Testing Laramide Hypotheses for the Colorado Front Range Arch Using Minor Faults: v. 43, p. 45–64.

Erslev, E.A., Holdaway, S.M., O'Meara, S.A., Jurista, B.K., and Selvig, B., 2004, Laramide minor faulting in the Colorado Front Range: New Mexico Bureau of Geology & Mineral Resources, Bulletin 160, p. 181-204

Evanoff, E., 1996, Rocks of the Cañon City Basin: Stratigraphic Column. https://royalgorgeregion.com/the-history-of-the-canon-city-area/

Haun, J. D. and Kent, H. C., 1965, Geologic history of Rocky Mountain region: AAPG Bulletin, v. 49, p. ?? doi:10.1306/A6633866-16C0-11D7-8645000102C1865D.

Heitmann, E.O., Hyland, E.G., Schoettle-Greene, P., Brigham, C.A.P., and Huntington, K.W., 2021, Rise of the Colorado Plateau: a synthesis of paleoelevation constraints from the region and a path forward using temperature-based elevation proxies: Frontiers in Earth Science, v. 9, https://doi.org/10.3389/feart.2021.648605.

Hernández-Uribe, D., and Palin, R.M., 2019, Catastrophic shear-removal of subcontinental lithospheric mantle beneath the Colorado Plateau by the subducted Farallon slab: Scientific Reports, v. 9, p. 8153, doi:10.1038/s41598-019-44628-y.

Hill, C.A., Polyak, V.J., Asmerom, Y. and P. Provencio, P., 2016. Constraints on a Late Cretaceous uplift, denudation, and incision of the Grand Canyon region, southwestern Colorado Plateau, USA, from U-Pb dating of lacustrine limestone. Tectonics, 35(4), pp.896-906.

Horstwood, M.S.A. et al., 2016, Community-derived standards for LA-ICP-MS U-(Th-)Pb geochronology – uncertainty propagation, age interpretation and data reporting: Geostandards and Geoanalytical Research, v. 40, p. 311–332, doi:10.1111/j.1751-908X.2016.00379.x.

Jacob, A.F., and Albertus, R.G. “Jerry,” 1985, Thrusting, Petroleum Seeps, and Seismic Exploration Front Range South of Denver, Colorado: , p. 77–96.

Jahn, B., and Cuvellier, H., 1994, Pb-Pb and U-Pb geochronology of carbonate rocks: an assessment: Chemical Geology, v. 115, p. 125–151, doi:10.1016/0009-2541(94)90149-X.

Karlstrom, K.E., Wilgus, J., Thacker, J.O., Schmandt, B., Coblentz, D. and Albonico, M., 2022, Tectonics of the Colorado Plateau and its margins: annual review of earth and planetary sciences, v. 50, doi.org/10.1146/annurev-earth-032320-111432.

Karlstrom, K.E. et al., 2012, Mantle-driven dynamic uplift of the Rocky Mountains and Colorado Plateau and its surface response: Toward a unified hypothesis: Lithosphere, v. 4, p. 3–22, doi:10.1130/L150.1.

Li, Q., Parrish, R.R., Horstwood, M.S.A., and McArthur, J.M., 2014, U–Pb dating of cements in Mesozoic ammonites: Chemical Geology, v. 376, p. 76–83, doi:10.1016/j.chemgeo.2014.03.020.

Marshall, G., 1959, The related faults of the east side of the Cañon City Embayment, Colorado: Proceedings of the Iowa Academy of Science, v. 66(1), p. 328-333.

Paton, C., Woodhead, J.D., Hellstrom, J.C., Hergt, J.M., Greig, A., and Maas, R., 2010, Improved laser ablation U-Pb zircon geochronology through robust downhole fractionation correction: Geochemistry, Geophysics, Geosystems, v. 11, doi: 10.1029/2009GC002618.

Paton, C., Hellstrom, J., Paul, B., Woodhead, J., and Hergt, J., 2011. Iolite: Freeware for the visualisation and processing of mass spectrometry data: Journal of Analytical Atomic Spectrometry, v. 26, p. 2508-2518.

Porter, R., Hoisch, T., and Holt, W.E., 2017, The role of lower-crustal hydration in the tectonic evolution of the Colorado Plateau: Tectonophysics, v. 712–713, p. 221–231, doi:10.1016/j.tecto.2017.05.025.

Rasbury, E.T., and Cole, J.M., 2009, Directly dating geologic events: U-Pb dating of carbonates: Reviews of Geophysics, v. 47, p. RG3001, doi:10.1029/2007RG000246.

Rasbury, E.T., Hanson, G.N., Meyers, W.J., and Saller, A.H., 1997, Dating of the time of sedimentation using U-Pb ages for paleosol calcite: Geochimica et Cosmochimica Acta, v. 61, p. 1525–1529, doi:10.1016/S0016-7037(97)00043-4.

Rasbury, E.T., Present, T.M., Northrup, P., Tappero, R.V., Lanzirotti, A., Cole, J.M., Wooton, K.M., and Hatton, K., 2021, Tools for uranium characterization in carbonate samples: case studies of natural U–Pb geochronology reference materials: Geochronology, v. 3, p. 103–122, doi:10.5194/gchron-3-103-2021.

Richards, D.A., Bottrell, S.H., Cliff, R.A., Ströhle, K., and Rowe, P.J., 1998, U-Pb dating of a speleothem of Quaternary age: Geochimica et Cosmochimica Acta, v. 62, p. 3683–3688, doi:10.1016/S0016-7037(98)00256-7.

Roberts, N.M., Rasbury, E.T., Parrish, R.R., Smith, C.J., Horstwood, M.S. & Condon, D.J., 2017. Geochemistry, Geophysics, Geosystems 18(7), 2807-2814.

Roberts, N.M.W. et al., 2020, Laser ablation inductively coupled plasma mass spectrometry (LA-ICP-MS) U–Pb carbonate geochronology: strategies, progress, and limitations: Geochronology, v. 2, p. 33–61, doi:10.5194/gchron-2-33-2020.

Roberts, N.M.W., Rasbury, E.T., Parrish, R.R., Smith, C.J., Horstwood, M.S.A., and Condon, D.J., 2017, A calcite reference material for LA-ICP-MS U-Pb geochronology: CALCITE RM FOR LA-ICP-MS U-Pb DATING: Geochemistry, Geophysics, Geosystems, v. 18, p. 2807–2814, doi:10.1002/2016GC006784.

Roberts, N.M.W., and Walker, R.J., 2016, U-Pb geochronology of calcite-mineralized faults: Absolute timing of rift-related fault events on the northeast Atlantic margin: Geology, v. 44, p. 531–534, doi:10.1130/G37868.1.

Sahagian, D., Proussevitch, A., and Carlson, W., 2002, Timing of Colorado Plateau uplift: Initial constraints from vesicular basalt-derived paleoelevations: Geology, v. 30, p. 807, doi:10.1130/0091-7613(2002)030<0807:TOCPUI>2.0.CO;2.

Smeraglia, L., Looser, N., Fabbri, O., Choulet, F., Guillong, M., and Bernasconi, S.M., 2021, U–Pb dating of middle Eocene–Pliocene multiple tectonic pulses in the Alpine foreland: Solid Earth, v. 12, p. 2539–2551, doi:10.5194/se-12-2539-2021.

Vermeesch, P., 2018, IsoplotR: A free and open toolbox for geochronology: Geoscience Frontiers, v. 9, p. 1479–1493, doi:10.1016/j.gsf.2018.04.001.

Woodhead, J., and Petrus, J., 2019, Exploring the advantages and limitations of in situ U–Pb carbonate geochronology using speleothems: Geochronology, v. 1, p. 69–84, doi:10.5194/gchron-1-69-2019.

Woodhead, J., Hellstrom, J., Maas, R., Drysdale, R., Zanchetta, G., Devine, P., and Taylor, E., 2006, U–Pb geochronology of speleothems by MC-ICPMS: Quaternary Geochronology, v. 1, p. 208–221, doi:10.1016/j.quageo.2006.08.002.

Woodhead, J., Hellstrom, J., Pickering, R., Drysdale, R., Paul, B., and Bajo, P., 2012, U and Pb variability in older speleothems and strategies for their chronology: Quaternary Geochronology, v. 14, p. 105–113, doi:10.1016/j.quageo.2012.02.028.

Woodhead, J., Reisz, R., Fox, D., Drysdale, R., Hellstrom, J., Maas, R., Cheng, H., and Edwards, R.L., 2010, Speleothem climate records from deep time? Exploring the potential with an example from the Permian: Geology, v. 38, p. 455–458, doi:10.1130/G30354.1.

# Appendix A: U-Pb Data Session 1

**Table 2.** Laser ablation ICP-MS U-Th-Pb Data for reference material DBTL

| Data for Tera-Wasserburg plot | | | | | | | Concentrations | | | | |
|---|---|---|---|---|---|---|---|---|---|---|---|
| **Identifier** | **238U/206Pb** | **Prop2SE** | **207Pb/206Pb** | **Prop2SE** | **err.corr.** | **Approx_U_PPM** | **Approx_U_PPM_Int2SE** | **Approx_Th_PPM** | **Approx_Th_PPM_Int2SE** | **Approx_Pb_PPM** | **Approx_Pb_PPM_Int2SE** |
| DBTL_1 | 57.8770 | 2.0060 | 0.3534 | 0.0051 | -0.5531 | 15.31 | 0.43 | 0.0994 | 0.0032 | 0.45 | 0.02 |
| DBTL_2 | 20.3103 | 0.8707 | 0.6195 | 0.0093 | -0.1034 | 5.67 | 0.3 | 0.0524 | 0.0026 | 0.871 | 0.032 |
| DBTL_3 | 40.8257 | 1.6958 | 0.4480 | 0.0074 | -0.1963 | 9.43 | 0.31 | 0.0895 | 0.0028 | 0.531 | 0.032 |
| DBTL_4 | 48.6762 | 2.1578 | 0.3960 | 0.0086 | -0.7081 | 12.1 | 0.4 | 0.0942 | 0.003 | 0.511 | 0.04 |
| DBTL_5 | 60.2047 | 2.2487 | 0.3180 | 0.0072 | -0.7449 | 14.94 | 0.23 | 0.1032 | 0.0029 | 0.384 | 0.022 |
| DBTL_6 | 49.3498 | 1.7182 | 0.3993 | 0.0057 | -0.5730 | 11.57 | 0.29 | 0.087 | 0.0036 | 0.446 | 0.019 |
| DBTL_7 | 50.4797 | 2.1350 | 0.3952 | 0.0095 | -0.7132 | 11.92 | 0.28 | 0.0784 | 0.0033 | 0.461 | 0.031 |
| DBTL_8 | 62.8902 | 1.9882 | 0.3081 | 0.0046 | 0.0274 | 14.02 | 0.43 | 0.0951 | 0.0029 | 0.326 | 0.012 |
| DBTL_9 | 66.7322 | 2.1938 | 0.2821 | 0.0041 | -0.3485 | 14.79 | 0.16 | 0.0959 | 0.0027 | 0.2988 | 0.0066 |
| DBTL_10 | 62.3405 | 2.1437 | 0.3242 | 0.0053 | -0.1301 | 13.51 | 0.19 | 0.0487 | 0.0026 | 0.331 | 0.011 |
| DBTL_11 | 64.4616 | 2.2409 | 0.3035 | 0.0064 | -0.4787 | 14.26 | 0.16 | 0.0564 | 0.0027 | 0.327 | 0.012 |
| DBTL_12 | 66.8794 | 2.2323 | 0.2839 | 0.0069 | -0.5168 | 15.2 | 0.3 | 0.0941 | 0.003 | 0.305 | 0.01 |
| DBTL_13 | 61.0843 | 2.4412 | 0.3042 | 0.0097 | -0.6077 | 13.03 | 0.17 | 0.1023 | 0.0036 | 0.315 | 0.021 |
| DBTL_14 | 60.9308 | 2.2173 | 0.3136 | 0.0077 | -0.5806 | 13.93 | 0.13 | 0.094 | 0.0033 | 0.339 | 0.014 |
| DBTL_15 | 62.2765 | 2.1400 | 0.3141 | 0.0064 | -0.3525 | 14.69 | 0.2 | 0.091 | 0.0031 | 0.355 | 0.013 |
| DBTL_16 | 53.6515 | 1.8237 | 0.3618 | 0.0068 | -0.1510 | 11.86 | 0.26 | 0.0698 | 0.003 | 0.402 | 0.011 |
| DBTL_17 | 65.9338 | 2.2389 | 0.2902 | 0.0051 | -0.0291 | 15.46 | 0.28 | 0.0661 | 0.0035 | 0.328 | 0.012 |
| DBTL_18 | 69.4856 | 2.3152 | 0.2682 | 0.0047 | 0.1918 | 15.63 | 0.33 | 0.0698 | 0.0033 | 0.277 | 0.01 |
| DBTL_19 | 67.4749 | 2.3285 | 0.2772 | 0.0056 | -0.1541 | 15.86 | 0.26 | 0.0492 | 0.0025 | 0.299 | 0.01 |
| DBTL_20 | 64.5646 | 2.1326 | 0.3028 | 0.0056 | -0.0136 | 17.01 | 0.51 | 0.0582 | 0.0058 | 0.377 | 0.014 |
| DBTL_21 | 51.8172 | 2.3184 | 0.3770 | 0.0101 | -0.5781 | 13.33 | 0.16 | 0.0632 | 0.0028 | 0.474 | 0.024 |
| DBTL_22 | 72.6497 | 2.5696 | 0.2546 | 0.0058 | -0.3269 | 16.83 | 0.32 | 0.0427 | 0.002 | 0.269 | 0.012 |
| DBTL_23 | 62.5657 | 2.4622 | 0.3220 | 0.0101 | -0.6854 | 16.31 | 0.2 | 0.0533 | 0.0027 | 0.393 | 0.021 |
| DBTL_24 | 68.2343 | 2.1831 | 0.2618 | 0.0046 | 0.0838 | 15.53 | 0.15 | 0.0505 | 0.0029 | 0.2795 | 0.0083 |
| DBTL_25 | 67.6631 | 2.3080 | 0.2774 | 0.0065 | -0.7271 | 14.85 | 0.15 | 0.0545 | 0.0025 | 0.28 | 0.012 |
| DBTL_26 | 65.2948 | 2.3204 | 0.2919 | 0.0092 | -0.7382 | 15.76 | 0.13 | 0.06 | 0.003 | 0.336 | 0.017 |
| DBTL_27 | 69.8861 | 2.3377 | 0.2660 | 0.0055 | -0.4400 | 16.37 | 0.2 | 0.0644 | 0.003 | 0.2877 | 0.008 |
| DBTL_28 | 57.9323 | 2.5175 | 0.3380 | 0.0111 | -0.2572 | 15.2 | 0.21 | 0.076 | 0.0045 | 0.414 | 0.021 |

**Table 3.** Laser ablation ICP-MS U-Th-Pb Data for reference material WC1

| Data for Tera-Wasserburg plot | | | | | | | Concentrations | | | | |
|---|---|---|---|---|---|---|---|---|---|---|---|
| **Identifier** | **238U/206Pb** | **Prop2SE** | **207Pb/206Pb** | **Prop2SE** | **err.corr.** | **Approx_U_PPM** | **Approx_U_PPM_Int2SE** | **Approx_Th_PPM** | **Approx_Th_PPM_Int2SE** | **Approx_Pb_PPM** | **Approx_Pb_PPM_Int2SE** |
| WC1_1 | 23.3178 | 0.9983 | 0.1010 | 0.0036 | 0.3321 | 4.323 | 0.073 | 0.00153 | 0.00045 | 0.0483 | 0.0033 |
| WC1_2 | 22.4958 | 0.8621 | 0.1107 | 0.0041 | -0.1300 | 3.792 | 0.072 | 0.00221 | 0.00048 | 0.0522 | 0.0029 |
| WC1_3 | 23.4985 | 0.8914 | 0.0813 | 0.0028 | -0.1709 | 4.183 | 0.082 | 0.00226 | 0.00045 | 0.0277 | 0.003 |
| WC1_4 | 23.0255 | 0.7859 | 0.0923 | 0.0018 | 0.2755 | 3.891 | 0.031 | 0.00104 | 0.00028 | 0.037 | 0.0019 |
| WC1_5 | 23.4849 | 0.7749 | 0.0843 | 0.0017 | 0.1569 | 4.019 | 0.053 | 0.00213 | 0.00043 | 0.0303 | 0.0018 |
| WC1_6 | 23.6359 | 0.8217 | 0.0722 | 0.0019 | -0.1096 | 4.58 | 0.073 | 0.00148 | 0.00031 | 0.0207 | 0.0021 |
| WC1_7 | 22.6217 | 0.8341 | 0.0837 | 0.0022 | 0.1096 | 4.43 | 0.12 | 0.00212 | 0.00043 | 0.0338 | 0.0021 |
| WC1_8 | 22.3961 | 0.7499 | 0.1206 | 0.0046 | -0.0762 | 4.222 | 0.045 | 0.00073 | 0.00024 | 0.0689 | 0.0046 |
| WC1_9 | 22.9645 | 0.8190 | 0.1008 | 0.0048 | 0.0293 | 4.028 | 0.052 | 0.00142 | 0.00035 | 0.0484 | 0.0044 |
| WC1_10 | 23.2062 | 0.7964 | 0.0942 | 0.0046 | -0.3122 | 4.335 | 0.042 | 0.00063 | 0.00022 | 0.0444 | 0.0054 |
| WC1_11 | 23.4803 | 0.8125 | 0.0835 | 0.0036 | -0.2714 | 4.597 | 0.057 | 0.00203 | 0.00041 | 0.035 | 0.0044 |
| WC1_12 | 24.2117 | 0.8157 | 0.0718 | 0.0020 | -0.0134 | 4.073 | 0.068 | 0.00222 | 0.00041 | 0.0177 | 0.0015 |
| WC1_13 | 23.2418 | 0.7985 | 0.0885 | 0.0034 | -0.2331 | 4.428 | 0.062 | 0.00258 | 0.00044 | 0.0379 | 0.0031 |
| WC1_14 | 24.0389 | 0.7669 | 0.0709 | 0.0018 | -0.1470 | 4.328 | 0.048 | 0.00247 | 0.00052 | 0.0186 | 0.0018 |
| WC1_15 | 23.5808 | 0.7802 | 0.0795 | 0.0035 | -0.4484 | 4.772 | 0.041 | 0.00194 | 0.00044 | 0.0324 | 0.0041 |
| WC1_16 | 23.3447 | 0.8045 | 0.0870 | 0.0020 | 0.1395 | 4.215 | 0.052 | 0.00141 | 0.00036 | 0.0349 | 0.0017 |
| WC1_17 | 23.6821 | 0.8637 | 0.0779 | 0.0021 | 0.1870 | 4.438 | 0.049 | 0.00175 | 0.00041 | 0.0252 | 0.0019 |
| WC1_18 | 23.2418 | 0.7985 | 0.0981 | 0.0020 | -0.2013 | 4.898 | 0.047 | 0.00184 | 0.00043 | 0.0528 | 0.0031 |
| WC1_19 | 23.0957 | 0.8270 | 0.0902 | 0.0022 | 0.2678 | 4.236 | 0.044 | 0.00133 | 0.00035 | 0.0383 | 0.0028 |
| WC1_20 | 23.9629 | 0.8816 | 0.0755 | 0.0015 | 0.1868 | 4.913 | 0.087 | 0.00294 | 0.00054 | 0.026 | 0.0016 |
| WC1_21 | 29.0216 | 0.9963 | 0.1148 | 0.0031 | 0.1823 | 3.303 | 0.056 | 0.0019 | 0.0004 | 0.0374 | 0.0019 |
| WC1_22 | 24.2505 | 0.9849 | 0.0776 | 0.0022 | 0.0579 | 4.8 | 0.22 | 0.00104 | 0.00046 | 0.0277 | 0.0018 |
| WC1_23 | 23.1619 | 0.7938 | 0.0973 | 0.0026 | -0.0704 | 4.012 | 0.032 | 0.00451 | 0.0007 | 0.0453 | 0.0029 |
| WC1_24 | 22.5544 | 0.7589 | 0.0914 | 0.0024 | -0.5347 | 4.302 | 0.03 | 0.00359 | 0.00078 | 0.0438 | 0.0048 |
| WC1_25 | 23.4985 | 0.8914 | 0.0820 | 0.0047 | -0.7846 | 4.43 | 0.053 | 0.00282 | 0.00055 | 0.039 | 0.015 |
| WC1_26 | 26.2849 | 0.9384 | 0.0870 | 0.0016 | 0.1226 | 4.269 | 0.05 | 0.00333 | 0.00081 | 0.0321 | 0.0023 |
| WC1_27 | 24.0104 | 0.8846 | 0.0828 | 0.0024 | 0.0926 | 4.93 | 0.068 | 0.00252 | 0.00058 | 0.0356 | 0.0026 |
| WC1_28 | 23.3178 | 0.8794 | 0.0884 | 0.0024 | 0.2844 | 5.09 | 0.11 | 0.00214 | 0.00042 | 0.0424 | 0.0034 |
| WC1_29 | 23.1398 | 0.8298 | 0.0897 | 0.0021 | 0.1479 | 4.143 | 0.039 | 0.0015 | 0.00045 | 0.033 | 0.002 |
| WC1_30 | 22.1668 | 0.8052 | 0.0995 | 0.0032 | -0.5687 | 4.701 | 0.041 | 0.00258 | 0.00055 | 0.0539 | 0.0038 |
| WC1_31 | 22.4708 | 0.7541 | 0.0834 | 0.0021 | -0.0074 | 4.266 | 0.036 | 0.00259 | 0.00054 | 0.0325 | 0.0027 |
| WC1_32 | 22.2890 | 0.7781 | 0.1066 | 0.0024 | 0.1428 | 4.231 | 0.041 | 0.0024 | 0.00061 | 0.0556 | 0.0034 |

**Table 4.** Laser ablation ICP-MS U-Th-Pb Data for sample MQ1-1

| Data for Tera-Wasserburg plot | | | | | | | Concentrations | | | | |
|---|---|---|---|---|---|---|---|---|---|---|---|
| **Identifier** | **238U/206Pb** | **Prop2SE** | **207Pb/206Pb** | **Prop2SE** | **err.corr.** | **Approx_U_PPM** | **Approx_U_PPM_Int2SE** | **Approx_Th_PPM** | **Approx_Th_PPM_Int2SE** | **Approx_Pb_PPM** | **Approx_Pb_PPM_Int2SE** |
| MQ1_1_1 | 0.1331 | 0.0079 | 0.8140 | 0.0144 | 0.7949 | 0.00783 | 0.00051 | 0.1193 | 0.003 | 0.2312 | 0.0061 |
| MQ1_1_2 | 0.1359 | 0.0083 | 0.7960 | 0.0125 | 0.1334 | 0.00829 | 0.00045 | 0.1025 | 0.0027 | 0.2382 | 0.0054 |
| MQ1_1_3 | 0.0740 | 0.0040 | 0.8196 | 0.0106 | 0.1604 | 0.00469 | 0.00021 | 0.1131 | 0.0033 | 0.2657 | 0.0066 |
| MQ1_1_4 | 0.1413 | 0.0066 | 0.8175 | 0.0106 | 0.3337 | 0.0125 | 0.00042 | 0.1071 | 0.0027 | 0.3713 | 0.0091 |
| MQ1_1_5 | 0.1585 | 0.0082 | 0.8191 | 0.0106 | 0.2944 | 0.011 | 0.00039 | 0.0879 | 0.0026 | 0.2843 | 0.0066 |
| MQ1_1_6 | 0.0516 | 0.0030 | 0.8203 | 0.0115 | 0.0698 | 0.00474 | 0.00026 | 0.1014 | 0.0024 | 0.369 | 0.0063 |
| MQ1_1_7 | 0.1164 | 0.0077 | 0.8137 | 0.0090 | 0.1540 | 0.01421 | 0.00062 | 0.1191 | 0.0028 | 0.51 | 0.01 |
| MQ1_1_8 | 0.0925 | 0.0038 | 0.8224 | 0.0106 | 0.0084 | 0.01265 | 0.00049 | 0.1145 | 0.0034 | 0.564 | 0.015 |
| MQ1_1_9 | 0.1278 | 0.0080 | 0.8138 | 0.0106 | 0.0165 | 0.01317 | 0.00057 | 0.1041 | 0.0028 | 0.426 | 0.01 |
| MQ1_1_10 | 0.0312 | 0.0021 | 0.8228 | 0.0098 | -0.0001 | 0.00322 | 0.00019 | 0.1286 | 0.0032 | 0.428 | 0.015 |
| MQ1_1_11 | 0.1295 | 0.0054 | 0.8104 | 0.0095 | 0.3298 | 0.01347 | 0.00041 | 0.1051 | 0.0039 | 0.4115 | 0.0092 |
| MQ1_1_12 | 0.1305 | 0.0084 | 0.8107 | 0.0095 | 0.2914 | 0.01184 | 0.00085 | 0.1024 | 0.0033 | 0.37 | 0.0091 |
| MQ1_1_13 | 0.1851 | 0.0079 | 0.8234 | 0.0099 | 0.2360 | 0.01743 | 0.00061 | 0.1082 | 0.0036 | 0.3925 | 0.0074 |
| MQ1_1_14 | 0.0938 | 0.0046 | 0.8096 | 0.0106 | 0.2803 | 0.0089 | 0.0004 | 0.0963 | 0.0029 | 0.3844 | 0.0077 |
| MQ1_1_15 | 0.1022 | 0.0047 | 0.8089 | 0.0106 | 0.4690 | 0.01371 | 0.0006 | 0.1319 | 0.0031 | 0.539 | 0.014 |
| MQ1_1_16 | 0.1998 | 0.0096 | 0.8110 | 0.0115 | 0.1389 | 0.02254 | 0.00081 | 0.115 | 0.0032 | 0.47 | 0.011 |
| MQ1_1_17 | 0.1490 | 0.0058 | 0.8100 | 0.0097 | 0.2916 | 0.02087 | 0.00058 | 0.1454 | 0.0029 | 0.566 | 0.014 |
| MQ1_1_18 | 0.1443 | 0.0092 | 0.8128 | 0.0096 | 0.0238 | 0.01392 | 0.00063 | 0.1459 | 0.0035 | 0.39 | 0.0068 |
| MQ1_1_19 | 0.0656 | 0.0031 | 0.8143 | 0.0090 | -0.0114 | 0.01396 | 0.00048 | 0.1961 | 0.0075 | 0.846 | 0.017 |
| MQ1_1_20 | 0.0901 | 0.0038 | 0.8167 | 0.0094 | 0.2899 | 0.01433 | 0.0004 | 0.1846 | 0.0043 | 0.654 | 0.014 |
| MQ1_1_21 | 0.1010 | 0.0085 | 0.8091 | 0.0083 | 0.1307 | 0.0216 | 0.0018 | 0.1487 | 0.0036 | 0.847 | 0.014 |
| MQ1_1_22 | 0.1158 | 0.0060 | 0.8161 | 0.0084 | 0.1893 | 0.02457 | 0.00096 | 0.1325 | 0.0041 | 0.88 | 0.013 |
| MQ1_1_23 | 0.0815 | 0.0049 | 0.8096 | 0.0088 | 0.3845 | 0.0217 | 0.0012 | 0.1701 | 0.0036 | 1.102 | 0.014 |
| MQ1_1_24 | 0.0962 | 0.0050 | 0.8127 | 0.0087 | 0.1917 | 0.01675 | 0.00086 | 0.1402 | 0.0051 | 0.751 | 0.025 |
| MQ1_1_25 | 0.1307 | 0.0081 | 0.8096 | 0.0103 | 0.1669 | 0.01708 | 0.0006 | 0.1438 | 0.0038 | 0.527 | 0.018 |
| MQ1_1_26 | 0.0342 | 0.0028 | 0.8179 | 0.0082 | -0.1020 | 0.00952 | 0.00055 | 0.1317 | 0.0039 | 1.092 | 0.031 |
| MQ1_1_27 | 0.0772 | 0.0056 | 0.8125 | 0.0084 | 0.1911 | 0.02 | 0.0011 | 0.0993 | 0.003 | 1.02 | 0.016 |
| MQ1_1_28 | 0.1250 | 0.0053 | 0.8080 | 0.0090 | 0.4058 | 0.02336 | 0.00047 | 0.1072 | 0.0028 | 0.747 | 0.015 |
| MQ1_1_29 | 0.1054 | 0.0042 | 0.8069 | 0.0091 | 0.1749 | 0.02061 | 0.00066 | 0.087 | 0.0028 | 0.801 | 0.01 |
| MQ1_1_30 | 0.2225 | 0.0129 | 0.8127 | 0.0091 | 0.1800 | 0.02859 | 0.00092 | 0.0851 | 0.0026 | 0.518 | 0.011 |
| MQ1_1_31 | 0.0772 | 0.0070 | 0.8092 | 0.0088 | 0.2462 | 0.01357 | 0.00097 | 0.0919 | 0.003 | 0.675 | 0.026 |
| MQ1_1_32 | 0.1449 | 0.0056 | 0.8055 | 0.0085 | 0.4127 | 0.02123 | 0.00058 | 0.0965 | 0.0028 | 0.6 | 0.01 |
| MQ1_1_33 | 0.0564 | 0.0033 | 0.8167 | 0.0097 | 0.1795 | 0.00754 | 0.0003 | 0.0967 | 0.0029 | 0.5406 | 0.0078 |
| MQ1_1_34 | 0.1563 | 0.0103 | 0.8191 | 0.0098 | 0.1423 | 0.0213 | 0.0011 | 0.0868 | 0.0029 | 0.551 | 0.011 |
| MQ1_1_35 | 0.1600 | 0.0086 | 0.8250 | 0.0115 | 0.3575 | 0.01638 | 0.00046 | 0.0848 | 0.0025 | 0.456 | 0.011 |
| MQ1_1_36 | 0.1533 | 0.0058 | 0.8161 | 0.0099 | 0.1723 | 0.02027 | 0.00046 | 0.0919 | 0.0027 | 0.5469 | 0.0076 |
| MQ1_1_37 | 0.0334 | 0.0020 | 0.8110 | 0.0115 | 0.1936 | 0.0039 | 0.0002 | 0.0848 | 0.0027 | 0.474 | 0.01 |
| MQ1_1_38 | 0.0415 | 0.0025 | 0.8163 | 0.0106 | 0.1448 | 0.00398 | 0.00024 | 0.0674 | 0.0024 | 0.3902 | 0.007 |
| MQ1_1_39 | 0.1137 | 0.0047 | 0.8060 | 0.0095 | 0.2710 | 0.01457 | 0.00054 | 0.0802 | 0.0025 | 0.526 | 0.011 |
| MQ1_1_40 | 0.1245 | 0.0061 | 0.8101 | 0.0106 | 0.2978 | 0.0127 | 0.00064 | 0.0732 | 0.003 | 0.414 | 0.01 |
| MQ1_1_41 | 0.2490 | 0.0165 | 0.8164 | 0.0105 | 0.1962 | 0.0254 | 0.0012 | 0.0717 | 0.0026 | 0.4081 | 0.0079 |
| MQ1_1_42 | 0.0569 | 0.0107 | 0.8193 | 0.0115 | 0.3967 | 0.039 | 0.012 | 0.094 | 0.013 | 0.86 | 0.12 |
| MQ1_1_43 | 0.0744 | 0.0169 | 0.8380 | 0.0116 | 0.2400 | 0.045 | 0.01 | 0.123 | 0.015 | 0.95 | 0.15 |
| MQ1_1_44 | 0.0886 | 0.0067 | 0.8122 | 0.0091 | 0.1842 | 0.01129 | 0.00051 | 0.0832 | 0.0026 | 0.517 | 0.016 |
| MQ1_1_45 | 0.0756 | 0.0049 | 0.8296 | 0.0116 | 0.0258 | 0.0084 | 0.001 | 0.0828 | 0.0041 | 0.41 | 0.023 |

**Table 5.** Laser ablation ICP-MS U-Th-Pb Data for sample MQ1-2

| | Data for Tera-Wasserburg plot | | | | | | Concentrations | | | | | |
|---|---|---|---|---|---|---|---|---|---|---|---|---|
| **Identifier** | **238U/206Pb** | **Prop2SE** | **207Pb/206Pb** | **Prop2SE** | **err.corr.** | **Approx_U_PPM** | **Approx_U_PPM_Int2SE** | **Approx_Th_PPM** | **Approx_Th_PPM_Int2SE** | **Approx_Pb_PPM** | **Approx_Pb_PPM_Int2SE** |
| MQ1_2_1 | 0.0234 | 0.0024 | 0.8180 | 0.0154 | 0.0566 | 0.00194 | 0.00014 | 0.0627 | 0.0025 | 0.4094 | 0.0072 |
| MQ1_2_2 | 0.0201 | 0.0017 | 0.8290 | 0.0144 | 0.4497 | 0.00189 | 0.00014 | 0.0486 | 0.0015 | 0.4342 | 0.0094 |
| MQ1_2_3 | 0.0000 | NaN | no value | NaN | NaN | 0.00133 | 0.00011 | 0.0451 | 0.0019 | 0.46 | 0.011 |
| MQ1_2_4 | 0.0141 | 0.0023 | 0.8020 | 0.0242 | -0.0717 | 0.00154 | 0.00014 | 0.0592 | 0.002 | 0.4663 | 0.0079 |
| MQ1_2_5 | 0.0144 | 0.0028 | 0.8220 | 0.0282 | 0.3543 | 0.00191 | 0.00071 | 0.0558 | 0.0023 | 0.466 | 0.011 |
| MQ1_2_6 | 0.0138 | 0.0016 | 0.8360 | 0.0213 | -0.5009 | 0.00165 | 0.00012 | 0.0566 | 0.0026 | 0.505 | 0.013 |
| MQ1_2_7 | 0.0159 | 0.0011 | 0.8121 | 0.0106 | 0.2511 | 0.00218 | 0.00013 | 0.0638 | 0.0023 | 0.5835 | 0.0096 |
| MQ1_2_8 | 0.0163 | 0.0012 | 0.7984 | 0.0099 | 0.2057 | 0.00224 | 0.00013 | 0.0638 | 0.0025 | 0.5497 | 0.0098 |
| MQ1_2_9 | 0.0119 | 0.0075 | 0.8710 | 0.0981 | 1.0000 | 0.00139 | 0.00015 | 0.0508 | 0.0019 | 0.576 | 0.029 |
| MQ1_2_10 | 0.0000 | NaN | no value | NaN | NaN | 0.00097 | 0.0001 | 0.0666 | 0.0034 | 0.627 | 0.017 |
| MQ1_2_11 | 0.0085 | 0.0007 | 0.8380 | 0.0671 | 1.0000 | 0.001153 | 0.000097 | 0.0474 | 0.0021 | 0.619 | 0.017 |
| MQ1_2_12 | 0.0155 | 0.0040 | 0.7790 | 0.0134 | 0.9874 | 0.001367 | 0.000089 | 0.045 | 0.0021 | 0.4162 | 0.0088 |
| MQ1_2_13 | 0.0152 | 0.0059 | 0.8270 | 0.0272 | -0.6016 | 0.00147 | 0.00012 | 0.0448 | 0.002 | 0.4394 | 0.0069 |
| MQ1_2_14 | 0.0125 | 0.0017 | 0.8250 | 0.0183 | 0.2523 | 0.00157 | 0.00023 | 0.0497 | 0.0018 | 0.606 | 0.012 |
| MQ1_2_15 | 0.0130 | 0.0017 | 0.8010 | 0.0213 | 0.2285 | 0.00172 | 0.00012 | 0.0512 | 0.0019 | 0.647 | 0.021 |
| MQ1_2_16 | 0.0000 | NaN | no value | NaN | NaN | 0.000875 | 0.000077 | 0.0723 | 0.0029 | 0.594 | 0.014 |
| MQ1_2_17 | 0.0000 | NaN | no value | NaN | NaN | 0.000828 | 0.000076 | 0.0812 | 0.0024 | 0.557 | 0.04 |
| MQ1_2_18 | 0.0181 | 0.0046 | 0.7800 | 0.0561 | -0.2969 | 0.00143 | 0.00011 | 0.0748 | 0.0027 | 0.3879 | 0.0067 |
| MQ1_2_19 | 0.0000 | NaN | no value | NaN | NaN | 0.00113 | 0.00013 | 0.0699 | 0.0025 | 0.458 | 0.013 |
| MQ1_2_20 | 0.0103 | 0.0007 | 0.8040 | 0.0173 | 0.3811 | 0.00154 | 0.000095 | 0.0748 | 0.0027 | 0.641 | 0.012 |
| MQ1_2_21 | 0.0162 | 0.0030 | 0.8080 | 0.0561 | -0.8089 | 0.00147 | 0.00011 | 0.0615 | 0.0024 | 0.464 | 0.011 |
| MQ1_2_22 | 0.0234 | 0.0030 | 0.8150 | 0.0144 | 0.1528 | 0.00202 | 0.00021 | 0.0767 | 0.0026 | 0.4205 | 0.0078 |
| MQ1_2_23 | 0.0159 | 0.0014 | 0.8250 | 0.0154 | 0.4216 | 0.00212 | 0.00014 | 0.0676 | 0.0022 | 0.595 | 0.015 |
| MQ1_2_24 | 0.0143 | 0.0020 | 0.8270 | 0.0203 | 0.0368 | 0.0018 | 0.00016 | 0.0703 | 0.0023 | 0.607 | 0.012 |
| MQ1_2_25 | 0.0000 | NaN | no value | NaN | NaN | 0.00098 | 0.00011 | 0.0892 | 0.0027 | 0.884 | 0.013 |
| MQ1_2_26 | 0.0171 | 0.0027 | 0.8300 | 0.0164 | -0.2804 | 0.00155 | 0.00019 | 0.0644 | 0.0024 | 0.586 | 0.014 |
| MQ1_2_27 | 0.0148 | 0.0020 | 0.8090 | 0.0164 | 0.0146 | 0.00186 | 0.00017 | 0.0848 | 0.0031 | 0.572 | 0.016 |
| MQ1_2_28 | 0.0187 | 0.0026 | 0.8060 | 0.0134 | 0.0715 | 0.0018 | 0.00013 | 0.1023 | 0.0031 | 0.4507 | 0.0099 |
| MQ1_2_29 | 0.0160 | 0.0017 | 0.8040 | 0.0144 | -0.0830 | 0.00172 | 0.00017 | 0.0954 | 0.0039 | 0.595 | 0.013 |
| MQ1_2_30 | 0.0165 | 0.0014 | 0.8170 | 0.0115 | 0.2247 | 0.00266 | 0.0002 | 0.113 | 0.0038 | 0.752 | 0.018 |
| MQ1_2_31 | 0.0158 | 0.0015 | 0.8166 | 0.0097 | 0.1963 | 0.00295 | 0.00037 | 0.1033 | 0.0033 | 0.653 | 0.023 |
| MQ1_2_32 | 0.0420 | 0.0046 | 0.8200 | 0.0125 | 0.0844 | 0.00608 | 0.00056 | 0.1043 | 0.0032 | 0.553 | 0.013 |
| MQ1_2_33 | 0.0192 | 0.0019 | 0.8010 | 0.0144 | -0.0282 | 0.00197 | 0.00015 | 0.0819 | 0.0025 | 0.4052 | 0.0079 |
| MQ1_2_34 | 0.0195 | 0.0026 | 0.8120 | 0.0135 | 0.0028 | 0.00212 | 0.00022 | 0.0894 | 0.0028 | 0.4662 | 0.0087 |
| MQ1_2_35 | 0.0198 | 0.0018 | 0.8250 | 0.0154 | 0.2466 | 0.00189 | 0.00017 | 0.0858 | 0.003 | 0.4705 | 0.0087 |
| MQ1_2_36 | 0.0225 | 0.0087 | 0.8450 | 0.0651 | 1.0000 | 0.00126 | 0.00012 | 0.0662 | 0.0026 | 0.3758 | 0.0088 |
| MQ1_2_37 | 0.0260 | 0.0021 | 0.8117 | 0.0103 | 0.3132 | 0.0026 | 0.0002 | 0.0785 | 0.0029 | 0.4113 | 0.0095 |
| MQ1_2_38 | 0.0225 | 0.0025 | 0.8040 | 0.0125 | 0.0170 | 0.00212 | 0.00018 | 0.0672 | 0.0022 | 0.4404 | 0.0089 |
| MQ1_2_39 | 0.0264 | 0.0063 | 0.8280 | 0.0392 | 0.2829 | 0.00147 | 0.00012 | 0.061 | 0.0027 | 0.3814 | 0.0078 |
| MQ1_2_40 | 0.0000 | NaN | no value | NaN | NaN | 0.00127 | 0.00011 | 0.0465 | 0.0021 | 0.3142 | 0.0059 |
| MQ1_2_41 | 0.0148 | 0.0034 | 0.8120 | 0.0272 | 0.0861 | 0.001424 | 0.000091 | 0.0769 | 0.0027 | 0.487 | 0.014 |

**Table 6.** Laser ablation ICP-MS U-Th-Pb Data for sample MQ2-1

| | Data for Tera-Wasserburg plot | | | | | | Concentrations | | | | | |
|---|---|---|---|---|---|---|---|---|---|---|---|---|
| **Identifier** | **238U/206Pb** | **Prop2SE** | **207Pb/206Pb** | **Prop2SE** | **err.corr.** | **Approx_U_PPM** | **Approx_U_PPM_Int2SE** | **Approx_Th_PPM** | **Approx_Th_PPM_Int2SE** | **Approx_Pb_PPM** | **Approx_Pb_PPM_Int2SE** |
| MQ2_1_1 | 0.0505 | 0.0039 | 0.7900 | 0.0134 | 0.3017 | 0.00305 | 0.00019 | 0.1026 | 0.0033 | 0.2447 | 0.0051 |
| MQ2_1_2 | 0.1549 | 0.0103 | 0.7894 | 0.0115 | 0.1947 | 0.01449 | 0.00093 | 0.1258 | 0.0046 | 0.3646 | 0.0095 |
| MQ2_1_3 | 0.1102 | 0.0162 | 0.7937 | 0.0115 | 0.1564 | 0.0112 | 0.0015 | 0.097 | 0.0035 | 0.3196 | 0.0059 |
| MQ2_1_4 | 0.4138 | 0.0266 | 0.7960 | 0.0115 | 0.1428 | 0.033 | 0.0019 | 0.0898 | 0.0026 | 0.3162 | 0.0058 |
| MQ2_1_5 | 0.2142 | 0.0157 | 0.8040 | 0.0095 | 0.1352 | 0.0204 | 0.0014 | 0.062 | 0.0026 | 0.3981 | 0.0074 |
| MQ2_1_6 | 0.0444 | 0.0030 | 0.7973 | 0.0099 | -0.1320 | 0.00437 | 0.00027 | 0.083 | 0.0027 | 0.4338 | 0.0073 |
| MQ2_1_7 | 0.0854 | 0.0175 | 0.7970 | 0.0115 | 0.0876 | 0.0151 | 0.0031 | 0.0948 | 0.0026 | 0.3469 | 0.005 |
| MQ2_1_8 | 0.1519 | 0.0177 | 0.8015 | 0.0092 | 0.3303 | 0.0254 | 0.0021 | 0.0665 | 0.0029 | 0.623 | 0.017 |
| MQ2_1_9 | 0.0836 | 0.0094 | 0.7986 | 0.0093 | -0.0605 | 0.01233 | 0.00097 | 0.0593 | 0.0021 | 0.614 | 0.011 |
| MQ2_1_10 | 0.0529 | 0.0038 | 0.8032 | 0.0099 | 0.1523 | 0.00823 | 0.00047 | 0.0707 | 0.0026 | 0.608 | 0.012 |
| MQ2_1_11 | 0.0537 | 0.0129 | 0.7983 | 0.0106 | -0.0155 | 0.0119 | 0.0024 | 0.0653 | 0.0027 | 0.543 | 0.012 |
| MQ2_1_12 | 0.1981 | 0.0303 | 0.8078 | 0.0100 | -0.0818 | 0.03 | 0.0044 | 0.0555 | 0.0021 | 0.4812 | 0.0076 |
| MQ2_1_13 | 0.0430 | 0.0042 | 0.8026 | 0.0097 | 0.0974 | 0.00478 | 0.00045 | 0.0612 | 0.0024 | 0.4239 | 0.0076 |
| MQ2_1_14 | 0.0972 | 0.0080 | 0.8060 | 0.0095 | 0.2007 | 0.0137 | 0.0012 | 0.0543 | 0.0023 | 0.5187 | 0.0081 |
| MQ2_1_15 | 0.0946 | 0.0051 | 0.8071 | 0.0104 | 0.0660 | 0.01065 | 0.00048 | 0.0954 | 0.0031 | 0.4609 | 0.0081 |
| MQ2_1_16 | 0.0793 | 0.0049 | 0.7991 | 0.0092 | -0.1416 | 0.01187 | 0.00084 | 0.0771 | 0.0032 | 0.607 | 0.018 |
| MQ2_1_17 | 0.0283 | 0.0043 | 0.8010 | 0.0090 | 0.0916 | 0.0052 | 0.0012 | 0.0727 | 0.0027 | 0.4703 | 0.0085 |
| MQ2_1_18 | 0.2254 | 0.0090 | 0.7999 | 0.0104 | 0.1750 | 0.03317 | 0.00087 | 0.0524 | 0.0025 | 0.586 | 0.011 |
| MQ2_1_19 | 0.2826 | 0.0136 | 0.7942 | 0.0083 | 0.0597 | 0.0716 | 0.003 | 0.2444 | 0.0094 | 1.018 | 0.019 |
| MQ2_1_20 | 0.1415 | 0.0106 | 0.8036 | 0.0086 | 0.2462 | 0.0267 | 0.0017 | 0.19 | 0.011 | 0.727 | 0.019 |
| MQ2_1_21 | 0.1041 | 0.0076 | 0.7926 | 0.0088 | 0.1529 | 0.0136 | 0.00091 | 0.1632 | 0.0048 | 0.5128 | 0.0093 |
| MQ2_1_22 | 0.0666 | 0.0114 | 0.8002 | 0.0106 | 0.0559 | 0.0095 | 0.0011 | 0.1315 | 0.0038 | 0.492 | 0.011 |
| MQ2_1_23 | 0.0978 | 0.0143 | 0.7980 | 0.0087 | 0.0042 | 0.0153 | 0.0024 | 0.0973 | 0.0042 | 0.4589 | 0.009 |
| MQ2_1_24 | 0.3911 | 0.0299 | 0.8000 | 0.0099 | 0.1073 | 0.0555 | 0.0038 | 0.0751 | 0.0024 | 0.554 | 0.017 |
| MQ2_1_25 | 0.2161 | 0.0152 | 0.8129 | 0.0103 | -0.0033 | 0.0237 | 0.0018 | 0.1416 | 0.0046 | 0.4236 | 0.0086 |
| MQ2_1_26 | 0.1083 | 0.0214 | 0.7990 | 0.0104 | 0.0331 | 0.0197 | 0.0033 | 0.0878 | 0.003 | 0.4545 | 0.0076 |
| MQ2_1_27 | 0.1705 | 0.0173 | 0.8099 | 0.0106 | 0.2172 | 0.0189 | 0.0019 | 0.0839 | 0.003 | 0.437 | 0.012 |
| MQ2_1_28 | 0.1003 | 0.0043 | 0.7990 | 0.0115 | 0.1171 | 0.00914 | 0.00031 | 0.0966 | 0.0032 | 0.3646 | 0.007 |
| MQ2_1_29 | 0.2392 | 0.0131 | 0.7920 | 0.0115 | 0.1941 | 0.01949 | 0.00095 | 0.0863 | 0.0028 | 0.3335 | 0.0056 |
| MQ2_1_30 | 0.1518 | 0.0186 | 0.8003 | 0.0106 | -0.0877 | 0.0159 | 0.002 | 0.1 | 0.0041 | 0.3683 | 0.0077 |
| MQ2_1_31 | 0.8661 | 0.1187 | 0.8031 | 0.0094 | 0.2385 | 0.187 | 0.026 | 0.14 | 0.01 | 0.739 | 0.044 |

**Table 7.** Laser ablation ICP-MS U-Th-Pb Data for sample MQ2-2

| | Data for Tera-Wasserburg plot | | | | | | Concentrations | | | | |
|---|---|---|---|---|---|---|---|---|---|---|---|
| **Identifier** | **238U/206Pb** | **Prop2SE** | **207Pb/206Pb** | **Prop2SE** | **err.corr.** | **Approx_U_PPM** | **Approx_U_PPM_Int2SE** | **Approx_Th_PPM** | **Approx_Th_PPM_Int2SE** | **Approx_Pb_PPM** | **Approx_Pb_PPM_Int2SE** |
| MQ2_2_1 | 3.5558 | 0.3301 | 0.7600 | 0.0134 | 0.1539 | 0.387 | 0.031 | 0.521 | 0.048 | 0.404 | 0.014 |
| MQ2_2_2 | 1.4366 | 0.0717 | 0.7530 | 0.0124 | 0.2022 | 0.1453 | 0.0072 | 0.317 | 0.018 | 0.386 | 0.012 |
| MQ2_2_3 | 0.7425 | 0.0394 | 0.7530 | 0.0173 | 0.4972 | 0.0527 | 0.0023 | 0.272 | 0.015 | 0.271 | 0.011 |
| MQ2_2_4 | 0.1166 | 0.0147 | 0.7776 | 0.0101 | -0.0737 | 0.01592 | 0.00092 | 0.1327 | 0.0051 | 0.52 | 0.046 |
| MQ2_2_5 | 0.2011 | 0.0126 | 0.7690 | 0.0092 | 0.2385 | 0.0237 | 0.0015 | 0.1166 | 0.0031 | 0.454 | 0.024 |
| MQ2_2_6 | 0.1225 | 0.0162 | 0.7803 | 0.0104 | 0.2513 | 0.0184 | 0.0029 | 0.1194 | 0.0034 | 0.528 | 0.013 |
| MQ2_2_7 | 0.0505 | 0.0062 | 0.7831 | 0.0087 | 0.0237 | 0.0088 | 0.00068 | 0.1355 | 0.0048 | 0.624 | 0.033 |
| MQ2_2_8 | 0.4330 | 0.0335 | 0.7800 | 0.0115 | 0.2586 | 0.0589 | 0.0044 | 0.1025 | 0.0054 | 0.576 | 0.014 |
| MQ2_2_9 | 0.1661 | 0.0149 | 0.7826 | 0.0104 | 0.2256 | 0.0209 | 0.0019 | 0.1387 | 0.0062 | 0.517 | 0.019 |
| MQ2_2_10 | 0.0334 | 0.0027 | 0.7790 | 0.0093 | -0.0261 | 0.00555 | 0.00036 | 0.139 | 0.0088 | 0.632 | 0.028 |
| MQ2_2_11 | 0.1410 | 0.0056 | 0.7770 | 0.0084 | 0.0537 | 0.0216 | 0.0011 | 0.1355 | 0.0051 | 0.597 | 0.02 |
| MQ2_2_12 | 0.0775 | 0.0035 | 0.7643 | 0.0099 | 0.3187 | 0.00569 | 0.0002 | 0.1391 | 0.005 | 0.2886 | 0.0071 |
| MQ2_2_13 | 0.2683 | 0.0129 | 0.7730 | 0.0090 | 0.2469 | 0.0381 | 0.0012 | 0.1614 | 0.0055 | 0.569 | 0.013 |
| MQ2_2_14 | 0.0848 | 0.0073 | 0.7779 | 0.0087 | 0.0091 | 0.01197 | 0.00084 | 0.1384 | 0.0052 | 0.547 | 0.015 |
| MQ2_2_15 | 0.0246 | 0.0021 | 0.7784 | 0.0076 | 0.1559 | 0.00528 | 0.00025 | 0.1335 | 0.0049 | 0.837 | 0.052 |
| MQ2_2_16 | 0.0294 | 0.0026 | 0.7762 | 0.0095 | 0.1618 | 0.00523 | 0.00025 | 0.1407 | 0.0085 | 0.68 | 0.043 |
| MQ2_2_17 | 0.0497 | 0.0034 | 0.7814 | 0.0086 | 0.0539 | 0.0081 | 0.00042 | 0.1421 | 0.0045 | 0.623 | 0.012 |
| MQ2_2_18 | 0.1064 | 0.0065 | 0.7784 | 0.0092 | 0.1521 | 0.0221 | 0.001 | 0.1622 | 0.0051 | 0.799 | 0.014 |
| MQ2_2_19 | 0.0400 | 0.0042 | 0.7806 | 0.0084 | 0.1577 | 0.00662 | 0.00074 | 0.1719 | 0.0063 | 0.644 | 0.042 |
| MQ2_2_20 | 0.0544 | 0.0043 | 0.7824 | 0.0078 | 0.0833 | 0.0114 | 0.0012 | 0.1681 | 0.0045 | 0.835 | 0.027 |
| MQ2_2_21 | 0.0529 | 0.0034 | 0.7796 | 0.0091 | 0.2319 | 0.01014 | 0.00056 | 0.1909 | 0.0054 | 0.785 | 0.019 |
| MQ2_2_22 | 0.0403 | 0.0024 | 0.7736 | 0.0092 | -0.1006 | 0.00715 | 0.00041 | 0.229 | 0.0067 | 0.693 | 0.014 |
| MQ2_2_23 | 0.0520 | 0.0031 | 0.7790 | 0.0088 | 0.2464 | 0.00832 | 0.00063 | 0.181 | 0.0047 | 0.635 | 0.021 |
| MQ2_2_24 | 0.0689 | 0.0045 | 0.7731 | 0.0081 | 0.1790 | 0.01087 | 0.0009 | 0.2611 | 0.008 | 0.62 | 0.02 |
| MQ2_2_25 | 0.0512 | 0.0044 | 0.7785 | 0.0083 | 0.0756 | 0.01055 | 0.00082 | 0.2934 | 0.0082 | 0.774 | 0.02 |
| MQ2_2_26 | 0.0398 | 0.0025 | 0.7781 | 0.0085 | -0.0060 | 0.00947 | 0.00043 | 0.3311 | 0.0064 | 0.94 | 0.017 |
| MQ2_2_27 | 0.0525 | 0.0035 | 0.7833 | 0.0083 | 0.0118 | 0.01005 | 0.00064 | 0.4003 | 0.009 | 0.798 | 0.013 |
| MQ2_2_28 | 0.1421 | 0.0128 | 0.7679 | 0.0099 | -0.0743 | 0.0268 | 0.0022 | 0.4151 | 0.0095 | 0.773 | 0.018 |
| MQ2_2_29 | 0.0983 | 0.0058 | 0.7816 | 0.0088 | 0.2253 | 0.0207 | 0.001 | 0.553 | 0.011 | 0.8322 | 0.0091 |
| MQ2_2_30 | 0.0311 | 0.0018 | 0.7777 | 0.0087 | 0.0949 | 0.00596 | 0.00034 | 0.4359 | 0.0068 | 0.732 | 0.01 |
| MQ2_2_31 | 0.0421 | 0.0019 | 0.7815 | 0.0099 | 0.2424 | 0.00643 | 0.00022 | 0.2742 | 0.0058 | 0.618 | 0.013 |
| MQ2_2_32 | 0.0514 | 0.0032 | 0.7820 | 0.0115 | 0.2656 | 0.00853 | 0.00035 | 0.29 | 0.0068 | 0.692 | 0.022 |
| MQ2_2_33 | 0.0692 | 0.0031 | 0.7710 | 0.0090 | 0.3686 | 0.00996 | 0.00055 | 0.2873 | 0.0062 | 0.644 | 0.034 |
| MQ2_2_34 | 0.0632 | 0.0044 | 0.7777 | 0.0097 | 0.0694 | 0.00961 | 0.00087 | 0.2614 | 0.0053 | 0.581 | 0.028 |
| MQ2_2_35 | 0.0385 | 0.0029 | 0.7746 | 0.0105 | -0.1241 | 0.00444 | 0.00021 | 0.2639 | 0.0066 | 0.454 | 0.019 |
| MQ2_2_36 | 0.0379 | 0.0022 | 0.7711 | 0.0084 | -0.0974 | 0.00745 | 0.00043 | 0.273 | 0.0072 | 0.773 | 0.019 |
| MQ2_2_37 | 0.0407 | 0.0024 | 0.7820 | 0.0115 | 0.1333 | 0.00584 | 0.00027 | 0.2452 | 0.006 | 0.575 | 0.015 |
| MQ2_2_38 | 0.0411 | 0.0022 | 0.7772 | 0.0088 | 0.1985 | 0.00613 | 0.00027 | 0.1715 | 0.006 | 0.5866 | 0.009 |
| MQ2_2_39 | 0.0748 | 0.0031 | 0.7720 | 0.0115 | 0.3558 | 0.01339 | 0.00049 | 0.1469 | 0.0071 | 0.696 | 0.018 |
| MQ2_2_40 | 1.4574 | 0.1120 | 0.7493 | 0.0105 | 0.1423 | 0.1091 | 0.0082 | 0.32 | 0.013 | 0.2776 | 0.0063 |
| MQ2_2_41 | 1.0904 | 0.0504 | 0.7430 | 0.0134 | 0.0373 | 0.0817 | 0.0031 | 0.209 | 0.01 | 0.2834 | 0.0066 |
| MQ2_2_42 | 1.6678 | 0.0614 | 0.7495 | 0.0095 | 0.4296 | 0.2373 | 0.0053 | 0.482 | 0.012 | 0.542 | 0.011 |

**Table 8.** Laser ablation ICP-MS U-Th-Pb Data for sample MQ3-1

| Data for Tera-Wasserburg plot | | | | | | | Concentrations | | | | |
|---|---|---|---|---|---|---|---|---|---|---|---|
| Identifier | 238U/206Pb | Prop2SE | 207Pb/206Pb | Prop2SE | err.corr. | Approx_U_PPM | Approx_U_PPM_Int2SE | Approx_Th_PPM | Approx_Th_PPM_Int2SE | Approx_Pb_PPM | Approx_Pb_PPM_Int2SE |
| MQ3_1 | 20.2425 | 0.7464 | 0.5149 | 0.0065 | 0.3191 | 4.026 | 0.09 | 3.29 | 0.11 | 0.528 | 0.011 |
| MQ3_2 | 23.0518 | 0.8243 | 0.4914 | 0.0062 | 0.3605 | 5.256 | 0.074 | 1.155 | 0.018 | 0.56 | 0.01 |
| MQ3_3 | 22.4958 | 1.1647 | 0.4820 | 0.0151 | -0.6587 | 6.27 | 0.19 | 1.125 | 0.064 | 0.661 | 0.036 |
| MQ3_4 | 32.2137 | 1.1194 | 0.3421 | 0.0046 | 0.3045 | 10.99 | 0.28 | 2.395 | 0.058 | 0.563 | 0.016 |
| MQ3_5 | 43.0737 | 1.4297 | 0.2341 | 0.0037 | 0.4364 | 26.2 | 0.51 | 1.868 | 0.068 | 0.626 | 0.011 |
| MQ3_6 | 49.0106 | 1.6321 | 0.1642 | 0.0020 | 0.3673 | 57.75 | 0.77 | 3.13 | 0.075 | 0.768 | 0.011 |
| MQ3_7 | 34.7528 | 1.2757 | 0.3380 | 0.0111 | -0.5000 | 12.63 | 0.43 | 1.813 | 0.028 | 0.579 | 0.017 |
| MQ3_8 | 19.6838 | 0.9388 | 0.5074 | 0.0090 | -0.2559 | 5.033 | 0.088 | 0.171 | 0.0042 | 0.65 | 0.025 |
| MQ3_9 | 21.3849 | 0.7568 | 0.5036 | 0.0068 | 0.4400 | 4.08 | 0.071 | 0.421 | 0.012 | 0.48 | 0.014 |
| MQ3_10 | 29.4302 | 1.3998 | 0.3980 | 0.0171 | -0.4632 | 7.51 | 0.59 | 0.323 | 0.011 | 0.4462 | 0.0094 |
| MQ3_11 | 21.7298 | 0.9492 | 0.5078 | 0.0095 | -0.5242 | 4.85 | 0.13 | 0.0799 | 0.0042 | 0.57 | 0.019 |
| MQ3_12 | 24.3479 | 0.9920 | 0.4843 | 0.0099 | -0.4728 | 4.67 | 0.18 | 0.606 | 0.011 | 0.447 | 0.022 |
| MQ3_13 | 19.5253 | 0.7831 | 0.5277 | 0.0080 | -0.1599 | 3.66 | 0.22 | 0.433 | 0.011 | 0.483 | 0.016 |
| MQ3_14 | 19.6519 | 0.6821 | 0.5285 | 0.0079 | 0.1854 | 3.36 | 0.13 | 0.2895 | 0.0086 | 0.451 | 0.019 |
| MQ3_15 | 20.5861 | 0.7387 | 0.5210 | 0.0081 | 0.2434 | 3.47 | 0.16 | 0.2473 | 0.0065 | 0.422 | 0.017 |
| MQ3_16 | 37.3084 | 1.2679 | 0.3193 | 0.0048 | 0.1897 | 10.57 | 0.19 | 0.385 | 0.021 | 0.4125 | 0.0082 |
| MQ3_17 | 31.7415 | 1.4573 | 0.3760 | 0.0101 | -0.6595 | 9.09 | 0.24 | 0.1097 | 0.0038 | 0.506 | 0.018 |
| MQ3_18 | 23.4531 | 0.9280 | 0.4772 | 0.0093 | -0.4983 | 7.656 | 0.08 | 0.3467 | 0.0063 | 0.754 | 0.025 |
| MQ3_19 | 41.9123 | 1.5235 | 0.2543 | 0.0050 | -0.3283 | 17.99 | 0.32 | 2.325 | 0.099 | 0.517 | 0.017 |
| MQ3_20 | 38.4318 | 1.3334 | 0.2895 | 0.0093 | -0.3451 | 15.28 | 0.7 | 1.076 | 0.024 | 0.515 | 0.011 |
| MQ3_21 | 29.0773 | 1.3054 | 0.4140 | 0.0121 | -0.7835 | 10.51 | 0.42 | 0.1406 | 0.0076 | 0.696 | 0.032 |
| MQ3_22 | 26.2451 | 1.6112 | 0.4300 | 0.0161 | -0.8472 | 8.1 | 0.25 | 1.333 | 0.063 | 0.634 | 0.049 |
| MQ3_23 | 33.2380 | 1.1811 | 0.3492 | 0.0075 | -0.1953 | 9.79 | 0.24 | 0.288 | 0.014 | 0.483 | 0.013 |
| MQ3_24 | 35.0440 | 1.2944 | 0.3210 | 0.0121 | -0.6771 | 11.05 | 0.63 | 0.658 | 0.05 | 0.4595 | 0.0075 |
| MQ3_25 | 46.6535 | 1.6219 | 0.1875 | 0.0030 | -0.2034 | 36.41 | 0.69 | 2.013 | 0.067 | 0.61 | 0.017 |
| MQ3_26 | 19.9757 | 0.7014 | 0.5272 | 0.0084 | -0.0276 | 3.493 | 0.085 | 1.121 | 0.022 | 0.457 | 0.01 |
| MQ3_27 | 17.5728 | 0.7400 | 0.5503 | 0.0101 | -0.3697 | 3.24 | 0.15 | 2.393 | 0.059 | 0.5112 | 0.0094 |
| MQ3_28 | 19.8449 | 0.7211 | 0.5323 | 0.0079 | -0.2474 | 3.75 | 0.11 | 3.58 | 0.084 | 0.5043 | 0.0088 |
| MQ3_29 | 28.0287 | 0.9936 | 0.4097 | 0.0077 | -0.0771 | 6.27 | 0.27 | 2.103 | 0.072 | 0.458 | 0.013 |
| MQ3_30 | 31.2990 | 1.0659 | 0.3746 | 0.0058 | 0.1665 | 8.33 | 0.11 | 2.231 | 0.03 | 0.4899 | 0.0088 |
| MQ3_31 | 20.0749 | 0.6521 | 0.5199 | 0.0071 | 0.0209 | 3.406 | 0.066 | 1.82 | 0.16 | 0.453 | 0.011 |
| MQ3_32 | 30.6968 | 1.4417 | 0.3930 | 0.0121 | -0.7564 | 7.76 | 0.58 | 0.522 | 0.056 | 0.424 | 0.021 |
| MQ3_33 | 30.9317 | 0.9802 | 0.3785 | 0.0050 | 0.5082 | 6.705 | 0.084 | 3.778 | 0.038 | 0.4099 | 0.0073 |
| MQ3_34 | 30.2526 | 1.0064 | 0.4020 | 0.0058 | 0.1236 | 6.62 | 0.12 | 0.36 | 0.017 | 0.426 | 0.011 |
| MQ3_35 | 23.0957 | 0.8270 | 0.4876 | 0.0079 | -0.2708 | 3.69 | 0.12 | 0.529 | 0.014 | 0.3788 | 0.0067 |
| MQ3_36 | 20.7553 | 0.6895 | 0.5128 | 0.0079 | -0.3422 | 3.248 | 0.098 | 0.4882 | 0.0095 | 0.3899 | 0.0077 |
| MQ3_37 | 23.7470 | 0.8283 | 0.4718 | 0.0071 | -0.0760 | 4.68 | 0.15 | 0.593 | 0.013 | 0.456 | 0.015 |
| MQ3_38 | 22.4126 | 1.0799 | 0.4900 | 0.0112 | -0.7041 | 4.03 | 0.28 | 0.331 | 0.017 | 0.4192 | 0.0096 |
| MQ3_39 | 31.2748 | 1.0645 | 0.3795 | 0.0073 | -0.2602 | 9.22 | 0.21 | 0.2619 | 0.0079 | 0.537 | 0.016 |
| MQ3_40 | 21.1610 | 0.8716 | 0.4951 | 0.0092 | 0.0111 | 4.066 | 0.094 | 0.313 | 0.013 | 0.454 | 0.011 |
| MQ3_41 | 20.3546 | 0.6956 | 0.5127 | 0.0070 | 0.2379 | 3.8 | 0.23 | 1.88 | 0.041 | 0.478 | 0.022 |
| MQ3_42 | 20.8337 | 0.7849 | 0.5093 | 0.0082 | -0.4472 | 4.14 | 0.12 | 1.877 | 0.046 | 0.498 | 0.017 |
| MQ3_43 | 23.8592 | 0.8350 | 0.4719 | 0.0066 | -0.0072 | 3.48 | 0.11 | 1.011 | 0.042 | 0.3405 | 0.008 |
| MQ3_44 | 23.4078 | 1.0052 | 0.4834 | 0.0098 | -0.6331 | 4.73 | 0.22 | 0.878 | 0.03 | 0.4738 | 0.0091 |
| MQ3_45 | 25.9086 | 0.9627 | 0.4518 | 0.0067 | -0.3505 | 5.4 | 0.11 | 2.189 | 0.052 | 0.458 | 0.011 |
| MQ3_46 | 40.1232 | 1.3685 | 0.2735 | 0.0072 | -0.1586 | 18.22 | 0.69 | 0.71 | 0.025 | 0.553 | 0.012 |
| MQ3_47 | 23.8827 | 0.7971 | 0.4767 | 0.0082 | 0.1868 | 3.862 | 0.04 | 0.244 | 0.011 | 0.3824 | 0.0076 |
| MQ3_48 | 24.4954 | 1.0470 | 0.4545 | 0.0074 | 0.0205 | 4.98 | 0.069 | 1.708 | 0.038 | 0.456 | 0.016 |
| MQ3_49 | 21.2723 | 0.7500 | 0.5079 | 0.0081 | -0.1877 | 2.65 | 0.12 | 0.787 | 0.03 | 0.314 | 0.0086 |
| MQ3_50 | 33.0568 | 1.1701 | 0.3642 | 0.0053 | -0.2965 | 12.06 | 0.27 | 1.284 | 0.029 | 0.641 | 0.016 |
| MQ3_51 | 32.4638 | 1.2085 | 0.3371 | 0.0042 | -0.3019 | 10.45 | 0.17 | 0.979 | 0.019 | 0.509 | 0.013 |
| MQ3_52 | 31.4533 | 1.0748 | 0.3553 | 0.0070 | -0.4242 | 10.88 | 0.23 | 1.286 | 0.038 | 0.583 | 0.02 |
| MQ3_53 | 43.9958 | 1.5620 | 0.2272 | 0.0045 | -0.4624 | 19.99 | 0.29 | 0.984 | 0.022 | 0.44 | 0.012 |

**Table 9.** Laser ablation ICP-MS U-Th-Pb Data for sample MQ3-2

| Data for Tera-Wasserburg plot | | | | | | | Concentrations | | | | | |
|---|---|---|---|---|---|---|---|---|---|---|---|---|
| **Identifier** | **238U/206Pb** | **Prop2SE** | **207Pb/206Pb** | **Prop2SE** | **err.corr.** | **Approx_U_PPM** | **Approx_U_PPM_Int2SE** | **Approx_Th_PPM** | **Approx_Th_PPM_Int2SE** | **Approx_Pb_PPM** | **Approx_Pb_PPM_Int2SE** |
| MQ3_2_1 | 0.1689 | 0.01544 | 0.8110 | 0.01807 | -0.0595 | 0.01070 | 0.0013 | 0.01520 | 0.0020 | 0.24900 | 0.0220 |
| MQ3_2_2 | 0.0516 | 0.00588 | 0.8200 | 0.00915 | 0.1496 | 0.00632 | 0.0006 | 0.02950 | 0.0016 | 0.47600 | 0.0240 |
| MQ3_2_3 | 0.0263 | 0.00262 | 0.8277 | 0.00876 | 0.1936 | 0.00393 | 0.0003 | 0.02700 | 0.0017 | 0.58800 | 0.0400 |
| MQ3_2_4 | 0.0000 | NaN | no value | NaN | NaN | 0.00018 | 0.0000 | 0.03350 | 0.0017 | 0.58400 | 0.0480 |
| MQ3_2_5 | 0.0000 | NaN | no value | NaN | NaN | 0.00043 | 0.0001 | 0.03160 | 0.0018 | 0.79000 | 0.0210 |
| MQ3_2_6 | 0.1090 | 0.00602 | 0.8140 | 0.01013 | 0.3694 | 0.01386 | 0.0005 | 0.03570 | 0.0029 | 0.53200 | 0.0140 |
| MQ3_2_7 | 0.0313 | 0.00237 | 0.7962 | 0.00973 | 0.0789 | 0.00678 | 0.0004 | 0.04540 | 0.0030 | 0.81900 | 0.0370 |
| MQ3_2_8 | 0.0499 | 0.00332 | 0.8154 | 0.00768 | 0.1015 | 0.01366 | 0.0007 | 0.06340 | 0.0022 | 1.13300 | 0.0240 |
| MQ3_2_9 | 0.0150 | 0.00135 | 0.8146 | 0.00885 | -0.3133 | 0.00389 | 0.0004 | 0.06300 | 0.0028 | 0.97600 | 0.0240 |
| MQ3_2_10 | 0.0216 | 0.00150 | 0.8148 | 0.00797 | 0.3440 | 0.00530 | 0.0003 | 0.13220 | 0.0050 | 1.02200 | 0.0290 |
| MQ3_2_11 | 0.0852 | 0.00548 | 0.8190 | 0.01609 | 0.5637 | 0.01263 | 0.0004 | 0.20130 | 0.0076 | 0.64800 | 0.0210 |
| MQ3_2_12 | 0.0411 | 0.00287 | 0.8140 | 0.01112 | 0.2527 | 0.00425 | 0.0003 | 0.10580 | 0.0035 | 0.40700 | 0.0130 |
| MQ3_2_13 | 0.0557 | 0.00465 | 0.8099 | 0.00994 | 0.1720 | 0.00632 | 0.0004 | 0.06010 | 0.0032 | 0.43400 | 0.0210 |
| MQ3_2_14 | 0.0395 | 0.00312 | 0.8210 | 0.01311 | -0.0213 | 0.00523 | 0.0004 | 0.04730 | 0.0029 | 0.53500 | 0.0190 |
| MQ3_2_15 | 0.0610 | 0.00548 | 0.8190 | 0.00837 | -0.0612 | 0.00926 | 0.0008 | 0.08500 | 0.0028 | 0.59700 | 0.0130 |
| MQ3_2_16 | 0.0196 | 0.00220 | 0.8160 | 0.00846 | 0.1081 | 0.00354 | 0.0003 | 0.07320 | 0.0027 | 0.71800 | 0.0150 |
| MQ3_2_17 | 0.0083 | 0.00071 | 0.8167 | 0.00768 | 0.1715 | 0.00242 | 0.0002 | 0.07310 | 0.0032 | 1.17900 | 0.0250 |
| MQ3_2_18 | 0.0000 | NaN | no value | NaN | NaN | 0.00033 | 0.0000 | 0.07160 | 0.0035 | 0.64900 | 0.0110 |
| MQ3_2_19 | 0.0286 | 0.00369 | 0.8040 | 0.01409 | -0.0280 | 0.00291 | 0.0003 | 0.05750 | 0.0034 | 0.42500 | 0.0190 |
| MQ3_2_20 | 0.0148 | 0.00108 | 0.8099 | 0.00729 | 0.1985 | 0.00443 | 0.0003 | 0.03920 | 0.0022 | 1.19500 | 0.0380 |
| MQ3_2_21 | 0.0000 | NaN | no value | NaN | NaN | 0.00016 | 0.0000 | 0.04780 | 0.0022 | 0.40410 | 0.0091 |
| MQ3_2_22 | 0.0281 | 0.00231 | 0.8320 | 0.01212 | 0.0057 | 0.00299 | 0.0002 | 0.26010 | 0.0076 | 0.44000 | 0.0150 |
| MQ3_2_23 | 0.0355 | 0.00431 | 0.8200 | 0.01311 | 0.1656 | 0.00832 | 0.0009 | 0.20500 | 0.0100 | 0.94300 | 0.0200 |
| MQ3_2_24 | 0.0239 | 0.00178 | 0.8190 | 0.01211 | 0.1242 | 0.00578 | 0.0004 | 0.27340 | 0.0091 | 1.04100 | 0.0220 |
| MQ3_2_25 | 0.0241 | 0.00164 | 0.8270 | 0.02605 | 0.0536 | 0.00442 | 0.0003 | 0.29300 | 0.0160 | 0.76400 | 0.0330 |
| MQ3_2_26 | 0.0000 | NaN | no value | NaN | NaN | 0.00040 | 0.0001 | 0.26320 | 0.0065 | 0.56000 | 0.0270 |
| MQ3_2_27 | 0.0151 | 0.00252 | 0.8280 | 0.01808 | -0.0421 | 0.00197 | 0.0004 | 0.33200 | 0.0120 | 0.47200 | 0.0180 |
| MQ3_2_28 | 0.0232 | 0.00173 | 0.8154 | 0.00994 | -0.0099 | 0.00238 | 0.0002 | 0.17350 | 0.0044 | 0.40420 | 0.0082 |
| MQ3_2_29 | 0.0000 | NaN | no value | NaN | NaN | 0.00031 | 0.0000 | 0.18400 | 0.0150 | 0.15360 | 0.0073 |
| MQ3_2_30 | 0.0000 | NaN | no value | NaN | NaN | 0.00050 | 0.0001 | 0.16050 | 0.0044 | 0.23730 | 0.0057 |
| MQ3_2_31 | 0.0695 | 0.00461 | 0.8336 | 0.01014 | 0.3059 | 0.00852 | 0.0005 | 0.15920 | 0.0048 | 0.50900 | 0.0110 |
| MQ3_2_32 | 0.0315 | 0.00549 | 0.8350 | 0.02506 | -0.1712 | 0.00232 | 0.0004 | 0.25000 | 0.0120 | 0.28350 | 0.0065 |
| MQ3_2_33 | 0.0000 | NaN | no value | NaN | NaN | 0.00007 | 0.0000 | 0.06000 | 0.0120 | 0.06000 | 0.0120 |
| MQ3_2_34 | 0.0376 | 0.00212 | 0.8170 | 0.01509 | 0.2173 | 0.00645 | 0.0004 | 0.11090 | 0.0037 | 0.69700 | 0.0400 |

# Appendix B: U-Pb Data Session 2

**Table 10.** Laser ablation ICP-MS U-Th-Pb Data for reference material DBTL

| Data for Tera-Wasserburg plot | | | | | | | Concentrations | | | | |
|---|---|---|---|---|---|---|---|---|---|---|---|
| **Identifier** | **238U/206Pb** | **Prop2SE** | **207Pb/206Pb** | **Prop2SE** | **err.corr.** | **Approx_U_PPM** | **Approx_U_PPM_Int2SE** | **Approx_Th_PPM** | **Approx_Th_PPM_Int2SE** | **Approx_Pb_PPM** | **Approx_Pb_PPM_Int2SE** |
| DBTL_1 | 54.8567 | 1.8602 | 0.3593 | 0.0058 | -0.5068 | 13.25 | 0.18 | 0.0687 | 0.0033 | 0.427 | 0.018 |
| DBTL_2 | 60.2865 | 2.1698 | 0.3309 | 0.0070 | -0.5176 | 19.05 | 0.31 | 0.0787 | 0.0033 | 0.521 | 0.03 |
| DBTL_3 | 69.4913 | 2.0291 | 0.2645 | 0.0032 | 0.2834 | 21.2 | 0.3 | 0.0544 | 0.0025 | 0.38 | 0.01 |
| DBTL_4 | 60.1697 | 2.2911 | 0.3346 | 0.0073 | -0.5408 | 16.63 | 0.15 | 0.0451 | 0.0019 | 0.447 | 0.023 |
| DBTL_5 | 61.5406 | 2.6339 | 0.3250 | 0.0110 | -0.8278 | 15.51 | 0.18 | 0.0525 | 0.0024 | 0.401 | 0.028 |
| DBTL_6 | 58.4433 | 1.8432 | 0.3454 | 0.0051 | -0.0660 | 13.59 | 0.36 | 0.045 | 0.0022 | 0.401 | 0.017 |
| DBTL_7 | 64.6465 | 2.3973 | 0.3050 | 0.0072 | -0.7155 | 15.64 | 0.37 | 0.0519 | 0.0033 | 0.371 | 0.025 |
| DBTL_8 | 58.1697 | 2.7009 | 0.3620 | 0.0140 | -0.8421 | 13.83 | 0.16 | 0.0416 | 0.0024 | 0.437 | 0.036 |
| DBTL_9 | 66.1963 | 2.5954 | 0.2910 | 0.0100 | -0.6761 | 16.88 | 0.21 | 0.052 | 0.0025 | 0.358 | 0.025 |
| DBTL_10 | 60.3451 | 2.6751 | 0.3180 | 0.0100 | -0.6953 | 14.32 | 0.13 | 0.0453 | 0.0025 | 0.368 | 0.025 |
| DBTL_11 | 67.9707 | 2.4905 | 0.2720 | 0.0069 | -0.6150 | 17.08 | 0.19 | 0.0439 | 0.0023 | 0.327 | 0.018 |
| DBTL_12 | 65.9504 | 2.4843 | 0.2938 | 0.0078 | -0.6194 | 15.89 | 0.15 | 0.0696 | 0.0029 | 0.339 | 0.016 |
| DBTL_13 | 66.3377 | 2.1716 | 0.2866 | 0.0060 | -0.3301 | 14.97 | 0.21 | 0.0625 | 0.0036 | 0.305 | 0.01 |
| DBTL_14 | 66.4441 | 2.3302 | 0.2770 | 0.0062 | -0.3844 | 15.54 | 0.24 | 0.0549 | 0.0027 | 0.302 | 0.012 |
| DBTL_15 | 67.5274 | 2.2391 | 0.2700 | 0.0048 | -0.0597 | 15.16 | 0.23 | 0.0494 | 0.0034 | 0.296 | 0.011 |
| DBTL_16 | 66.1963 | 2.1936 | 0.2898 | 0.0051 | -0.2927 | 14.93 | 0.21 | 0.0434 | 0.0022 | 0.303 | 0.012 |
| DBTL_17 | 65.9154 | 2.2374 | 0.2925 | 0.0066 | -0.2154 | 15.38 | 0.19 | 0.0403 | 0.0025 | 0.322 | 0.011 |
| DBTL_18 | 57.2319 | 1.8674 | 0.3534 | 0.0084 | -0.3535 | 14.15 | 0.37 | 0.0477 | 0.0082 | 0.424 | 0.015 |
| DBTL_19 | 61.5711 | 2.1723 | 0.3310 | 0.0120 | -0.6714 | 15.73 | 0.4 | 0.0379 | 0.003 | 0.42 | 0.028 |
| DBTL_20 | 60.9968 | 1.9827 | 0.3258 | 0.0058 | 0.5735 | 14.22 | 0.13 | 0.0516 | 0.0027 | 0.373 | 0.01 |
| DBTL_21 | 61.2675 | 2.0492 | 0.3268 | 0.0070 | -0.4462 | 15.96 | 0.22 | 0.0302 | 0.0024 | 0.415 | 0.016 |
| DBTL_22 | 52.6932 | 1.5859 | 0.3741 | 0.0048 | 0.4830 | 12.46 | 0.14 | 0.0402 | 0.0022 | 0.455 | 0.01 |
| DBTL_23 | 68.1945 | 2.3417 | 0.2838 | 0.0075 | -0.2860 | 15.08 | 0.18 | 0.0631 | 0.0033 | 0.292 | 0.014 |
| DBTL_24 | 67.0899 | 1.9734 | 0.2832 | 0.0040 | 0.0763 | 15.91 | 0.31 | 0.0724 | 0.0031 | 0.3204 | 0.0092 |
| DBTL_25 | 61.3886 | 1.9790 | 0.3224 | 0.0074 | -0.2554 | 16.47 | 0.28 | 0.0587 | 0.0031 | 0.434 | 0.016 |
| DBTL_26 | 61.5406 | 2.0651 | 0.3203 | 0.0061 | -0.3195 | 14.32 | 0.22 | 0.0614 | 0.0032 | 0.361 | 0.013 |
| DBTL_27 | 59.1106 | 1.8090 | 0.3333 | 0.0051 | -0.4206 | 13.76 | 0.12 | 0.0915 | 0.0037 | 0.382 | 0.011 |
| DBTL_28 | 56.5804 | 2.2365 | 0.3542 | 0.0083 | -0.5775 | 17.5 | 0.32 | 0.0497 | 0.0029 | 0.552 | 0.022 |
| DBTL_29 | 60.6396 | 2.5906 | 0.3250 | 0.0130 | -0.7186 | 14.72 | 0.16 | 0.0359 | 0.0023 | 0.389 | 0.03 |
| DBTL_30 | 67.3444 | 2.1361 | 0.2772 | 0.0056 | -0.0919 | 16.6 | 0.25 | 0.0568 | 0.0025 | 0.326 | 0.012 |
| DBTL_31 | 56.5032 | 1.8923 | 0.3546 | 0.0069 | -0.2895 | 15.57 | 0.41 | 0.0567 | 0.0027 | 0.478 | 0.027 |
| DBTL_32 | 39.8111 | 1.5638 | 0.4714 | 0.0092 | -0.4334 | 8.18 | 0.13 | 0.0273 | 0.0022 | 0.519 | 0.022 |
| DBTL_33 | 22.8528 | 0.7095 | 0.1077 | 0.0049 | -0.3325 | 3.795 | 0.047 | 0.00257 | 0.00062 | 0.0485 | 0.0045 |
| DBTL_34 | 47.6603 | 1.8087 | 0.4240 | 0.0101 | -0.6631 | 14.25 | 0.34 | 0.04 | 0.0024 | 0.665 | 0.044 |

**Table 11.** Laser ablation ICP-MS U-Th-Pb Data for reference material WC1

| Data for Tera-Wasserburg plot | | | | | | | Concentrations | | | | | |
|---|---|---|---|---|---|---|---|---|---|---|---|---|
| **Identifier** | **238U/206Pb** | **Prop2SE** | **207Pb/206Pb** | **Prop2SE** | **err.corr.** | **Approx_U_PPM** | **Approx_U_PPM_Int2SE** | **Approx_Th_PPM** | **Approx_Th_PPM_Int2SE** | **Approx_Pb_PPM** | **Approx_Pb_PPM_Int2SE** |
| WC1_1 | 22.1480 | 0.7733 | 0.1101 | 0.0040 | -0.4934 | 4.82 | 0.11 | 0.00176 | 0.00042 | 0.0715 | 0.0076 |
| WC1_2 | 21.6842 | 0.7452 | 0.1124 | 0.0045 | -0.2378 | 3.813 | 0.091 | 0.00219 | 0.00043 | 0.0551 | 0.0047 |
| WC1_3 | 21.2758 | 0.7524 | 0.1316 | 0.0030 | 0.1859 | 3.989 | 0.081 | 0.00126 | 0.00035 | 0.0807 | 0.0037 |
| WC1_4 | 22.7565 | 0.8110 | 0.0895 | 0.0031 | 0.2454 | 4.532 | 0.078 | 0.00288 | 0.00057 | 0.0411 | 0.0024 |
| WC1_5 | 22.0302 | 0.7325 | 0.0955 | 0.0025 | -0.1319 | 4.3 | 0.13 | 0.00145 | 0.00035 | 0.0428 | 0.0025 |
| WC1_6 | 22.5091 | 0.7956 | 0.1096 | 0.0031 | -0.1495 | 4.38 | 0.11 | 0.00097 | 0.00048 | 0.0599 | 0.0028 |
| WC1_7 | 21.3856 | 0.6960 | 0.1364 | 0.0026 | -0.2221 | 3.755 | 0.047 | 0.00093 | 0.0003 | 0.0802 | 0.0034 |
| WC1_8 | 22.5500 | 0.7627 | 0.1028 | 0.0026 | 0.0364 | 5.05 | 0.14 | 0.00177 | 0.00039 | 0.0599 | 0.0036 |
| WC1_9 | 22.7232 | 0.7027 | 0.0920 | 0.0023 | -0.1288 | 4.432 | 0.053 | 0.00263 | 0.00055 | 0.0461 | 0.0035 |
| WC1_10 | 22.5541 | 0.6939 | 0.0928 | 0.0034 | 0.1320 | 3.936 | 0.046 | 0.00177 | 0.00046 | 0.0398 | 0.003 |
| WC1_11 | 22.7149 | 0.7724 | 0.0957 | 0.0036 | 0.1180 | 4.077 | 0.044 | 0.00214 | 0.00048 | 0.0437 | 0.0028 |
| WC1_12 | 22.4684 | 0.7579 | 0.1126 | 0.0024 | 0.4822 | 3.959 | 0.054 | 0.00131 | 0.00041 | 0.0555 | 0.0033 |
| WC1_13 | 22.9414 | 0.7497 | 0.0899 | 0.0020 | -0.1814 | 3.25 | 0.055 | 0.00057 | 0.00027 | 0.0291 | 0.0014 |
| WC1_14 | 22.4279 | 0.7556 | 0.0885 | 0.0028 | -0.0820 | 3.709 | 0.035 | 0.00172 | 0.00047 | 0.0347 | 0.0032 |
| WC1_15 | 21.7983 | 0.7854 | 0.0836 | 0.0030 | -0.2421 | 3.61 | 0.082 | 0.00082 | 0.00029 | 0.0288 | 0.0034 |
| WC1_16 | 22.3071 | 0.7831 | 0.0789 | 0.0025 | 0.0842 | 3.699 | 0.085 | 0.00157 | 0.00038 | 0.0254 | 0.0025 |
| WC1_17 | 21.3489 | 0.6939 | 0.1136 | 0.0026 | 0.0055 | 3.936 | 0.08 | 0.00185 | 0.00053 | 0.0604 | 0.0026 |
| WC1_18 | 21.7601 | 0.7498 | 0.0892 | 0.0052 | -0.2754 | 4.198 | 0.068 | 0.00197 | 0.00049 | 0.0424 | 0.0075 |
| WC1_19 | 22.1480 | 0.7733 | 0.0830 | 0.0025 | -0.1145 | 3.67 | 0.06 | 0.00152 | 0.00043 | 0.0307 | 0.0024 |
| WC1_20 | 22.3472 | 0.7855 | 0.0754 | 0.0024 | -0.0298 | 4.16 | 0.1 | 0.0018 | 0.00041 | 0.024 | 0.0022 |
| WC1_21 | 22.4684 | 0.7579 | 0.0983 | 0.0027 | 0.1156 | 4.171 | 0.084 | 0.00185 | 0.00049 | 0.0479 | 0.0028 |
| WC1_22 | 22.1480 | 0.8427 | 0.0862 | 0.0020 | 0.1872 | 5.53 | 0.071 | 0.00292 | 0.00058 | 0.0468 | 0.0027 |
| WC1_23 | 22.7607 | 0.7396 | 0.0869 | 0.0029 | -0.3966 | 3.644 | 0.04 | 0.00161 | 0.00049 | 0.0303 | 0.0028 |
| WC1_24 | 23.1465 | 0.7612 | 0.0944 | 0.0029 | -0.3689 | 4.358 | 0.061 | 0.00255 | 0.00056 | 0.0444 | 0.004 |
| WC1_25 | 23.3641 | 0.7366 | 0.1018 | 0.0034 | -0.1657 | 4.69 | 0.058 | 0.00156 | 0.0005 | 0.0545 | 0.0034 |
| WC1_26 | 23.8485 | 0.8016 | 0.0798 | 0.0034 | -0.2122 | 3.877 | 0.05 | 0.00252 | 0.00053 | 0.0247 | 0.0032 |
| WC1_27 | 23.5056 | 0.7817 | 0.0792 | 0.0026 | 0.0613 | 3.993 | 0.068 | 0.00244 | 0.00062 | 0.0263 | 0.0027 |
| WC1_28 | 22.7149 | 0.7724 | 0.1119 | 0.0025 | 0.0454 | 3.742 | 0.052 | 0.00083 | 0.00031 | 0.0533 | 0.0031 |
| WC1_29 | 23.0520 | 0.9056 | 0.1129 | 0.0030 | -0.8043 | 4.594 | 0.056 | 0.00208 | 0.00051 | 0.076 | 0.023 |
| WC1_30 | 24.3820 | 0.7921 | 0.0760 | 0.0018 | -0.1374 | 4.343 | 0.06 | 0.00186 | 0.00052 | 0.0261 | 0.0021 |
| WC1_31 | 21.9912 | 0.9020 | 0.0982 | 0.0070 | 0.1549 | 0.766 | 0.018 | 0.00019 | 0.00015 | 0.00719 | 0.00081 |
| WC1_32 | 22.5500 | 0.7627 | 0.0927 | 0.0048 | -0.0414 | 4.42 | 0.085 | 0.00446 | 0.0007 | 0.0425 | 0.004 |
| WC1_33 | 22.3875 | 0.8953 | 0.1141 | 0.0070 | -0.7689 | 3.658 | 0.059 | 0.00197 | 0.0005 | 0.061 | 0.014 |
| WC1_34 | 23.2679 | 0.7681 | 0.1006 | 0.0048 | -0.4058 | 4.55 | 0.075 | 0.00498 | 0.00086 | 0.0556 | 0.0063 |
| WC1_35 | 22.3071 | 0.7831 | 0.1130 | 0.0052 | -0.1648 | 4.304 | 0.074 | 0.00281 | 0.00071 | 0.064 | 0.006 |
| WC1_36 | 22.7982 | 0.7417 | 0.0898 | 0.0025 | 0.1747 | 4.229 | 0.055 | 0.00297 | 0.00067 | 0.0377 | 0.0027 |
| WC1_37 | 22.5910 | 0.7651 | 0.0924 | 0.0023 | 0.1007 | 4.454 | 0.044 | 0.00418 | 0.0007 | 0.0433 | 0.0033 |
| WC1_38 | 22.6321 | 0.8032 | 0.0980 | 0.0077 | -0.4570 | 4.431 | 0.062 | 0.0039 | 0.00069 | 0.05 | 0.01 |
| WC1_39 | 22.8528 | 0.7095 | 0.1077 | 0.0049 | -0.3325 | 3.795 | 0.047 | 0.00257 | 0.00062 | 0.0485 | 0.0045 |
| WC1_40 | 23.5323 | 0.7456 | 0.0833 | 0.0032 | -0.1414 | 5.816 | 0.098 | 0.00531 | 0.00077 | 0.0462 | 0.0045 |

**Table 12.** Laser ablation ICP-MS U-Th-Pb Data for sample MQ2-2

| Data for Tera-Wasserburg plot | | | | | | | Concentrations | | | | |
|---|---|---|---|---|---|---|---|---|---|---|---|
| **Identifier** | **238U/206Pb** | **Prop2SE** | **207Pb/206Pb** | **Prop2SE** | **err.corr.** | **Approx_U_PPM** | **Approx_U_PPM_Int2SE** | **Approx_Th_PPM** | **Approx_Th_PPM_Int2SE** | **Approx_Pb_PPM** | **Approx_Pb_PPM_Int2SE** |
| MQ2_2_1 | 3.5000 | 0.1690 | 0.7470 | 0.0152 | 0.4955 | 0.601 | 0.019 | 0.964 | 0.047 | 0.684 | 0.016 |
| MQ2_2_2 | 1.9354 | 0.0743 | 0.7594 | 0.0099 | 0.3868 | 0.482 | 0.016 | 0.944 | 0.045 | 1.007 | 0.031 |
| MQ2_2_3 | 2.1722 | 0.0986 | 0.7530 | 0.0142 | 0.4019 | 0.2497 | 0.0088 | 0.468 | 0.014 | 0.456 | 0.015 |
| MQ2_2_4 | 2.5576 | 0.0860 | 0.7440 | 0.0112 | 0.6141 | 0.307 | 0.015 | 0.566 | 0.043 | 0.463 | 0.02 |
| MQ2_2_5 | 0.5221 | 0.0513 | 0.7719 | 0.0089 | 0.0511 | 0.0871 | 0.0066 | 0.185 | 0.016 | 0.652 | 0.02 |
| MQ2_2_6 | 1.3898 | 0.0652 | 0.7440 | 0.0152 | 0.3645 | 0.097 | 0.0055 | 0.1541 | 0.0072 | 0.271 | 0.011 |
| MQ2_2_7 | 1.8712 | 0.0906 | 0.7540 | 0.0152 | 0.5238 | 0.1916 | 0.0084 | 0.321 | 0.018 | 0.407 | 0.012 |
| MQ2_2_8 | 0.1920 | 0.0172 | 0.7540 | 0.0122 | -0.0461 | 0.0166 | 0.0013 | 0.1213 | 0.0057 | 0.3067 | 0.0084 |
| MQ2_2_9 | 0.2627 | 0.0178 | 0.7820 | 0.0172 | 0.2690 | 0.0242 | 0.0018 | 0.1313 | 0.0057 | 0.377 | 0.014 |
| MQ2_2_10 | 0.1198 | 0.0068 | 0.7770 | 0.0122 | 0.1553 | 0.00975 | 0.0004 | 0.1256 | 0.0052 | 0.316 | 0.012 |
| MQ2_2_11 | 1.9536 | 0.1157 | 0.7800 | 0.0122 | -0.0438 | 0.199 | 0.014 | 0.194 | 0.023 | 0.406 | 0.01 |
| MQ2_2_12 | 1.7852 | 0.0735 | 0.7464 | 0.0088 | 0.3342 | 0.365 | 0.016 | 0.852 | 0.066 | 0.801 | 0.03 |
| MQ2_2_13 | 1.9414 | 0.0802 | 0.7490 | 0.0122 | 0.2972 | 0.283 | 0.014 | 0.497 | 0.021 | 0.557 | 0.026 |
| MQ2_2_14 | 2.0953 | 0.1188 | 0.7500 | 0.0122 | 0.2988 | 0.232 | 0.014 | 0.38 | 0.028 | 0.44 | 0.014 |
| MQ2_2_15 | 0.2599 | 0.0201 | 0.7740 | 0.0113 | 0.0070 | 0.0279 | 0.0026 | 0.1257 | 0.0044 | 0.45 | 0.023 |
| MQ2_2_16 | 1.3024 | 0.0758 | 0.7560 | 0.0122 | 0.1847 | 0.1114 | 0.0067 | 0.1803 | 0.007 | 0.331 | 0.017 |
| MQ2_2_17 | 1.4481 | 0.0913 | 0.7500 | 0.0132 | 0.0842 | 0.1214 | 0.0087 | 0.216 | 0.023 | 0.33 | 0.011 |
| MQ2_2_18 | 2.9654 | 0.1308 | 0.7480 | 0.0103 | 0.1832 | 0.257 | 0.015 | 0.289 | 0.021 | 0.324 | 0.021 |
| MQ2_2_19 | 1.5302 | 0.1125 | 0.7530 | 0.0172 | 0.2604 | 0.1136 | 0.0076 | 0.199 | 0.011 | 0.2921 | 0.0096 |
| MQ2_2_20 | 0.3742 | 0.0192 | 0.7510 | 0.0112 | 0.1212 | 0.0394 | 0.0024 | 0.1716 | 0.0068 | 0.405 | 0.016 |
| MQ2_2_21 | 0.1117 | 0.0079 | 0.7840 | 0.0122 | 0.0372 | 0.01241 | 0.00084 | 0.1063 | 0.0041 | 0.449 | 0.014 |
| MQ2_2_22 | 0.2153 | 0.0132 | 0.7590 | 0.0132 | 0.2383 | 0.0203 | 0.0013 | 0.1089 | 0.0049 | 0.357 | 0.012 |
| MQ2_2_23 | 0.3278 | 0.0158 | 0.7640 | 0.0113 | 0.4111 | 0.031 | 0.0013 | 0.0759 | 0.0037 | 0.371 | 0.011 |
| MQ2_2_24 | 0.7458 | 0.0323 | 0.7622 | 0.0081 | 0.3219 | 0.429 | 0.023 | 0.807 | 0.099 | 2.254 | 0.077 |
| MQ2_2_25 | 0.2863 | 0.0236 | 0.7659 | 0.0101 | -0.0120 | 0.0319 | 0.0026 | 0.1422 | 0.0077 | 0.4276 | 0.0085 |
| MQ2_2_26 | 0.0718 | 0.0064 | 0.7800 | 0.0113 | 0.5238 | 0.0141 | 0.0016 | 0.098 | 0.0041 | 0.723 | 0.013 |
| MQ2_2_27 | 0.1863 | 0.0111 | 0.7410 | 0.0172 | 0.3620 | 0.01894 | 0.00084 | 0.0906 | 0.005 | 0.395 | 0.012 |
| MQ2_2_28 | 0.5752 | 0.0647 | 0.7760 | 0.0251 | -0.0434 | 0.0566 | 0.0064 | 0.163 | 0.016 | 0.369 | 0.014 |
| MQ2_2_29 | 0.4585 | 0.0381 | 0.7590 | 0.0103 | 0.2381 | 0.0442 | 0.0032 | 0.1179 | 0.0081 | 0.3629 | 0.0096 |
| MQ2_2_30 | 1.2278 | 0.0597 | 0.7540 | 0.0103 | -0.0352 | 0.1046 | 0.0054 | 0.1574 | 0.0074 | 0.319 | 0.0086 |
| MQ2_2_31 | 0.4270 | 0.0288 | 0.7549 | 0.0087 | 0.1304 | 0.0389 | 0.0027 | 0.1052 | 0.0077 | 0.3496 | 0.008 |
| MQ2_2_32 | 0.4636 | 0.0239 | 0.7552 | 0.0096 | 0.2706 | 0.0452 | 0.0021 | 0.1804 | 0.0068 | 0.379 | 0.012 |
| MQ2_2_33 | 0.3219 | 0.0240 | 0.7690 | 0.0122 | 0.2202 | 0.0325 | 0.0021 | 0.1485 | 0.005 | 0.394 | 0.0093 |
| MQ2_2_34 | 0.1502 | 0.0098 | 0.7522 | 0.0101 | 0.1167 | 0.01265 | 0.00077 | 0.0469 | 0.0034 | 0.318 | 0.0073 |
| MQ2_2_35 | 0.9692 | 0.0635 | 0.7480 | 0.0103 | 0.0333 | 0.0943 | 0.007 | 0.18 | 0.013 | 0.362 | 0.012 |
| MQ2_2_36 | 3.5500 | 0.2120 | 0.7610 | 0.0113 | 0.3195 | 0.386 | 0.017 | 0.43 | 0.022 | 0.418 | 0.012 |
| MQ2_2_37 | 1.1526 | 0.0764 | 0.7320 | 0.0142 | 0.3850 | 0.0847 | 0.0048 | 0.168 | 0.012 | 0.28 | 0.013 |
| MQ2_2_38 | 1.2314 | 0.0544 | 0.7670 | 0.0172 | 0.4878 | 0.1326 | 0.0053 | 0.206 | 0.0083 | 0.421 | 0.016 |
| MQ2_2_39 | 0.4241 | 0.0271 | 0.7548 | 0.0093 | 0.0348 | 0.0363 | 0.0023 | 0.1518 | 0.0056 | 0.3294 | 0.0076 |
| MQ2_2_40 | 0.0476 | 0.0039 | 0.7776 | 0.0088 | 0.0828 | 0.00802 | 0.00058 | 0.0928 | 0.0043 | 0.633 | 0.017 |
| MQ2_2_41 | 0.4636 | 0.0440 | 0.7552 | 0.0099 | 0.0590 | 0.0515 | 0.0045 | 0.162 | 0.011 | 0.412 | 0.011 |

**Table 13.** Laser ablation ICP-MS U-Th-Pb Data for sample MQ2-2 continued

| Data for Tera-Wasserburg plot | | | | | | | Concentrations | | | | |
|---|---|---|---|---|---|---|---|---|---|---|---|
| **Identifier** | **238U/206Pb** | **Prop2SE** | **207Pb/206Pb** | **Prop2SE** | **err.corr.** | **Approx_U_PPM** | **Approx_U_PPM_Int2SE** | **Approx_Th_PPM** | **Approx_Th_PPM_Int2SE** | **Approx_Pb_PPM** | **Approx_Pb_PPM_Int2SE** |
| MQ2_2_42 | 1.4152 | 0.0904 | 0.7470 | 0.0152 | 0.3487 | 0.1406 | 0.0096 | 0.215 | 0.014 | 0.374 | 0.012 |
| MQ2_2_43 | 3.3957 | 0.1260 | 0.7390 | 0.0172 | 0.5267 | 0.3201 | 0.0074 | 0.313 | 0.01 | 0.356 | 0.011 |
| MQ2_2_44 | 4.7136 | 0.1555 | 0.7550 | 0.0122 | 0.2552 | 0.381 | 0.012 | 0.346 | 0.015 | 0.305 | 0.012 |
| MQ2_2_45 | 1.7929 | 0.1155 | 0.7600 | 0.0152 | 0.1539 | 0.1249 | 0.0099 | 0.1509 | 0.0095 | 0.2686 | 0.0092 |
| MQ2_2_46 | 0.0894 | 0.0091 | 0.7827 | 0.0100 | 0.2045 | 0.016 | 0.0013 | 0.1312 | 0.0066 | 0.659 | 0.021 |
| MQ2_2_47 | 0.7975 | 0.0413 | 0.7460 | 0.0132 | 0.3885 | 0.085 | 0.0039 | 0.2176 | 0.0088 | 0.4065 | 0.0086 |
| MQ2_2_48 | 1.9536 | 0.0982 | 0.7710 | 0.0201 | 0.2829 | 0.221 | 0.01 | 0.386 | 0.017 | 0.454 | 0.022 |
| MQ2_2_49 | 4.2406 | 0.1886 | 0.7510 | 0.0152 | 0.5502 | 0.478 | 0.014 | 0.385 | 0.027 | 0.441 | 0.022 |
| MQ2_2_50 | 2.9098 | 0.1647 | 0.7660 | 0.0162 | 0.4707 | 0.322 | 0.027 | 0.297 | 0.035 | 0.481 | 0.062 |
| MQ2_2_51 | 1.8517 | 0.0786 | 0.7608 | 0.0085 | 0.2149 | 0.598 | 0.022 | 0.923 | 0.088 | 1.322 | 0.076 |
| MQ2_2_52 | 1.3714 | 0.0622 | 0.7640 | 0.0152 | 0.5141 | 0.0974 | 0.0042 | 0.2501 | 0.0088 | 0.2862 | 0.0064 |
| MQ2_2_53 | 0.0894 | 0.0066 | 0.7829 | 0.0097 | 0.0615 | 0.01344 | 0.0009 | 0.1239 | 0.0044 | 0.583 | 0.011 |
| MQ2_2_54 | 0.1173 | 0.0075 | 0.7670 | 0.0113 | 0.4107 | 0.01025 | 0.00082 | 0.144 | 0.0045 | 0.321 | 0.011 |
| MQ2_2_55 | 0.0634 | 0.0040 | 0.7840 | 0.0152 | 0.0575 | 0.00649 | 0.00037 | 0.1342 | 0.0081 | 0.413 | 0.017 |
| MQ2_2_56 | 1.1711 | 0.0466 | 0.7510 | 0.0152 | 0.4265 | 0.0626 | 0.0018 | 0.2881 | 0.0089 | 0.2077 | 0.0053 |
| MQ2_2_57 | 4.4953 | 0.1601 | 0.7444 | 0.0102 | 0.2466 | 0.438 | 0.01 | 0.348 | 0.035 | 0.375 | 0.014 |
| MQ2_2_58 | 1.5493 | 0.0553 | 0.7460 | 0.0152 | 0.4564 | 0.1484 | 0.0036 | 0.1277 | 0.0054 | 0.3701 | 0.0095 |
| MQ2_2_59 | 0.5798 | 0.0256 | 0.7610 | 0.0142 | 0.0970 | 0.0519 | 0.0044 | 0.256 | 0.016 | 0.347 | 0.021 |
| MQ2_2_60 | 0.4654 | 0.0208 | 0.7720 | 0.0103 | 0.1115 | 0.063 | 0.0015 | 0.1101 | 0.0037 | 0.54 | 0.017 |
| MQ2_2_61 | 0.0392 | 0.0029 | 0.7750 | 0.0122 | 0.0095 | 0.00729 | 0.00046 | 0.1323 | 0.006 | 0.748 | 0.026 |
| MQ2_2_62 | 0.0230 | 0.0013 | 0.7741 | 0.0096 | 0.1185 | 0.00413 | 0.00022 | 0.1312 | 0.0036 | 0.707 | 0.016 |
| MQ2_2_63 | 0.0578 | 0.0044 | 0.7773 | 0.0091 | 0.1068 | 0.00697 | 0.00041 | 0.1342 | 0.0043 | 0.479 | 0.018 |
| MQ2_2_64 | 1.8656 | 0.0647 | 0.7500 | 0.0122 | 0.4869 | 0.1874 | 0.0061 | 0.369 | 0.016 | 0.388 | 0.011 |
| MQ2_2_65 | 2.5672 | 0.1102 | 0.7591 | 0.0101 | 0.1995 | 0.339 | 0.014 | 0.477 | 0.031 | 0.503 | 0.019 |
| MQ2_2_66 | 1.1970 | 0.0527 | 0.7470 | 0.0122 | 0.2642 | 0.1305 | 0.0043 | 0.1931 | 0.0082 | 0.419 | 0.012 |
| MQ2_2_67 | 2.6606 | 0.1125 | 0.7410 | 0.0098 | 0.6825 | 0.3177 | 0.0076 | 0.737 | 0.023 | 0.439 | 0.016 |
| MQ2_2_68 | 1.6157 | 0.0690 | 0.7400 | 0.0162 | 0.3796 | 0.144 | 0.0077 | 0.552 | 0.016 | 0.343 | 0.014 |
| MQ2_2_69 | 0.0218 | 0.0012 | 0.7816 | 0.0097 | -0.0558 | 0.00463 | 0.00021 | 0.1141 | 0.0042 | 0.858 | 0.016 |
| MQ2_2_70 | 1.4916 | 0.0863 | 0.7440 | 0.0112 | -0.0304 | 0.196 | 0.014 | 0.66 | 0.028 | 0.509 | 0.02 |
| MQ2_2_71 | 1.7801 | 0.0708 | 0.7578 | 0.0094 | 0.3958 | 0.2371 | 0.0072 | 0.408 | 0.018 | 0.518 | 0.016 |
| MQ2_2_72 | 2.7308 | 0.1071 | 0.7680 | 0.0122 | 0.4332 | 0.33 | 0.017 | 0.399 | 0.05 | 0.478 | 0.022 |
| MQ2_2_73 | 1.0871 | 0.0529 | 0.7490 | 0.0112 | 0.3761 | 0.1187 | 0.0048 | 0.211 | 0.012 | 0.412 | 0.01 |
| MQ2_2_74 | 0.9392 | 0.0456 | 0.7390 | 0.0132 | 0.1283 | 0.101 | 0.0051 | 0.327 | 0.012 | 0.413 | 0.01 |
| MQ2_2_75 | 0.0296 | 0.0027 | 0.7794 | 0.0084 | -0.0124 | 0.00602 | 0.00043 | 0.1298 | 0.0057 | 0.772 | 0.017 |
| MQ2_2_76 | 0.4453 | 0.0221 | 0.7510 | 0.0122 | -0.0380 | 0.0463 | 0.002 | 0.2639 | 0.0086 | 0.4 | 0.011 |
| MQ2_2_77 | 1.7162 | 0.0749 | 0.7460 | 0.0122 | 0.1567 | 0.1978 | 0.0077 | 0.286 | 0.015 | 0.451 | 0.01 |
| MQ2_2_78 | 2.6476 | 0.0865 | 0.7470 | 0.0103 | 0.3227 | 0.3339 | 0.0057 | 0.458 | 0.012 | 0.493 | 0.014 |
| MQ2_2_79 | 1.5970 | 0.0713 | 0.7490 | 0.0112 | -0.0081 | 0.1836 | 0.0053 | 0.303 | 0.015 | 0.455 | 0.011 |
| MQ2_2_80 | 0.3847 | 0.0328 | 0.7490 | 0.0112 | 0.2286 | 0.0658 | 0.0062 | 0.296 | 0.012 | 0.638 | 0.018 |
| MQ2_2_81 | 1.2627 | 0.0570 | 0.7560 | 0.0152 | 0.4224 | 0.1338 | 0.004 | 0.498 | 0.013 | 0.412 | 0.013 |
| MQ2_2_82 | 2.0743 | 0.0970 | 0.7471 | 0.0090 | 0.0540 | 0.28 | 0.015 | 0.452 | 0.047 | 0.52 | 0.015 |
| MQ2_2_83 | 2.3622 | 0.0827 | 0.7497 | 0.0090 | 0.3981 | 0.468 | 0.012 | 0.541 | 0.02 | 0.772 | 0.025 |
| MQ2_2_84 | 1.5340 | 0.0560 | 0.7440 | 0.0103 | 0.4002 | 0.1583 | 0.0095 | 0.272 | 0.016 | 0.391 | 0.022 |
| MQ2_2_85 | 2.1312 | 0.1192 | 0.7450 | 0.0142 | 0.0518 | 0.193 | 0.019 | 0.442 | 0.031 | 0.362 | 0.02 |
| MQ2_2_86 | 0.0489 | 0.0026 | 0.7809 | 0.0080 | 0.2131 | 0.00604 | 0.00042 | 0.1114 | 0.005 | 0.535 | 0.019 |
| MQ2_2_87 | 1.4809 | 0.0604 | 0.7560 | 0.0132 | 0.2293 | 0.1182 | 0.0054 | 0.357 | 0.011 | 0.3069 | 0.0094 |
| MQ2_2_88 | 2.6952 | 0.1205 | 0.7514 | 0.0096 | 0.1867 | 0.233 | 0.012 | 0.345 | 0.014 | 0.323 | 0.017 |
| MQ2_2_89 | 1.6656 | 0.0896 | 0.7730 | 0.0241 | 0.6129 | 0.0962 | 0.0067 | 0.141 | 0.013 | 0.23 | 0.014 |
| MQ2_2_90 | 2.9030 | 0.1511 | 0.7280 | 0.0132 | 0.5632 | 0.2248 | 0.0072 | 0.31 | 0.015 | 0.2939 | 0.0092 |

**Table 14.** Laser ablation ICP-MS U-Th-Pb Data for sample SR1

| Data for Tera-Wasserburg plot | | | | | | | Concentrations | | | | |
|---|---|---|---|---|---|---|---|---|---|---|---|
| Identifier | 238U/206Pb | Prop2SE | 207Pb/206Pb | Prop2SE | err.corr. | Approx_U_PPM | Approx_U_PPM_Int2SE | Approx_Th_PPM | Approx_Th_PPM_Int2SE | Approx_Pb_PPM | Approx_Pb_PPM_Int2SE |
| SR1_1 | 5.8664 | 0.2951 | 0.7555 | 0.0077 | 0.2737 | 1.651 | 0.07 | 0.1388 | 0.0089 | 1.081 | 0.045 |
| SR1_2 | 16.6779 | 0.7107 | 0.5080 | 0.0111 | 0.5236 | 0.917 | 0.013 | 0.0051 | 0.0024 | 0.1387 | 0.0056 |
| SR1_3 | 11.1435 | 0.7547 | 0.5380 | 0.0141 | -0.3319 | 0.994 | 0.028 | 0.0279 | 0.0051 | 0.254 | 0.023 |
| SR1_4 | 9.8377 | 0.6086 | 0.7200 | 0.0181 | 0.1420 | 1.108 | 0.058 | 0.236 | 0.0084 | 0.417 | 0.015 |
| SR1_5 | 5.1556 | 0.2517 | 0.7210 | 0.0191 | 0.6005 | 0.584 | 0.022 | 0.243 | 0.017 | 0.411 | 0.023 |
| SR1_6 | 13.1204 | 0.8886 | 0.6990 | 0.0191 | 0.1971 | 3.961 | 0.072 | 0.262 | 0.019 | 1.126 | 0.089 |
| SR1_7 | 36.1193 | 1.6950 | 0.5490 | 0.0161 | 0.2598 | 2.2 | 0.16 | 0.0253 | 0.0052 | 0.164 | 0.013 |
| SR1_8 | 0.0184 | 0.0010 | 0.7692 | 0.0083 | 0.0175 | 0.00376 | 0.00027 | 0.00018 | 0.00013 | 0.769 | 0.026 |
| SR1_9 | 12.8757 | 0.6657 | 0.4830 | 0.0082 | 0.3632 | 0.913 | 0.04 | 0.00355 | 0.00087 | 0.1702 | 0.004 |
| SR1_10 | 22.1086 | 1.2784 | 0.4910 | 0.0095 | 0.3931 | 1.514 | 0.084 | 0.00345 | 0.00068 | 0.1666 | 0.0044 |
| SR1_11 | 55.7177 | 3.3888 | 0.4920 | 0.0111 | 0.1338 | 2.13 | 0.12 | 0.00113 | 0.00039 | 0.09 | 0.0032 |
| SR1_12 | 42.1188 | 2.8094 | 0.4913 | 0.0097 | -0.0471 | 1.763 | 0.098 | 0.0091 | 0.0012 | 0.1054 | 0.0039 |
| SR1_13 | 5.7926 | 0.2580 | 0.7321 | 0.0094 | 0.2722 | 2.721 | 0.093 | 0.48 | 0.1 | 1.739 | 0.049 |
| SR1_14 | 14.6868 | 1.0218 | 0.5110 | 0.0097 | -0.2463 | 1.093 | 0.047 | 0.00712 | 0.00096 | 0.1856 | 0.0094 |
| SR1_15 | 33.7637 | 1.6660 | 0.4983 | 0.0096 | 0.3690 | 1.225 | 0.056 | 0.00093 | 0.00036 | 0.0962 | 0.0041 |
| SR1_16 | 19.5979 | 0.6786 | 0.5010 | 0.0111 | 0.5056 | 1.169 | 0.021 | 0.115 | 0.014 | 0.1557 | 0.0045 |
| SR1_17 | 3.6870 | 0.1559 | 0.5215 | 0.0080 | 0.2930 | 0.286 | 0.015 | 0.035 | 0.007 | 0.2074 | 0.0056 |
| SR1_18 | 17.8778 | 0.8796 | 0.4731 | 0.0086 | -0.0211 | 1.029 | 0.026 | 0 | 0.05 | 0.1356 | 0.0038 |
| SR1_19 | 64.0136 | 2.6512 | 0.4890 | 0.0101 | 0.1674 | 3.81 | 0.11 | 0.0528 | 0.0038 | 0.1477 | 0.0063 |
| SR1_20 | 0.1670 | 0.0065 | 0.7239 | 0.0092 | 0.2458 | 0.01997 | 0.00057 | 0.0384 | 0.0023 | 0.453 | 0.016 |
| SR1_21 | 12.0632 | 0.4602 | 0.4823 | 0.0085 | 0.3795 | 0.789 | 0.015 | 0.011 | 0.0011 | 0.1646 | 0.0058 |
| SR1_22 | 21.1310 | 1.9043 | 0.4677 | 0.0091 | 0.2157 | 1.052 | 0.064 | 0.00005 | 0.00007 | 0.1178 | 0.0044 |
| SR1_23 | 5.5469 | 0.7491 | 0.6970 | 0.0099 | -0.6088 | 2.2 | 0.36 | 0.46 | 0.13 | 0.979 | 0.023 |
| SR1_24 | 35.1984 | 2.6634 | 0.4794 | 0.0096 | -0.1121 | 1.95 | 0.15 | 0.00184 | 0.00042 | 0.1349 | 0.0045 |
| SR1_25 | 13.0105 | 0.4788 | 0.5022 | 0.0084 | 0.1972 | 0.939 | 0.025 | 0.119 | 0.013 | 0.1926 | 0.0082 |
| SR1_26 | 16.3703 | 1.0735 | 0.4865 | 0.0083 | 0.3747 | 0.995 | 0.02 | 0.00515 | 0.00089 | 0.1491 | 0.0073 |
| SR1_27 | 34.4184 | 1.6381 | 0.3950 | 0.0200 | 0.2148 | 0.751 | 0.019 | 0.00189 | 0.00076 | 0.0413 | 0.0024 |
| SR1_28 | 11.8334 | 1.2566 | 0.5470 | 0.0181 | -0.5352 | 1.392 | 0.06 | 0.07 | 0.012 | 0.314 | 0.031 |
| SR1_29 | 43.8273 | 1.8627 | 0.4270 | 0.0121 | 0.6760 | 2.249 | 0.054 | 0.00056 | 0.00047 | 0.1095 | 0.0035 |
| SR1_30 | 30.0122 | 2.0253 | 0.6500 | 0.0221 | 0.4380 | 2.7 | 0.12 | 0.0204 | 0.0023 | 0.283 | 0.015 |
| SR1_31 | 113.0578 | 8.1603 | 0.5020 | 0.0141 | 0.2501 | 3.95 | 0.14 | 0.028 | 0.0029 | 0.085 | 0.004 |
| SR1_32 | 27.1883 | 1.3912 | 0.4610 | 0.0230 | -0.3966 | 1.401 | 0.049 | 0.0164 | 0.0027 | 0.121 | 0.015 |
| SR1_33 | 15.2081 | 0.7202 | 0.6090 | 0.0092 | 0.1761 | 1.21 | 0.02 | 0.0264 | 0.0034 | 0.236 | 0.01 |
| SR1_34 | 58.2242 | 2.1363 | 0.4180 | 0.0131 | 0.2255 | 1.865 | 0.017 | 0.00245 | 0.00067 | 0.063 | 0.0027 |
| SR1_35 | 16.5888 | 0.7038 | 0.5550 | 0.0121 | 0.0302 | 1.688 | 0.079 | 0.0517 | 0.0069 | 0.275 | 0.02 |
| SR1_36 | 14.5834 | 0.5571 | 0.3900 | 0.0111 | 0.3359 | 0.4088 | 0.0055 | 0.00151 | 0.00048 | 0.0575 | 0.0025 |
| SR1_37 | 27.4284 | 2.2310 | 0.5270 | 0.0280 | 0.0672 | 1.885 | 0.066 | 0.024 | 0.0036 | 0.179 | 0.018 |
| SR1_38 | 30.0122 | 0.9523 | 0.4230 | 0.0101 | 0.3713 | 1.868 | 0.029 | 0.0138 | 0.002 | 0.1312 | 0.0055 |
| SR1_39 | 39.0479 | 1.3909 | 0.3840 | 0.0076 | 0.4384 | 3.297 | 0.063 | 0.00061 | 0.00029 | 0.1524 | 0.0038 |
| SR1_40 | 75.3033 | 8.3181 | 0.5650 | 0.0301 | 0.3393 | 3.55 | 0.18 | 0.0131 | 0.0054 | 0.132 | 0.015 |
| SR1_41 | 13.1066 | 0.5979 | 0.6280 | 0.0221 | 0.1737 | 1.76 | 0.14 | 0.124 | 0.018 | 0.441 | 0.044 |
| SR1_42 | 44.2487 | 1.6963 | 0.3970 | 0.0098 | 0.7457 | 1.666 | 0.021 | 0 | 0.05 | 0.0724 | 0.0022 |
| SR1_43 | 209.8825 | 14.6410 | 0.4570 | 0.0420 | -0.2726 | 3.457 | 0.056 | 0.006 | 0.002 | 0.0357 | 0.0036 |
| SR1_44 | 19.3838 | 0.6920 | 0.4210 | 0.0101 | 0.5443 | 1.182 | 0.03 | 0.27 | 0.016 | 0.1307 | 0.0049 |
| SR1_45 | 60.9370 | 3.0015 | 0.4200 | 0.0111 | -0.0060 | 1.648 | 0.033 | 0.00142 | 0.00048 | 0.0577 | 0.0035 |
| SR1_46 | 20.7430 | 1.0342 | 0.4750 | 0.0121 | 0.4865 | 1.653 | 0.072 | 0.1288 | 0.0095 | 0.1888 | 0.0099 |
| SR1_47 | 96.3182 | 18.7409 | 0.5130 | 0.0171 | 0.2343 | 9.9 | 1.8 | 0.18 | 0.022 | 0.241 | 0.018 |
| SR1_48 | 342.2878 | 19.7711 | 0.2800 | 0.0200 | 0.4542 | 3.126 | 0.073 | 0.00113 | 0.0008 | 0.0125 | 0.002 |
| SR1_49 | 205.0338 | 10.1189 | 0.2940 | 0.0360 | 0.2566 | 2.482 | 0.061 | 0.0021 | 0.001 | 0.0173 | 0.0029 |
| SR1_50 | 117.2174 | 4.5688 | 0.3930 | 0.0151 | 0.1890 | 2.349 | 0.031 | 0.0001 | 0.0001 | 0.0405 | 0.0019 |
| SR1_51 | 84.5241 | 3.4857 | 0.4200 | 0.0131 | 0.4467 | 1.838 | 0.039 | 0.00009 | 0.00012 | 0.0466 | 0.0029 |
| SR1_52 | 167.9060 | 13.4785 | 0.4840 | 0.0201 | -0.2123 | 4.89 | 0.14 | 0.0078 | 0.0021 | 0.071 | 0.0082 |
| SR1_53 | 25.3056 | 0.8890 | 0.4640 | 0.0099 | 0.7429 | 0.911 | 0.015 | 0.0134 | 0.0015 | 0.0865 | 0.0031 |

**Table 15.** Laser ablation ICP-MS U-Th-Pb Data for sample SR2

| Data for Tera-Wasserburg plot | | | | | | | Concentrations | | | | |
|---|---|---|---|---|---|---|---|---|---|---|---|
| Identifier | 238U/206Pb | Prop2SE | 207Pb/206Pb | Prop2SE | err.corr. | Approx_U_PPM | Approx_U_PPM_Int2SE | Approx_Th_PPM | Approx_Th_PPM_Int2SE | Approx_Pb_PPM | Approx_Pb_PPM_Int2SE |
| SR2_1 | 0.0028 | 0.0001 | 0.8720 | 0.0041 | -0.0286 | 0.01042 | 0.00046 | 0.7144 | 0.0097 | 15.75 | 0.12 |
| SR2_2 | 14.7042 | 0.5346 | 0.7270 | 0.0181 | 0.0333 | 1.534 | 0.065 | 0.0095 | 0.0026 | 0.394 | 0.028 |
| SR2_3 | 33.1335 | 1.2844 | 0.6850 | 0.0251 | 0.8543 | 1.579 | 0.013 | 0.00135 | 0.00075 | 0.1686 | 0.0078 |
| SR2_4 | 116.8866 | 6.0666 | 0.6920 | 0.0221 | -0.0818 | 2.985 | 0.026 | 0.0209 | 0.0022 | 0.0878 | 0.0043 |
| SR2_5 | 70.0003 | 2.4513 | 0.6660 | 0.0241 | 0.3529 | 3.232 | 0.045 | 0.00058 | 0.00041 | 0.1554 | 0.0096 |
| SR2_6 | 103.4558 | 4.9054 | 0.7260 | 0.0321 | 0.1157 | 2.463 | 0.075 | 0.0011 | 0.0004 | 0.0843 | 0.0043 |
| SR2_7 | 30.6564 | 1.0519 | 0.6060 | 0.0121 | 0.6186 | 2.416 | 0.024 | 0.00148 | 0.00071 | 0.247 | 0.0099 |
| SR2_8 | 22.2671 | 0.8155 | 0.6030 | 0.0181 | 0.8497 | 1.609 | 0.017 | 0.00397 | 0.00096 | 0.225 | 0.013 |
| SR2_9 | 38.9256 | 1.3094 | 0.5587 | 0.0096 | 0.5118 | 1.836 | 0.029 | 0.00165 | 0.00056 | 0.1352 | 0.0056 |
| SR2_10 | 14.0396 | 0.5918 | 0.5470 | 0.0151 | 0.4577 | 0.426 | 0.016 | 0 | 0.05 | 0.0847 | 0.0033 |
| SR2_11 | 28.3677 | 1.0890 | 0.5580 | 0.0131 | 0.4298 | 2.235 | 0.034 | 0.165 | 0.013 | 0.2199 | 0.0084 |
| SR2_12 | 40.7379 | 1.5110 | 0.5370 | 0.0121 | 0.5132 | 2.519 | 0.034 | 0.1081 | 0.0061 | 0.1654 | 0.0068 |
| SR2_13 | 81.1034 | 4.0629 | 0.5210 | 0.0201 | 0.3865 | 0.794 | 0.027 | 0.00082 | 0.00032 | 0.0256 | 0.0016 |
| SR2_14 | 17.2331 | 0.5842 | 0.5229 | 0.0085 | 0.6001 | 2.036 | 0.025 | 0.1187 | 0.0055 | 0.3092 | 0.0059 |
| SR2_15 | 20.8125 | 0.6644 | 0.5287 | 0.0096 | 0.5999 | 2.066 | 0.038 | 0.1225 | 0.0071 | 0.2742 | 0.0088 |
| SR2_16 | 28.3031 | 1.2009 | 0.5200 | 0.0161 | 0.3555 | 0.4609 | 0.0096 | 0 | 0.05 | 0.0426 | 0.0023 |
| SR2_17 | 14.4645 | 0.4757 | 0.5518 | 0.0075 | 0.5534 | 1.738 | 0.024 | 0.515 | 0.047 | 0.3319 | 0.008 |
| SR2_18 | 18.0073 | 0.5641 | 0.5500 | 0.0121 | 0.5887 | 1.853 | 0.029 | 0.252 | 0.026 | 0.2909 | 0.0093 |
| SR2_19 | 17.4020 | 0.5942 | 0.5145 | 0.0083 | 0.4109 | 1.155 | 0.013 | 0.1031 | 0.0093 | 0.1758 | 0.004 |
| SR2_20 | 45.6803 | 2.1654 | 0.5100 | 0.0191 | 0.5993 | 1.355 | 0.021 | 0.00009 | 0.00018 | 0.0753 | 0.0038 |
| SR2_21 | 21.8443 | 0.6895 | 0.5300 | 0.0111 | 0.6593 | 1.386 | 0.018 | 0.182 | 0.017 | 0.1686 | 0.0045 |
| SR2_22 | 41.4860 | 1.4755 | 0.5130 | 0.0131 | 0.6520 | 1.367 | 0.018 | 0.00044 | 0.00022 | 0.0873 | 0.0022 |
| SR2_23 | 52.5594 | 2.0782 | 0.5230 | 0.0161 | 0.6575 | 1.299 | 0.026 | 0 | 0.05 | 0.0654 | 0.0036 |
| SR2_24 | 36.3624 | 1.4242 | 0.5270 | 0.0151 | -0.0673 | 0.964 | 0.015 | 0 | 0.05 | 0.0689 | 0.002 |
| SR2_25 | 67.5641 | 2.4641 | 0.5470 | 0.0161 | 0.7896 | 1.736 | 0.016 | 0.00035 | 0.00021 | 0.07 | 0.0026 |
| SR2_26 | 23.6218 | 1.0282 | 0.5170 | 0.0181 | 0.6143 | 0.7943 | 0.0089 | 0 | 0.05 | 0.0869 | 0.0042 |
| SR2_27 | 35.8070 | 1.8609 | 0.5210 | 0.0211 | 0.5318 | 1.042 | 0.022 | 0 | 0.05 | 0.0777 | 0.0045 |
| SR2_28 | 23.5769 | 1.1909 | 0.6080 | 0.0181 | -0.2572 | 1.616 | 0.043 | 0.04 | 0.011 | 0.2074 | 0.0088 |
| SR2_29 | 18.3260 | 0.6040 | 0.5117 | 0.0065 | 0.5451 | 1.634 | 0.02 | 0.0164 | 0.0024 | 0.236 | 0.0062 |
| SR2_30 | 23.9357 | 0.7291 | 0.5092 | 0.0067 | 0.5046 | 2.115 | 0.019 | 0.00373 | 0.00092 | 0.2297 | 0.0051 |
| SR2_31 | 50.6938 | 2.0586 | 0.5600 | 0.0141 | 0.3507 | 2.084 | 0.037 | 0.00272 | 0.00081 | 0.1154 | 0.0059 |
| SR2_32 | 106.5613 | 4.2601 | 0.5360 | 0.0171 | 0.6745 | 1.678 | 0.022 | 0 | 0.05 | 0.0437 | 0.0021 |
| SR2_33 | 0.1162 | 0.0049 | 0.7882 | 0.0055 | 0.0690 | 0.1818 | 0.0051 | 0.0325 | 0.0023 | 6.158 | 0.067 |
| SR2_34 | 36.6954 | 1.4479 | 0.6108 | 0.0092 | 0.5044 | 3.808 | 0.057 | 0.327 | 0.013 | 0.322 | 0.012 |
| SR2_35 | 0.5474 | 0.0610 | 0.8702 | 0.0058 | 0.0662 | 1.02 | 0.11 | 0.5178 | 0.0094 | 7.441 | 0.097 |
| SR2_36 | 0.7949 | 0.0312 | 0.8355 | 0.0050 | 0.2550 | 1.277 | 0.028 | 0.924 | 0.016 | 6.8 | 0.21 |
| SR2_37 | 128.3579 | 5.2672 | 0.4226 | 0.0082 | -0.6963 | 96.1 | 1.2 | 7.615 | 0.061 | 1.521 | 0.071 |
| SR2_38 | 1.2640 | 0.0455 | 0.8211 | 0.0056 | 0.2848 | 5.28 | 0.13 | 1.088 | 0.08 | 17.23 | 0.25 |
| SR2_39 | 0.0026 | 0.0007 | 0.8285 | 0.0052 | 0.0770 | 0.168 | 0.046 | 0.157 | 0.045 | 25.56 | 0.59 |
| SR2_40 | 0.3900 | 0.0151 | 0.8453 | 0.0054 | -0.0334 | 1.062 | 0.031 | 1.121 | 0.023 | 11.26 | 0.12 |
| SR2_41 | 0.1133 | 0.0058 | 0.8667 | 0.0052 | 0.1629 | 0.309 | 0.013 | 0.464 | 0.011 | 11.47 | 0.13 |
| SR2_42 | 1.7451 | 0.0864 | 0.8399 | 0.0093 | 0.3440 | 0.605 | 0.019 | 0.436 | 0.017 | 1.464 | 0.025 |
| SR2_43 | 227.1490 | 8.8188 | 0.2586 | 0.0044 | -0.6709 | 162.2 | 3.8 | 9.84 | 0.11 | 0.853 | 0.027 |
| SR2_44 | 0.0531 | 0.0046 | 0.8700 | 0.0052 | 0.1593 | 0.241 | 0.015 | 0.59 | 0.016 | 18.56 | 0.45 |
| SR2_45 | 161.5741 | 6.1396 | 0.4260 | 0.0210 | -0.8262 | 131.5 | 4.8 | 8.73 | 0.33 | 1.74 | 0.19 |
| SR2_46 | 0.6539 | 0.0428 | 0.8115 | 0.0061 | -0.1360 | 1.07 | 0.066 | 1.016 | 0.028 | 6.56 | 0.11 |
| SR2_47 | 2.3894 | 0.0884 | 0.7075 | 0.0062 | 0.2099 | 2.792 | 0.086 | 1.759 | 0.041 | 4.278 | 0.059 |
| SR2_48 | 5.8609 | 0.3735 | 0.7007 | 0.0097 | -0.3223 | 7.4 | 0.43 | 1.336 | 0.055 | 4.76 | 0.13 |
| SR2_49 | 10.2517 | 0.5778 | 0.6673 | 0.0049 | -0.3271 | 9.85 | 0.4 | 3.121 | 0.064 | 3.236 | 0.077 |
| SR2_50 | 1.7525 | 0.1562 | 0.6945 | 0.0049 | -0.1092 | 2.49 | 0.22 | 1.547 | 0.042 | 4.892 | 0.069 |
| SR2_51 | 126.7862 | 4.8023 | 0.3971 | 0.0060 | -0.2580 | 140.7 | 5.4 | 13.49 | 0.42 | 2.12 | 0.12 |
| SR2_52 | 100.6892 | 3.9192 | 0.5940 | 0.0171 | -0.6901 | 145.6 | 4.7 | 11.01 | 0.3 | 4.04 | 0.15 |
| SR2_53 | 151.7099 | 4.8508 | 0.3557 | 0.0061 | 0.1235 | 158.8 | 4.1 | 12.17 | 0.12 | 1.776 | 0.048 |
| SR2_54 | 7.9140 | 0.3975 | 0.1670 | 0.0035 | 0.5674 | 12.41 | 0.59 | 7.97 | 0.6 | 1.305 | 0.072 |
| SR2_55 | 5.5994 | 0.2633 | 0.7070 | 0.0112 | 0.2776 | 4.74 | 0.14 | 11.89 | 0.27 | 3.01 | 0.11 |
| SR2_56 | 9.6768 | 0.4682 | 0.8460 | 0.0133 | -0.3128 | 2.331 | 0.05 | 0.0503 | 0.0046 | 0.959 | 0.035 |

**Table 16.** Laser ablation ICP-MS U-Th-Pb Data for sample SR2_surf

| Data for Tera-Wasserburg plot | | | | | | | Concentrations | | | | |
|---|---|---|---|---|---|---|---|---|---|---|---|
| Identifier | 238U/206Pb | Prop2SE | 207Pb/206Pb | Prop2SE | err.corr. | Approx_U_PPM | Approx_U_PPM_Int2SE | Approx_Th_PPM | Approx_Th_PPM_Int2SE | Approx_Pb_PPM | Approx_Pb_PPM_Int2SE |
| SR2surf_1 | 17.2092 | 1.0675 | 0.6590 | 0.0181 | -0.0473 | 1.959 | 0.047 | 0.241 | 0.031 | 0.39 | 0.027 |
| SR2surf_2 | 18.3802 | 1.0294 | 0.6400 | 0.0211 | 0.1785 | 1.327 | 0.024 | 0.059 | 0.019 | 0.24 | 0.018 |
| SR2surf_3 | 2.6836 | 0.3969 | 0.6820 | 0.0211 | -0.0345 | 0.638 | 0.024 | 0.179 | 0.029 | 0.85 | 0.14 |
| SR2surf_4 | 46.3621 | 3.3838 | 0.5780 | 0.0171 | 0.5488 | 9.87 | 0.4 | 1.259 | 0.081 | 0.604 | 0.038 |
| SR2surf_5 | 15.4348 | 1.5760 | 0.7320 | 0.0371 | 0.2887 | 1.574 | 0.03 | 0.074 | 0.01 | 0.362 | 0.041 |
| SR2surf_6 | 7.1821 | 0.5944 | 0.7090 | 0.0152 | 0.5207 | 2.024 | 0.056 | 0.349 | 0.028 | 1.027 | 0.089 |
| SR2surf_7 | 18.8258 | 3.1546 | 0.7380 | 0.0241 | 0.2280 | 2.476 | 0.063 | 0.099 | 0.011 | 0.503 | 0.069 |
| SR2surf_8 | 3.8707 | 0.2503 | 0.7680 | 0.0371 | 0.1177 | 0.7109 | 0.0093 | 0.105 | 0.018 | 0.692 | 0.032 |
| SR2surf_9 | 5.5718 | 0.5335 | 0.7320 | 0.0271 | 0.3918 | 1.873 | 0.041 | 0.414 | 0.046 | 1.25 | 0.11 |
| SR2surf_10 | 7.9648 | 0.7280 | 0.7090 | 0.0251 | -0.1394 | 1.478 | 0.086 | 0.16 | 0.019 | 0.702 | 0.081 |
| SR2surf_11 | 36.8696 | 3.7743 | 0.6850 | 0.0311 | 0.3036 | 2.39 | 0.13 | 0.073 | 0.015 | 0.22 | 0.02 |
| SR2surf_12 | 36.1193 | 7.7951 | 0.4400 | 0.1100 | -0.3433 | 0.75 | 0.041 | 0.0069 | 0.0012 | 0.0339 | 0.0079 |
| SR2surf_13 | 4.7606 | 0.4993 | 0.7180 | 0.0171 | 0.3485 | 1.735 | 0.041 | 0.268 | 0.026 | 1.26 | 0.12 |
| SR2surf_14 | 80.6821 | 25.7097 | 0.4890 | 0.0700 | -0.6100 | 2.91 | 0.15 | 0.028 | 0.0097 | 0.094 | 0.035 |
| SR2surf_15 | 10.8044 | 0.6388 | 0.7340 | 0.0281 | -0.1746 | 2.312 | 0.099 | 0.219 | 0.016 | 0.822 | 0.064 |
| SR2surf_16 | 54.4958 | 5.5780 | 0.8400 | 0.3100 | 0.3692 | 3.05 | 0.094 | 0.079 | 0.036 | 0.209 | 0.03 |
| SR2surf_17 | 217.2211 | 34.0077 | 0.6110 | 0.0370 | 0.4110 | 5.21 | 0.26 | 0.0166 | 0.0025 | 0.072 | 0.017 |
| SR2surf_18 | 4.6711 | 0.8293 | 0.6960 | 0.0112 | -0.1967 | 1.537 | 0.057 | 0.16 | 0.024 | 1.11 | 0.15 |
| SR2surf_19 | 26.1030 | 2.4550 | 0.6650 | 0.0191 | 0.0655 | 1.606 | 0.077 | 0.083 | 0.01 | 0.223 | 0.019 |
| SR2surf_20 | 1.5728 | 0.2207 | 0.7180 | 0.0102 | 0.0823 | 1.673 | 0.046 | 0.97 | 0.14 | 3.73 | 0.45 |
| SR2surf_21 | 33.8557 | 2.2015 | 0.6550 | 0.0251 | -0.0387 | 1.877 | 0.017 | 0.0593 | 0.0062 | 0.183 | 0.013 |
| SR2surf_22 | 22.2273 | 1.7527 | 0.7050 | 0.0221 | -0.1194 | 3.454 | 0.054 | 0.152 | 0.018 | 0.549 | 0.041 |
| SR2surf_23 | 20.0404 | 4.5386 | 0.7100 | 0.1000 | 0.2561 | 0.721 | 0.019 | 0.0273 | 0.0065 | 0.109 | 0.024 |
| SR2surf_24 | 10.8992 | 1.2572 | 0.6320 | 0.0241 | 0.1047 | 1.341 | 0.035 | 0.354 | 0.075 | 0.439 | 0.06 |
| SR2surf_25 | 35.0001 | 5.7505 | 0.6150 | 0.0410 | -0.4451 | 1.556 | 0.056 | 0.0337 | 0.0077 | 0.143 | 0.026 |
| SR2surf_26 | 3.3133 | 0.1942 | 0.7430 | 0.0132 | -0.0020 | 1.515 | 0.049 | 0.387 | 0.024 | 1.807 | 0.096 |
| SR2surf_27 | 10.1181 | 0.5950 | 0.7310 | 0.0241 | 0.3282 | 2.089 | 0.059 | 0.189 | 0.016 | 0.793 | 0.074 |
| SR2surf_28 | 4.0081 | 0.2553 | 0.7310 | 0.0162 | 0.1673 | 1.047 | 0.028 | 0.318 | 0.018 | 1.029 | 0.081 |
| SR2surf_29 | 38.4676 | 3.4007 | 0.2780 | 0.0470 | -0.1616 | 0.759 | 0.039 | 0.0084 | 0.0026 | 0.0266 | 0.0049 |
| SR2surf_30 | 104.5000 | 8.9738 | 0.1900 | 0.0390 | 0.0503 | 0.869 | 0.018 | 0.00031 | 0.00036 | 0.0066 | 0.0013 |
| SR2surf_31 | 149.6993 | 18.2220 | 0.5320 | 0.0560 | 0.1141 | 1.482 | 0.034 | 0.0036 | 0.0016 | 0.0283 | 0.0045 |
| SR2surf_32 | 165.4467 | 20.4699 | 0.0880 | 0.0810 | 0.5320 | 0.87 | 0.032 | 0.00046 | 0.00062 | 0.0085 | 0.002 |
| SR2surf_33 | 12.5506 | 1.0001 | 0.6500 | 0.0211 | -0.0793 | 0.913 | 0.012 | 0.0691 | 0.0072 | 0.243 | 0.023 |
| SR2surf_34 | 3.6760 | 0.5367 | 0.6940 | 0.0112 | -0.2187 | 1.234 | 0.081 | 0.442 | 0.044 | 1.14 | 0.12 |
| SR2surf_35 | 205.0338 | 12.6887 | 0.6160 | 0.0361 | 0.0647 | 4.45 | 0.17 | 0.0083 | 0.0013 | 0.0657 | 0.0054 |
| SR2surf_36 | 16.7453 | 2.1188 | 0.6970 | 0.0261 | 0.0022 | 2.4 | 0.11 | 0.131 | 0.016 | 0.485 | 0.055 |
| SR2surf_37 | 2.7859 | 0.4461 | 0.7110 | 0.0102 | -0.4492 | 1.778 | 0.046 | 0.53 | 0.093 | 2.25 | 0.38 |
| SR2surf_38 | 3.2526 | 0.4041 | 0.7040 | 0.0122 | 0.0438 | 1.426 | 0.033 | 0.67 | 0.15 | 1.72 | 0.21 |
| SR2surf_39 | 3.7652 | 0.5176 | 0.7110 | 0.0122 | 0.0318 | 1.814 | 0.036 | 0.305 | 0.038 | 1.88 | 0.26 |
| SR2surf_40 | 4.9306 | 0.4197 | 0.7150 | 0.0122 | 0.0421 | 1.528 | 0.016 | 0.266 | 0.016 | 1.121 | 0.09 |
| SR2surf_41 | 2.3667 | 0.2736 | 0.7261 | 0.0087 | -0.0660 | 1.432 | 0.091 | 0.575 | 0.045 | 2.27 | 0.15 |
| SR2surf_42 | 12.7698 | 0.8687 | 0.7230 | 0.0331 | 0.3329 | 2.449 | 0.052 | 0.195 | 0.018 | 0.707 | 0.059 |
| SR2surf_43 | 10.2942 | 0.8714 | 0.7420 | 0.0132 | 0.2105 | 4.045 | 0.061 | 0.449 | 0.073 | 1.51 | 0.11 |
| SR2surf_44 | 3.3856 | 0.5658 | 0.7350 | 0.0122 | 0.1322 | 1.576 | 0.091 | 0.28 | 0.031 | 1.66 | 0.19 |
| SR2surf_45 | 14.0714 | 1.2667 | 0.7120 | 0.0181 | 0.0675 | 4.57 | 0.15 | 0.264 | 0.027 | 1.22 | 0.11 |
| SR2surf_46 | 22.6734 | 1.6207 | 0.7100 | 0.0181 | 0.7427 | 3.18 | 0.11 | 0.158 | 0.017 | 0.505 | 0.025 |
| SR2surf_47 | 38.9500 | 1.9521 | 0.6470 | 0.0311 | -0.0689 | 3.795 | 0.031 | 0.105 | 0.012 | 0.329 | 0.019 |
| SR2surf_48 | 20.4696 | 2.1540 | 0.7300 | 0.0221 | -0.3616 | 3.466 | 0.086 | 0.119 | 0.011 | 0.671 | 0.089 |
| SR2surf_49 | 28.4978 | 3.4993 | 0.6520 | 0.0191 | -0.1300 | 1.518 | 0.066 | 0.063 | 0.013 | 0.194 | 0.03 |
| SR2surf_50 | 36.9793 | 2.6113 | 0.7370 | 0.0201 | 0.4691 | 6.12 | 0.15 | 0.246 | 0.032 | 0.658 | 0.044 |
| SR2surf_51 | 40.2105 | 3.7098 | 0.3750 | 0.0480 | 0.3343 | 0.422 | 0.04 | 0.0049 | 0.0022 | 0.0194 | 0.0041 |
| SR2surf_52 | 28.4326 | 3.5478 | 0.6880 | 0.0211 | -0.2903 | 2.76 | 0.14 | 0.0623 | 0.0093 | 0.35 | 0.055 |
| SR2surf_53 | 28.8955 | 2.2735 | 0.7240 | 0.0231 | 0.5164 | 4.59 | 0.29 | 0.1136 | 0.0093 | 0.567 | 0.045 |
| SR2surf_54 | 7.8145 | 0.6531 | 0.6640 | 0.0211 | 0.7782 | 1.748 | 0.072 | 0.162 | 0.015 | 0.729 | 0.036 |
| SR2surf_55 | 10.1017 | 0.9202 | 0.7260 | 0.0311 | 0.0664 | 1.754 | 0.075 | 0.062 | 0.0084 | 0.643 | 0.051 |
| SR2surf_56 | 4.0211 | 0.7191 | 0.7180 | 0.0201 | 0.2654 | 2.207 | 0.068 | 0.415 | 0.074 | 1.88 | 0.31 |
| SR2surf_57 | 6.6444 | 0.4761 | 0.7450 | 0.0122 | -0.0236 | 3.305 | 0.091 | 0.275 | 0.028 | 1.94 | 0.11 |
| SR2surf_58 | 52.4264 | 3.6543 | 0.2580 | 0.0430 | 0.0404 | 0.517 | 0.018 | 0.00158 | 0.00066 | 0.0116 | 0.0017 |
| SR2surf_59 | 96.3182 | 9.1142 | 0.6200 | 0.1100 | 0.3896 | 2.019 | 0.046 | 0.0055 | 0.002 | 0.057 | 0.0056 |
| SR2surf_60 | 167.6795 | 11.6822 | 0.5590 | 0.0410 | 0.2981 | 2.1 | 0.056 | 0.00149 | 0.00091 | 0.0353 | 0.0045 |
| SR2surf_61 | 306.0356 | 27.6504 | 0.5010 | 0.0460 | -0.3112 | 5.24 | 0.14 | 0.0259 | 0.0055 | 0.039 | 0.0037 |

**Table 17.** Laser ablation ICP-MS U-Th-Pb Data for sample TC2_surf

| Data for Tera-Wasserburg plot | | | | | | | Concentrations | | | | |
|---|---|---|---|---|---|---|---|---|---|---|---|
| Identifier | 238U/206Pb | Prop2SE | 207Pb/206Pb | Prop2SE | err.corr. | Approx_U_PPM | Approx_U_PPM_Int2SE | Approx_Th_PPM | Approx_Th_PPM_Int2SE | Approx_Pb_PPM | Approx_Pb_PPM_Int2SE |
| TC2surf_1 | 0.0243 | 0.0012 | 0.8330 | 0.0192 | 0.3968 | 0.363 | 0.032 | 1.99 | 0.25 | 70.2 | 8.1 |
| TC2surf_2 | 0.0619 | 0.0029 | 0.8510 | 0.0113 | 0.0615 | 0.31 | 0.034 | 0.754 | 0.073 | 21.5 | 2.2 |
| TC2surf_3 | 0.0357 | 0.0017 | 0.8568 | 0.0086 | 0.1549 | 0.294 | 0.029 | 1.091 | 0.061 | 31.7 | 1.7 |
| TC2surf_4 | 0.0452 | 0.0032 | 0.8540 | 0.0133 | 0.0694 | 0.35 | 0.049 | 0.924 | 0.094 | 32.8 | 2.9 |
| TC2surf_5 | 0.0271 | 0.0011 | 0.8538 | 0.0092 | 0.1500 | 0.184 | 0.016 | 0.598 | 0.041 | 29.3 | 2.9 |
| TC2surf_6 | 0.0369 | 0.0017 | 0.8642 | 0.0090 | 0.0562 | 0.292 | 0.016 | 0.886 | 0.044 | 33.4 | 2 |
| TC2surf_7 | 0.0331 | 0.0014 | 0.8560 | 0.0113 | 0.3738 | 0.2169 | 0.0097 | 0.918 | 0.056 | 27.9 | 1.1 |
| TC2surf_8 | 0.0248 | 0.0017 | 0.8560 | 0.0152 | 0.5082 | 0.175 | 0.022 | 0.69 | 0.46 | 28.6 | 2.8 |
| TC2surf_9 | 0.0147 | 0.0005 | 0.8584 | 0.0086 | 0.2737 | 0.1234 | 0.0074 | 0.678 | 0.039 | 38.2 | 2.7 |
| TC2surf_10 | 0.0152 | 0.0054 | 0.9030 | 0.0681 | 0.2845 | 0.0039 | 0.0021 | 1 | 1.7 | 0.89 | 0.46 |
| TC2surf_11 | 0.0343 | 0.0015 | 0.8585 | 0.0098 | 0.4429 | 0.1581 | 0.0085 | 0.697 | 0.018 | 19.66 | 0.83 |
| TC2surf_12 | 0.0457 | 0.0023 | 0.8650 | 0.0143 | 0.5587 | 0.326 | 0.013 | 1.179 | 0.038 | 31.3 | 1.6 |
| TC2surf_13 | 0.0718 | 0.0059 | 0.8480 | 0.0202 | 0.1926 | 0.33 | 0.038 | 1.149 | 0.041 | 19.8 | 1.3 |
| TC2surf_14 | 0.1172 | 0.0134 | 0.8330 | 0.0142 | -0.2272 | 0.215 | 0.026 | 0.697 | 0.075 | 7.44 | 0.53 |
| TC2surf_15 | 0.0444 | 0.0045 | 0.8570 | 0.0113 | -0.2474 | 0.409 | 0.046 | 1.015 | 0.075 | 37.4 | 3.1 |
| TC2surf_16 | 0.0482 | 0.0031 | 0.8559 | 0.0076 | 0.4753 | 0.297 | 0.028 | 0.842 | 0.041 | 26 | 1.8 |
| TC2surf_17 | 0.0601 | 0.0025 | 0.8550 | 0.0104 | 0.5987 | 0.26 | 0.015 | 0.717 | 0.031 | 19 | 1.1 |
| TC2surf_18 | 0.0374 | 0.0017 | 0.8560 | 0.0075 | 0.2891 | 0.283 | 0.014 | 1.191 | 0.037 | 31.9 | 1 |
| TC2surf_19 | 0.0389 | 0.0029 | 0.8547 | 0.0101 | 0.0102 | 0.288 | 0.038 | 1.12 | 0.11 | 31.8 | 3.5 |
| TC2surf_20 | 0.0411 | 0.0019 | 0.8570 | 0.0133 | 0.0681 | 0.184 | 0.011 | 0.831 | 0.027 | 19.4 | 0.86 |
| TC2surf_21 | 0.0408 | 0.0016 | 0.8547 | 0.0072 | 0.3181 | 0.198 | 0.02 | 1.24 | 0.17 | 21.6 | 2.1 |
| TC2surf_22 | 0.0545 | 0.0032 | 0.8504 | 0.0091 | 0.1442 | 0.302 | 0.025 | 1.125 | 0.054 | 22.2 | 1 |
| TC2surf_23 | 0.0668 | 0.0055 | 0.8537 | 0.0088 | 0.0770 | 0.571 | 0.072 | 1.132 | 0.088 | 35.2 | 2.2 |
| TC2surf_24 | 0.0570 | 0.0025 | 0.8540 | 0.0192 | 0.1079 | 0.409 | 0.033 | 1.13 | 0.13 | 31.8 | 3 |
| TC2surf_25 | 0.0520 | 0.0034 | 0.8540 | 0.0123 | 0.2054 | 0.454 | 0.028 | 1.077 | 0.062 | 37.1 | 3.3 |
| TC2surf_26 | 0.0882 | 0.0037 | 0.8560 | 0.0113 | 0.1473 | 0.444 | 0.017 | 0.919 | 0.035 | 22 | 0.65 |
| TC2surf_27 | 0.0857 | 0.0067 | 0.8330 | 0.0241 | 0.3875 | 0.299 | 0.051 | 1.11 | 0.21 | 15 | 2.7 |
| TC2surf_28 | 0.0581 | 0.0034 | 0.8470 | 0.0113 | 0.4172 | 0.1004 | 0.0068 | 0.606 | 0.028 | 7.34 | 0.36 |
| TC2surf_29 | 0.0560 | 0.0034 | 0.8440 | 0.0162 | 0.4266 | 0.1532 | 0.0091 | 0.473 | 0.03 | 11.52 | 0.65 |
| TC2surf_30 | 0.0583 | 0.0028 | 0.8550 | 0.0104 | 0.4020 | 0.241 | 0.016 | 1.202 | 0.057 | 17.8 | 1.4 |
| TC2surf_31 | 0.0628 | 0.0037 | 0.8520 | 0.0133 | 0.2817 | 0.264 | 0.017 | 0.915 | 0.078 | 17.6 | 1.1 |
| TC2surf_32 | 0.9103 | 0.0679 | 0.8469 | 0.0096 | 0.2315 | 3.67 | 0.46 | 2.05 | 0.17 | 17.1 | 1.1 |
| TC2surf_33 | 0.0769 | 0.0037 | 0.8480 | 0.0113 | 0.2137 | 0.201 | 0.013 | 0.635 | 0.038 | 11.09 | 0.62 |
| TC2surf_34 | 0.0646 | 0.0035 | 0.7840 | 0.0391 | 0.3301 | 0.864 | 0.073 | 3.59 | 0.34 | 54 | 4.4 |
| TC2surf_35 | 0.0489 | 0.0018 | 0.7520 | 0.0700 | 0.3139 | 0.96 | 0.14 | 0.857 | 0.061 | 83 | 13 |
| TC2surf_36 | 0.0326 | 0.0013 | 0.8650 | 0.0113 | 0.4512 | 0.35 | 0.012 | 0.717 | 0.026 | 47.4 | 2.4 |
| TC2surf_37 | 0.0905 | 0.0054 | 0.8560 | 0.0133 | 0.4087 | 0.275 | 0.016 | 0.747 | 0.045 | 13.25 | 0.71 |
| TC2surf_38 | 0.0613 | 0.0026 | 0.8528 | 0.0099 | 0.4659 | 0.428 | 0.017 | 1.319 | 0.046 | 30.6 | 1.4 |
| TC2surf_39 | 0.0657 | 0.0027 | 0.8590 | 0.0113 | 0.1524 | 0.988 | 0.04 | 2.12 | 0.24 | 66.5 | 3 |
| TC2surf_40 | 0.0470 | 0.0017 | 0.8561 | 0.0072 | -0.0359 | 0.493 | 0.025 | 1.231 | 0.044 | 45.2 | 2.7 |
| TC2surf_41 | 0.0390 | 0.0015 | 0.8526 | 0.0083 | 0.4590 | 0.359 | 0.016 | 1.097 | 0.034 | 39.1 | 1.7 |
| TC2surf_42 | 0.0339 | 0.0018 | 0.8530 | 0.0123 | 0.3575 | 0.377 | 0.034 | 1.027 | 0.044 | 49.2 | 5 |
| TC2surf_43 | 0.0284 | 0.0011 | 0.8574 | 0.0093 | 0.4098 | 0.267 | 0.017 | 0.893 | 0.06 | 40.3 | 2.1 |
| TC2surf_44 | 0.0364 | 0.0028 | 0.8590 | 0.0101 | 0.0035 | 0.209 | 0.015 | 1.132 | 0.052 | 24.1 | 1.7 |
| TC2surf_45 | 0.0345 | 0.0016 | 0.8520 | 0.0123 | 0.6181 | 0.362 | 0.018 | 1.4 | 0.041 | 45.3 | 2 |
| TC2surf_46 | 0.7965 | 0.0929 | 0.8106 | 0.0089 | -0.3097 | 7.49 | 0.76 | 6.87 | 0.48 | 36.7 | 1.3 |
| TC2surf_47 | 0.0373 | 0.0021 | 0.8620 | 0.0113 | 0.1607 | 0.429 | 0.044 | 1.108 | 0.066 | 46.1 | 2.7 |
| TC2surf_48 | 0.0457 | 0.0023 | 0.8480 | 0.0123 | 0.5702 | 0.235 | 0.015 | 0.876 | 0.045 | 22.1 | 1 |
| TC2surf_49 | 0.0914 | 0.0149 | 0.8330 | 0.0261 | 0.5308 | 0.606 | 0.092 | 1 | 0.1 | 25.6 | 2 |
| TC2surf_50 | 0.0483 | 0.0028 | 0.8760 | 0.0192 | 0.4361 | 0.1391 | 0.0083 | 0.489 | 0.028 | 12.24 | 0.77 |
| TC2surf_51 | 0.0446 | 0.0019 | 0.8551 | 0.0090 | 0.3284 | 0.346 | 0.021 | 1 | 0.037 | 33.4 | 2.7 |
| TC2surf_52 | 0.0665 | 0.0035 | 0.8563 | 0.0101 | 0.5573 | 0.3302 | 0.0091 | 1.081 | 0.062 | 21.98 | 0.46 |
| TC2surf_53 | 0.0519 | 0.0019 | 0.8441 | 0.0095 | 0.1803 | 0.36 | 0.02 | 1.64 | 0.1 | 29.8 | 1.9 |
| TC2surf_54 | 0.0685 | 0.0026 | 0.8400 | 0.0103 | 0.3474 | 0.197 | 0.024 | 0.625 | 0.071 | 12.5 | 1.7 |
| TC2surf_55 | 0.0740 | 0.0040 | 0.8430 | 0.0113 | 0.1770 | 0.164 | 0.013 | 0.692 | 0.035 | 8.79 | 0.44 |
| TC2surf_56 | 0.0697 | 0.0039 | 0.8420 | 0.0103 | 0.1849 | 0.207 | 0.011 | 1.097 | 0.036 | 12.51 | 0.44 |